



MONASH University

Examining the Mechanisms of How Surface Modification Alters the Flow of Fine Powders

Geoffrey Tan

Bachelor of Pharmaceutical Sciences (Honours)

A thesis submitted for the degree of Doctor of Philosophy at
Monash University in 2021

Drug Delivery, Disposition and Dynamics, Monash Institute of Pharmaceutical
Sciences. 381 Royal Parade, Parkville, VIC, 3052, Australia

Table of Contents

<i>Copyright notice</i>	<i>vi</i>
<i>Abstract</i>	<i>vii</i>
<i>Declaration</i>	<i>ix</i>
<i>Publications</i>	<i>x</i>
<i>Published works declaration</i>	<i>xi</i>
<i>Acknowledgements</i>	<i>xiii</i>
<i>Chapter 1: Introduction</i>	<i>15</i>
1.1. <i>Commentary</i>	<i>15</i>
1.2. <i>Introduction</i>	<i>15</i>
1.3. <i>Theoretical Background</i>	<i>16</i>
1.3.1. <i>Powder Flow</i>	<i>16</i>
1.4. <i>Adhesive and Cohesive Contacts</i>	<i>16</i>
1.5. <i>Inter-particle interactions</i>	<i>17</i>
1.5.1. <i>Van der Waals Interactions</i>	<i>17</i>
1.5.1.1. <i>Surface Energy</i>	<i>19</i>
1.5.2. <i>Capillary Forces</i>	<i>20</i>
1.5.3. <i>Solid Bridging</i>	<i>21</i>
1.5.4. <i>Electrical Interactions</i>	<i>22</i>
1.5.5. <i>Mechanical Interlocking</i>	<i>22</i>
1.6. <i>Flow–No Flow Postulate</i>	<i>23</i>
1.7. <i>External Factors Influencing the Flow of Powders</i>	<i>23</i>
1.7.1. <i>Particle Shape, Size and Distribution</i>	<i>24</i>
1.7.2. <i>Hardness (or Softness) of Particles</i>	<i>24</i>
1.7.3. <i>Consolidation (or Aeration) State of Powders</i>	<i>25</i>
1.7.4. <i>Surface and Geometry of Containers</i>	<i>25</i>
1.7.5. <i>Relative Humidity</i>	<i>25</i>
1.8. <i>Measuring the Flow of Powders</i>	<i>26</i>
1.8.1. <i>Powder Densities and their Indices</i>	<i>26</i>
1.8.2. <i>Powder Avalanche</i>	<i>31</i>
1.8.3. <i>Angle of Repose</i>	<i>34</i>
1.8.4. <i>Flow Through an Orifice and the Critical Orifice Diameter</i>	<i>37</i>
1.8.5. <i>Powder Rheometer</i>	<i>40</i>

1.8.6. Shear Cells.....	42
1.9. Improving the Flow of Powders	46
1.9.1. Surface Modification.....	47
1.9.1.1. Intensive Mechanical Dry Coating	47
1.10. Surface Property Measurements.....	49
1.10.1. Wettability Measurement.....	49
1.10.1.1. Liquid Intrusion	49
1.11. Surface Energy Measurements.....	52
1.11.1. Contact Angles.....	52
1.11.1.1. Zisman's Method: the Critical Surface Tension	53
1.11.1.2. Fowkes' Method	53
1.11.1.3. Owens-Wendt: the Two Components Method	54
1.11.1.4. Wu's Harmonic Mean Method	54
1.11.1.5. Good-van Oss: the Three Components Method	55
1.11.2. Inverse Gas Chromatography	55
1.12. Thesis Statement	59
1.13. Aims and Objectives.....	59
1.14. References.....	60
Chapter 2: Surface Modification and Physical Characterisation of a Model Pharmaceutical Powder	72
2.1. Commentary.....	72
2.2. Materials.....	72
2.3. Methods	73
2.3.1. Particle Engineering via Dry Coating.....	73
2.3.2. Laser Diffraction	73
2.3.3. Scanning Electron Microscopy	74
2.3.4. Statistical Analysis.....	74
2.4. Results	74
2.4.1. Observations	74
2.4.2. Particle Size Analysis	74
2.4.3. Powder Morphology	76
2.5. Conclusions.....	77

2.6. References.....	78
Chapter 3: Development of New Experimental Methods.....	80
3.1. Commentary.....	80
3.2. Part I: A Strategy to Evaluate the Surface Energy of High Packing Efficiency Fine Powders via Inverse Gas Chromatography.....	81
3.2.1. Introduction	81
3.2.2. Materials and Methods	82
3.2.2.1. Materials	82
3.2.2.2. Dry Coating	83
3.2.2.3. Blending Fine Powders with Carrier Particles	83
3.2.2.4. Surface Energy Measurements	84
3.2.2.5. Statistical Analysis	86
3.2.3. Results and Discussions	86
3.2.4. Conclusions.....	91
3.2.5. Acknowledgements	92
3.2.6. References.....	92
3.3. Part II: Strategies to Analyse Data Obtained from Liquid Intrusion Experiments of Loose Porous Materials.....	94
3.3.1. Introduction	94
3.3.1.1. Measurement of Contact Angles	94
3.3.2. Background	95
3.3.2.1. The Reference Liquid	98
3.3.2.2. Analysis of Multiple Measurements	99
3.3.3. Materials and Methods	100
3.3.3.1. Materials	100
3.3.3.2. Selecting the Most Appropriate Reference Liquid	100
3.3.3.3. Analysing Multiple Sets of Reference and Probe Liquid Data	101
3.3.3.4. Case Study	104
3.3.3.5. Statistical Analysis	106
3.3.4. Results and Discussions	106
3.3.5. Conclusions.....	110
3.3.6. Acknowledgements	111

3.3.7. References.....	111
Chapter 4: Evaluating the Flow of Surface Modified Fine Powders with Varying Amounts of Magnesium Stearate Through Different Flowability Tests.....	115
4.1. Commentary.....	115
4.2. Abstract.....	115
4.3. Introduction.....	116
4.4. Materials and Methods.....	123
4.4.1. Materials.....	123
4.4.2. Methods.....	123
4.4.2.1. Sample Pre-conditioning.....	123
4.4.2.2. Powder Densities and their Carr Indices.....	123
4.4.2.3. Compressibility Measurements.....	124
4.4.2.4. Basic Flowability Energy.....	124
4.4.2.5. Flow Rate.....	125
4.4.2.6. Shear Cell Testing.....	125
4.4.2.7. Statistical Analysis.....	125
4.5. Results.....	126
4.6. Discussion.....	133
4.7. Conclusion.....	135
4.8. Acknowledgements.....	136
4.9. References.....	136
Chapter 5: Characterising the Surface Properties of Surface Modified Fine Powders.....	141
5.1. Commentary.....	141
5.2. Abstract.....	141
5.3. Introduction.....	142
5.4. Materials and Methods.....	147
5.4.1. Materials.....	147
5.4.2. Methods.....	147
5.4.2.1. Time-of-Flight Secondary Ion Mass Spectrometry.....	147
5.4.2.2. X-ray Photoelectron Spectroscopy.....	148
5.4.2.3. Surface Energy Measurements.....	149

5.4.2.4. Surface Hydrophobicity Measurements	151
5.4.2.5. Statistical Analysis	152
5.5. Results and Discussion	152
5.5.1. Surface Composition of MGB After Dry Coating with Varying Amounts of MgSt	152
5.5.2. The Effect of a MgSt Coating on the Surface Energy of MGB	157
5.5.3. Hydrophobicity of MgSt Coated MGB	159
5.6. Conclusion	161
5.7. Acknowledgements	162
5.8. References	162
Chapter 6: Conclusions and Future Work	168
6.1. Conclusions	168
6.1.1. Thesis Summary	177
6.2. Future Work	178
6.3. References	179
Appendix	180

Copyright notice

© Geoffrey Tan (2021).

I certify that I have made all reasonable efforts to secure copyright permissions for third-party content included in this thesis and have not knowingly added copyright content to my work without the owner's permission.

Abstract

This thesis examined the mechanisms of how modifying the surface of a cohesive fine powder altered the flow behaviours of the fine powder. To this end, a model pharmaceutical fine powder (micron-sized glass beads (MGB, $d_{50} \approx 10 \mu\text{m}$) was dry coated with different amounts of the pharmaceutical lubricant magnesium stearate (MgSt) (0.05% to 2% w/w MgSt). The flowability of the powders was evaluated with a number of techniques. To understand how the MgSt coating altered powder flow, the surface coatings, surface energies and the hydrophobicities of the powders were also examined.

Modified MGB flowed better than uncoated MGB. Best flow was obtained with 0.1% w/w MgSt to 0.25% w/w MgSt. With 0.05% w/w MgSt, better flow was only possible when the powder underwent unconfined flow or confined mechanical flow. Powders with excess amounts of MgSt ($\geq 0.5\%$ w/w MgSt) were unable to flow as freely as powders with optimal amounts of MgSt.

ToF-SIMS showed the MgSt coating to be dependent on the amount of MgSt used and varied from being a partial coating of MgSt (0.05% w/w MgSt) to a near-complete coating of MgSt (0.1-0.25% w/w MgSt) to a thicker near-complete coating of MgSt ($\geq 0.5\%$ w/w MgSt). XPS measurements suggested the hydrocarbon tail of MgSt was likely presented at the surface of the powder.

With a change in the surface of the MgSt coated powders, the surface energies of the powders were altered. MgSt coated powders had significantly lower surface energies than uncoated MGB. Powders with 0.1% w/w MgSt or more exhibited the same surface energies, which coincides well with the results from ToF-SIMS and XPS measurements.

Hydrophobicities of the powders were evaluated by measuring the contact angle of water to the powders with the liquid intrusion method. The contact angle of water to MGB was approximately 80° , thus capillary forces within MGB were weak.

Hydrophobicity of MgSt coated powders increased. This eliminated the presence of capillary forces.

Modifying the surfaces of cohesive fine powders with MgSt can have a complex effect on the flow of MgSt coated powders. The principal mechanism by which MgSt improved flow was by significantly lowering the surface energy of the powder, and to a lesser extent, eliminating capillary forces. Furthermore, the flow of MgSt coated powders was also influenced by the extent and thickness of the coating. Partial coatings of MgSt affect the type of contacts that are possible during flow. Thicker coatings of MgSt result in small increases in cohesivity as deformation of the coating may occur, especially when powders undergo flow processes where powder consolidation occurs.

Declaration

This thesis is an original work of my research and contains no material which has been accepted for the award of any other degree or diploma at any university or equivalent institution and that, to the best of my knowledge and belief, this thesis contains no material previously published or written by another person, except where due reference is made in the text of the thesis.

Signature:

Print Name: Geoffrey Tan

Date: 30th January 2021

Publications

Mangal S, Meiser F, Tan G, Gengenbach T, Denman J, Rowles MR, et al., Relationship between surface concentration of l-leucine and bulk powder properties in spray dried formulations, *Eur J Pharm Biopharm.* 94(2015) 160-9.

Tan G, Morton DAV, Larson I, On the methods to measure powder flow, *Current Pharmaceutical Design.* 21(2015) 5751-65.

Mangal S, Meiser F, Tan G, Gengenbach T, Morton DAV, Larson I, Applying surface energy derived cohesive-adhesive balance model in predicting the mixing, flow and compaction behaviour of interactive mixtures, *Eur J Pharm Biopharm.* 104(2016) 110-6.

Tan G, Morton DAV, Larson I, Strategies to analyse data obtained from liquid intrusion experiments of loose porous materials, *J Pharm Biomed Anal.* 145(2017) 711-7.

Tan G, Qu L, Morton DAV, Larson I, A strategy to evaluate the surface energy of high packing efficiency fine powders via inverse gas chromatography, *Powder Technol.* 320(2017) 470-3.

Published works declaration

I hereby declare that this thesis contains no material which has been accepted for the award of any other degree or diploma at any university or equivalent institution and that, to the best of my knowledge and belief, this thesis contains no material previously published or written by another person, except where due reference is made in the text of the thesis.

This thesis includes 3 original papers published in peer reviewed journals. The papers form the basis of chapters one and three. The ideas, development and writing of the papers in the thesis were my responsibility under the supervision of Dr. Ian Larson and Prof. David Morton.

My contribution to these chapters was:

Thesis Chapter	Publication Title	Nature and % of student contribution	Co-author name(s) Nature and % of Co-author's contribution*	Co-author(s), Monash student Y/N*
1	On the methods to measure powder flow	Initiation of key ideas, literature review, writing up (70%)	1) Ian Larson: Input of ideas, editing (15) 2) David Morton: Input of ideas, editing (15%)	1) No 2) No
3	Strategies to analyse data obtained from liquid intrusion experiments of loose porous materials	Initiation of key ideas, development of new methods, design of study, developed laboratory work, data collection, analysis and interpretation of data, writing. (80%)	1) Ian Larson: Input of ideas, editing (10) 2) David Morton: Input of ideas, editing (10%)	1) No 2) No

3	A strategy to evaluate the surface energy of high packing efficiency fine powders via inverse gas chromatography	Initiation of key ideas, development of new method, design of study, developed laboratory work, data collection, analysis and interpretation of data, writing. (78%)	1) Li Qu: laboratory work (2%) 2) Ian Larson: Input ideas, editing (10) 3) David Morton: Input ideas, editing (10%)	1) Yes 2) No 3) No
---	--	--	---	--------------------------

I renumbered sections of submitted or published papers for consistent presentation within the thesis.

Student name: Geoffrey Tan

Student signature: 

Date: 30th January 2021

Acknowledgements

I would like to express my deepest and most sincere gratitude to my supervisions Dr. Ian Larson and Prof. David Morton for their continued presence, guidance, support and endless encouragement throughout the entirety of my studies. I appreciate all the time and effort you have put into helping me develop my scientific and interpersonal skills and allowing me the freedom to explore my scientific curiosities. If not for your inputs, ideas and many stimulating discussions, many of this research would never have been possible.

I would also like to thank my colleagues and friends within Drug Delivery, Disposition and Dynamics, Monash Institute of Pharmaceutical Sciences, Monash University. Their support, advice and understanding has made my studies an enjoyable and memorable experience. I am also grateful for their reminders to find a balance in my life and for providing much needed distractions from my work every so often.

I would like to thank Dr. Aidan Sudbury and Dr. Daniel Tokarev for the fruitful discussions during the development of new approaches to analyse data obtained from liquid intrusion experiments when working with powders. I would like to thank Dr. John Denman for conducting ToF-SIMS experiments and for the discussions relating to the analysis of the ToF-SIMS data. I would like to thank Dr. Thomas Gengenbach for conducting XPS experiments and for the discussions relating to the analysis of the XPS data.

I would also like to thank Graduate Research, Monash University, for providing a Monash Equity Scholarship.

Last but not least, I would like to express my deepest heartfelt gratitude to my family for their constant and endless support and encouragement throughout my studies.

Geoffrey Tan

Chapter 1: Introduction

Geoffrey Tan

Bachelor of Pharmaceutical Sciences (Honours)

Drug Delivery, Disposition and Dynamics, Monash Institute of Pharmaceutical
Sciences. 381 Royal Parade, Parkville, VIC, 3052, Australia

Chapter 1: Introduction

1.1. Commentary

Portions of this chapter were published in: *Tan G, Morton DAV, Larson I, On the methods to measure powder flow, Current Pharmaceutical Design. 21(2015) 5751-65* and *Tan G, Morton DAV, Larson I, Strategies to analyse data obtained from liquid intrusion experiments of loose porous materials, J Pharm Biomed Anal. 145(2017) 711-7.*

1.2. Introduction

The flow of fine powders is of particular interest to the pharmaceutical industry as it can affect a multitude of processes within the pharmaceutical industry such as handling, transporting, blending, fluidising and dispensing [1-3]. Many of these processes require good, consistent and predictable flow to ensure efficient and optimal manufacturing of quality products. For example, to rapidly manufacture quality and satisfactory tablets, the precursor tablet particulate blend has to possess good, consistent and reliable flow which allows the consistent filling of the tablet dies [4]. Any erratic flow behaviour can have a negative impact on the quality of the resultant tablets—that is, some tablets may be out of specification due to over or under filling of the tablet die [5]. However, as fine powders are naturally cohesive due to relatively strong inter-particle interactions, their inherently poor flowability can often hinder the optimal production of pharmaceutical products which results in economic loss [2, 3, 6-8].

Consequently, numerous strategies have been explored to improve the flow of fine powders, including those that modify the surfaces of powders through particle engineering such as dry coating. Through dry coating methods such as mechanofusion, the flow of fine powders has been improved [9-17]. However, the mechanisms of how such improvements occur remain relatively poorly understood and deserves further investigation.

1.3. Theoretical Background

1.3.1. Powder Flow

The concept of powder flow can be defined as the relative movement of particles amongst adjacent particles or along a containing surface [18]. However, in spite of this, powders can often flow in a highly complex fashion. In fact, not only can powders behave as solids, they can also behave as liquids or even gases depending on the state of the powder [19]. Despite the importance and ubiquitousness of powders in industries, the flow behaviour of powders remains relatively poorly understood [3]. To date, perhaps the most successful attempts to describe the mechanics of powder flow are those where the bulk powder is viewed as a solid body undergoing elastic/plastic deformation (see, for example, [20-25]) and mechanical failure (see, for example, [26-28]).

As a force is applied to a bulk powder material, the initial reaction of the bulk powder is to deform. If the applied force is removed and the material returns to its original position, the powder is said to have undergone elastic deformation [22]. However, such elastic deformation of bulk powders does not play a critical role in powder flow as particles do not move relative to one another. Instead, if the magnitude of the applied force increases beyond the elastic point of the bulk powder, the particles pressing against one another will slip past one another and the bulk powder is described to have undergone plastic deformation. At this point, a shear failure plane is formed leading to powder flow. From this point onwards, deformation of the bulk powder is completely plastic and powder flow occurs from layers of particles slipping over other layers where contacts are continuously breaking and reforming dynamically [6, 22, 29].

1.4. Adhesive and Cohesive Contacts

The cohesiveness of fine powders results from inter-particle interactions which are a collection of concurrently acting attractive forces that keep particles in contact with one

another to form agglomerates [2, 30]. These contacts are referred to as adhesive and cohesive contacts. Adhesion is defined as the attractive forces between dissimilar materials, while cohesion is defined as the attractive forces between similar materials [31].

1.5. Inter-particle interactions

The inter-particle interactions are primarily comprised of: van der Waals interactions, the capillary force, solid bridging, electrostatic forces and mechanical interlocking [22].

1.5.1. Van der Waals Interactions

Johannes D. van der Waals first hypothesised the existence of attractive molecular interactions in his doctoral thesis in 1873 after observing the non-ideality of gases. Another five decades past before the attractive interactions were shown to comprise of three different interactions: dipole-dipole interactions, first described by Keesom (1921) [32]; dipole-induced dipole interactions, first described by Debye (1920) [33]; and dispersive (London) interactions, first described by London (1930) [34]. Collectively, these three different interactions are now termed van der Waals interactions and are innate interactions as they stem from the electron densities of molecules. That is, the van der Waals interactions are always present between molecules that are in close proximity to one another.

In 1937, Hamaker developed a model for determining the strength of the van der Waals interaction between two macroscopic bodies by summing all the molecular van der Waals forces within the two macroscopic bodies [35]. The attractive force of the van der Waals interaction between two spherical bodies with radius r_1 and r_2 as a function of their separation distance z_0 , where r_1 and $r_2 \gg z_0$ and $z_0 \neq 0$, is described by Equation (1.1) [35]:

$$F_{vdW} = -\frac{A_H r_1 r_2}{6(r_1 + r_2)z_0^2} \quad (1.1)$$

where A_H is the Hamaker constant which is dependent on the molecular properties of the two bodies.

The significance of the Hamaker model for van der Waals interactions between macroscopic bodies is that the strength of the van der Waals force is proportional to z_0^{-2} as opposed to the molecular van der Waals interaction, which is proportional to z_0^{-7} [36]. Consequently, for macroscopic bodies, the van der Waals interactions does not diminish as rapidly over increasing distances; thus, van der Waals interactions can be considered long ranged forces when dealing with macroscopic bodies [37]. However, it must be noted that the Hamaker model only holds true when particles are separated by a finite non-zero distance—that is, when the particles are not in contact.

When the particles are in contact, however, the strength of the van der Waals interaction is equivalent to the pull-off force as described in contact mechanics such as JKR (Johnson–Kendall–Roberts) or DMT (Derjaguin–Muller–Toporov) Theory provided that no other attractive forces are present [38-40]. Here, contact mechanics describes the adhesive force (that is, the pull-off force) between contacting surfaces as a function of the surface energy of the contacting surfaces. For two contacting spherical particles with radius r_1 and r_2 and without external loading (that is, the particles are not externally pushed together), the pull-off force is given by Equation (1.2) [38, 41]:

$$F_{po} = -n\pi w_A R^* \quad (1.2)$$

where $w_A = \gamma_1 + \gamma_2 - \gamma_{12}$ and is termed the work of adhesion, $R^* = \frac{r_1 r_2}{r_1 + r_2}$ and is termed the reduced radius. γ_1 and γ_2 are the surface energies of materials 1 and 2, respectively, and γ_{12} is the interfacial energy between materials 1 and 2. n is a constant that is either equal to $\frac{3}{2}$ for the JKR Theory or is equal to 2 for the DMT Theory.

It should be noted, if the contacting materials are similar, the work of cohesion, w_c , is used instead where $w_c = 2\gamma_1$.

1.5.1.1. Surface Energy

As seen above, the surface energy of powders plays an important role in the adhesive/cohesive forces and therefore, theoretically, powder flow. So, what is this surface energy? Johnson, Kendall and Roberts simply defined it as: “*the energy required to create unit area of new surface*” [38]. It arises from the net inward intermolecular force exerted by the molecules found at the surface of materials and is analogous to the surface tension of liquids [31].

The surface energy, γ_s , comprises two major interactions [42]. The first being the innate dispersive (London) interaction which is present between all molecules. The second is the polar interaction (sometimes referred to as the acid-base interaction or the “specific interaction” as it is only evident when an acidic moiety interacts with a basic moiety and vice versa) [42, 43]. Therefore, the surface energy of any material can be split into two major components—a dispersive component, γ_s^D , which is always present and a polar (specific) component, γ_s^P , which only arises when acid-base interactions are present [44].

In order to further analyse the influences of the components of surface energy on the adhesive contacts of particles, the work of adhesion, w_A , and the work of cohesion, w_c , can also be written in their surface energy component form [37, 45, 46]:

$$w_A = 2 \left(\sqrt{\gamma_{S1}^D \gamma_{S2}^D} + \sqrt{\gamma_{S1}^P \gamma_{S2}^P} \right) \quad (1.3)$$

$$w_c = 2 \left(\sqrt{\gamma_{S1}^D \gamma_{S1}^D} + \sqrt{\gamma_{S1}^P \gamma_{S1}^P} \right) \quad (1.3a)$$

where subscripts 1 and 2 represent solids 1 and 2, respectively.

For powders with a large surface energy, the pull-off force is likely to be high as the high surface energy would result in larger work of adhesion/cohesion. Therefore, powders with large surface energies would, in theory, be poorer flowing. In contrast, powders with lower surface energies, the pull-off force is likely to be lower as the low surface energy would result in lower work of adhesion/cohesion. Thus, powders with lower surface energies would, in theory, be better flowing.

1.5.2. Capillary Forces

Voids between neighbouring particles act as very fine capillaries in which moisture from the atmosphere can condense even at low relative humidity (RH) and ambient temperatures, as illustrated in Figure 1-1. This phenomenon is explained with the Kelvin equation [47], which relates the equilibrium vapour pressure of a liquid to the curvature of the liquid-vapour interface at different temperatures.

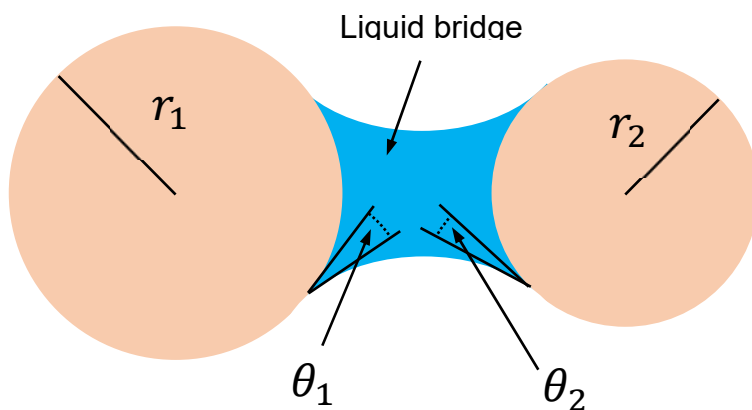


Figure 1-1: Liquid bridging between two spherical bodies.

The capillary force is always attractive as the force stems from the surface tension of the liquid and the negative pressure as a result of a concave curvature on the liquid-vapour interface [48]. The strength of the capillary force for two smooth spherical particles of radius, r_1 and r_2 (see Figure 1-1) can be determined by Equation (1.4) [49]:

$$F_c = -2\pi\gamma_l R^* (\cos \theta_1 + \cos \theta_2) \quad (1.4)$$

where γ_l is the surface tension of the liquid and θ_1 and θ_2 are the angles the liquid makes to the surface of each particle.

As can be seen, the strength of the capillary force is dependent on the wettability (or hydrophilicity/hydrophobicity when water is considered) of powders where the maximum capillary force occurs when the liquid perfectly wets the powder, that is, when $\theta = 0^\circ$. Moreover, the capillary force is generally considered as a relatively strong force that can potentially dominate other adhesive forces [48]. However, unlike the van der Waals interactions, the capillary force is not always present—it cannot exist without the presence of a liquid bridge between adjacent particles [48].

1.5.3. Solid Bridging

If a liquid bridge exists, the surfaces of the particles can dissolve until the solubility of the material is reached. If drying subsequently occurs, perhaps due to small changes in relative humidity, recrystallization of the solute can physically link adjacent particles [2]. Such links are depicted in Figure 1-2 and are referred to as solid bridges. Thus, it is not uncommon to find the presence of solid bridges following liquid bridging [50]. However, similar to the capillary force, solid bridging is not always present, for instance when the particles are insoluble in the liquid.

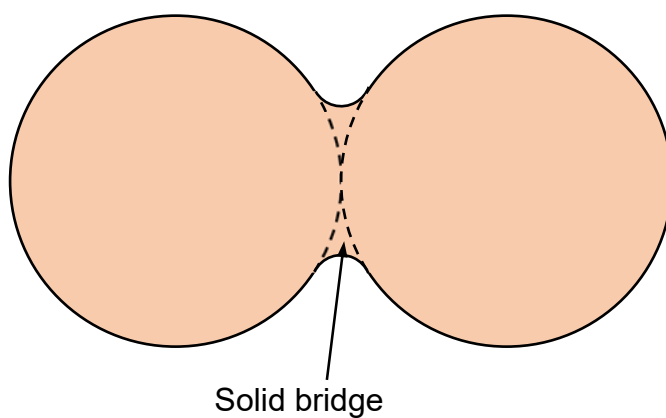


Figure 1-2: Solid bridge between two spherical particles.

1.5.4. Electrical Interactions

When two charges approach one another, the charges will either attract one another in the case of opposite charges or repel one another in the case of similar charges. Macroscopic bodies may carry charge due to triboelectrification where dissimilar initially uncharged surfaces are rubbed against one another [51]. Such charges will either cause the macroscopic bodies to repel or attract depending on the nature of their charge. The amount of charge at the two surfaces determines the overall strength of the electrical force.

However, the amount of charge on the surfaces of particles does not remain constant over time, the charge diminishes, thus resulting in reduced electrical forces. In addition, if either of the contacting materials are conductive or if water is present in the voids, the charge will also decay resulting in reduced electrical forces [48, 52]. Therefore, with suitable storage conditions and adequate storage periods, the electrical force may be considered negligible.

1.5.5. Mechanical Interlocking

Real surfaces are rarely truly smooth—there will always be some form of asperity, even if it is on a nanometre scale. When two surfaces are in contact the peak of one surface may align directly in the trough of the other surface as depicted in Figure 1-3. This is known as mechanical interlocking which hinders the relative movement of adjacent particles and thus inhibits powder flow [52].

Mechanical interlocking

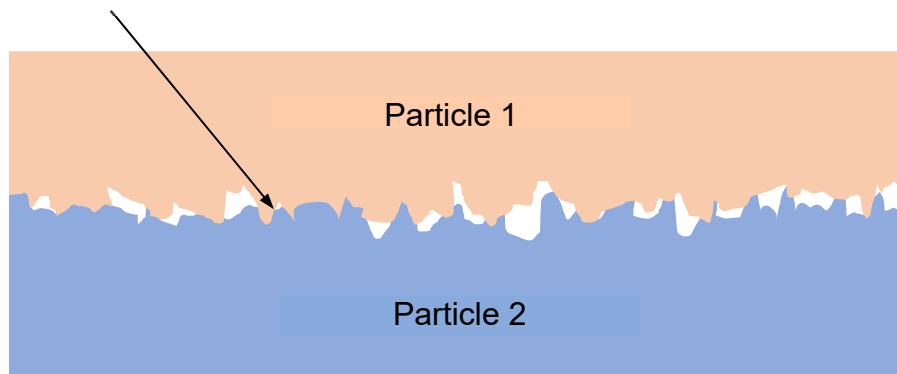


Figure 1-3: Mechanical interlocking between two rough surfaces.

1.6. Flow–No Flow Postulate

As inter-particle interactions act concurrently to hinder powder flow by keeping particles in contact with one another [2, 30], these interactions must be overcome before powder flow is possible. Consequently, the flow of powders is the result of an imbalance of two opposing forces: the flow promoting force, F_p , which is any force that acts to cause powder flow, and the cohesive force, which results from the presence of the inter-particle interactions, F_{ip} [3, 6, 18, 22, 29, 31].

Thus, powder flow occurs when $F_p > F_{ip}$ is satisfied, while powders do not flow when $F_p \leq F_{ip}$ is satisfied.

where $F_{ip} = F_{vdw} + F_c + F_s + F_e + F_i$. F_{vdw} is the force due to van der Waals interactions, F_c is the capillary force, F_s is the force due to solid bridging, F_e is the electrostatic force and F_i is the force due to mechanical interlocking.

1.7. External Factors Influencing the Flow of Powders

In addition to the inter-particle interactions, the flow of powders is also influenced by a multitude of external factors such as the shape of the particles, their size and size

distribution, the hardness of the particles, the consolidation (or aeration) state of the powder, the surface geometry of the containing walls and the relative humidity of the surrounding environment.

1.7.1. Particle Shape, Size and Distribution

Pharmaceutical particles are rarely spherical in shape. They can be elongated such as needles and rods, prismatic with defined geometric parameters, flat such as plates or even irregularly shaped. For all but the simplest shape, it is difficult to determine the exact influence that particle shape has on flowability. Generally, however, as the particles become more rounded, the flow tends to improve, that is, spherical particles generally flow more easily than elongated or plate-like particles [53-55].

Particle size can have a substantial effect on the flowability of bulk powders. Small particles are often poor flowing as they are typically more cohesive than larger particles [31, 55]. This is because the weight of smaller particles is often insufficient to overcome the relatively strong inter-particle interactions.

It is also important to recognize that powders are rarely monodispersed, there is always some level of distribution in the size of the particles. This distribution can have a significant impact on flow, the flow can either improve or worsen depending on the size distribution of the particles. For instance, Liu, 2008 [56] observed poorer powder flow for samples with a smaller particle size and wider size distribution. Alternatively, Danish, 1971 [57] showed a more complex relationship between size distribution and flow. These authors found that increasing the fines content increased the flowability of the powder to a finite level before the flowability was observed to worsen with further increase in fines content [57].

1.7.2. Hardness (or Softness) of Particles

As powders consolidate, the constituent particles compress against one another. This compression can cause the contacting particles to deform and flatten around their contact points, thereby effectively increasing the contact area between adjacent

particles [58]. With more of the surface in contact, more inter-particle interactions, such as van der Waals interactions, can occur between the contacting surfaces. The larger amounts of inter-particle interactions result in an increase in the overall cohesiveness of the powder, which translates to poorer powder flowability. Consequently, softer particles are likely to flow more poorly than harder particles as softer particles are likely to deform more easily than harder particles.

1.7.3. Consolidation (or Aeration) State of Powders

Powder flow is not only dependent on the constituting particles, but also the state at which the powder is in, especially its state of consolidation. For instance, with the exception of a few cases, as powders consolidate, their flowabilities typically decrease. The decrease in flowability can be so severe that powders are unable to flow out of hoppers [27]. This decreased flowability occurs because of an increase in the average number of contacts between adjacent particles [8, 59]. Consequently, there are more inter-particle interactions, thus increasing the overall cohesive force [8, 59]. Alternatively, when aerated, powders can behave as a liquid or when suspended in a gas, powders can behave as a gas [19]. Consequently, the consolidation (or aeration) state of powders can have dramatic effects on how powders behave [3].

1.7.4. Surface and Geometry of Containers

The flow of powders is also influenced by the surfaces on which they are to slide over as well as the geometry of the surfaces [3, 60]. For example, the same powder may flow easily and steadily in one hopper and show erratic and uncontrollable flow in a different hopper [3].

1.7.5. Relative Humidity

The effect of relative humidity (RH) on the flow of powders is not necessarily simple. In the previous section (Chapter 1: Section 1.5.2), it was discussed that liquid bridges can form and thus lead to capillary forces. Typically, this results in the immobilisation

of the particles and thus decrease flow [61-64]. On the other hand, the adsorption of a molecularly thin layer of water onto the surfaces of particles may improve powder flow as the water acts as a lubricant [65]. Alternatively, the water can indirectly affect the flow of powders by altering the surface energy of the powder or altering the localised crystallinity of the surfaces of the particles [61, 62]. The presence of water may even soften the particles, which, as discussed in Chapter 1: Section 1.7.2, makes them easier to deform, which ultimately increases the cohesiveness of the powder and thus results in poorer flow [7, 66]. Furthermore, the relative humidity may also expedite the decay of any electrostatic charge that may be present on the powder, thus removing the effect of the electrostatic force [67], thereby improving flowability.

1.8. Measuring the Flow of Powders

Although there are numerous methods available to assess the flow of powders, they can be very broadly categorised as: confined, unconfined or consolidated flow. Confined flow occurs when powders start from an unconsolidated (or low consolidated) state and powder flow results in significant increases in powder consolidation, while unconfined flow occurs when the flow of powders does not result in significant increases in powder consolidation. In contrast to confined flow, when powders are already in a consolidated state, due to a consolidating stress, and flow occurs while the powders are still under consolidation, then consolidated flow is said to have occurred. These types of flow can be further subcategorised into gravitational or mechanical flow depending on whether the flow inducing force is due to gravity or a mechanically exerted force, respectively.

1.8.1. Powder Densities and their Indices

When a powder is poured into a container, it will occupy a volume termed the initial volume, V_0 . This initial volume is dependent on the spatial arrangement of the individual particles. That is, the resulting powder bed consists of both particles and void spaces, see Figure 1-4a, which result from a variety of factors including inter-particle interactions [54, 68, 69]. The ratio of the mass of powder to the initial volume

(V_0) is known as the bulk density, ρ_b (or the initial or poured density). If the container is disturbed by, for instance, tapping, the energy applied from the taps (provided the energy is sufficient) will break and re-form the cohesive contacts between the constituent particles of the powder. The result is the powder forms a more consolidated state and the volume will consequently decrease to a new volume, V_n , where n is the number of taps. As n increases, the volume of the powder reaches a minimum as no further consolidation occurs [70, 71], as depicted in Figure 1-4b. Because the mass of the powder remains constant, a new density is obtained, which is termed the tapped density, ρ_t , or the final density.

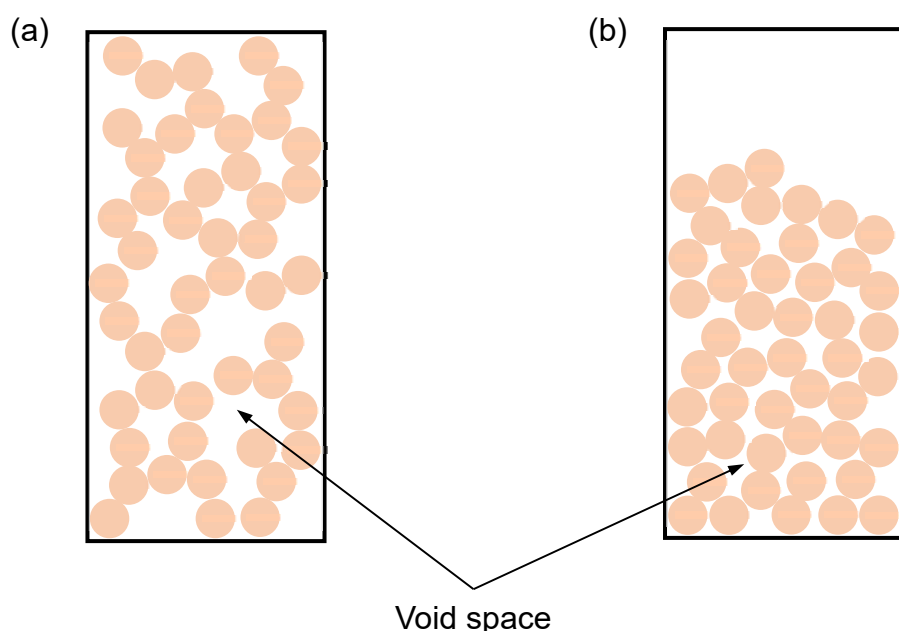


Figure 1-4: Spatial arrangement of cohesive particles in a confined space. (a) Before tapping and (b) after tapping.

There are a number of methods available to measure the bulk and tapped density of powders. The United States Pharmacopeia (USP38-NF33 Chapter 616) [71], for example, recommends the use of a graduated cylinder, such as a calibrated volumetric cylinder, or a 100 ml cylindrical container of specific dimensions to measure the bulk density of powders. For the determination of tapped densities, automatic tapping apparatus are normally used. These are normally designed to conform to standards such as the those outlined in the United States Pharmacopeia (USP38-NF33 Chapter

616) [71]. Examples of such apparatus include the Autotap™ by Quantachrome Instruments, USA and the Tapped Density Testers Series JV by Copley Scientific Ltd., UK [72, 73].

In the case of cohesive powders, the packing efficiency of the particles is poor, that is, there are many large voids because of relatively strong inter-particle interactions that exist between neighbouring particles that dominate over the gravitational force. A loosely packed powder bed is formed. Conversely, for free-flowing powders, the inter-particle interactions are not dominant over the gravitational force. The individual particles will flow and slide past one another when poured to form a powder bed with a higher packing efficiency.

Bulk and tapped densities are not indicators of powder flow [70]. However, in 1965 Carr [70] noted a relationship between the bulk density, ρ_b , and the tapped density, ρ_t , of bulk powders and their flowability. He described this relationship in the form now commonly known as the Carr index, CI , (sometimes expressed as a percentage) which is defined as:

$$CI = \frac{\rho_t - \rho_b}{\rho_t} \quad (1.5)$$

Similarly, Hausner in 1967 [68] noticed the same relationship and defined the quotient of the tapped density and the bulk density as the Hausner ratio, HR :

$$HR = \frac{\rho_t}{\rho_b} \quad (1.6)$$

Because tap density measurements result in powders consolidating with each tap (provided that powder flow occurs) and the flow inducing force is gravity, Carr indices and Hausner ratios can be considered examples of indirect measurements of confined gravitational flow. The advantages of the Carr index and Hausner ratio are: they are quick, simple and cost-effective methods to indirectly assess the relative strength of inter-particle interactions of bulk powders. Limitation of both the Carr index and Hausner ratio includes their inability to take into account the effect of powder

consolidation on the flow of powders and they are not suitable to assess the flow of highly cohesive powders that are very poor flowing (see below).

For poor flowing powders, the difference between the bulk and tapped densities is usually larger than those for free-flowing powders, thus resulting in larger Carr indices and larger Hausner ratios. As a general guide, the transition between free-flowing and poor flowing powder is in the region of approximately $CI = 0.2$, which results in an equivalent Hausner ratio of around 1.25 [68-70]. Table 1-1 provides a qualitative description of powder flowability as measured by the density indices [70]:

Table 1-1: Qualitative description of flow properties of powders as measured by both the Carr index and the Hausner ratio.

Carr index	Hausner ratio	Flow Property
≤0.10	1.00-1.11	Excellent
0.11-0.15	1.12-1.18	Good
0.16-0.20	1.19-1.25	Fair
0.21-0.25	1.26-1.34	Passable
0.26-0.31	1.35-1.45	Poor
0.32-0.37	1.46-1.59	Very poor
>0.38	1.60	Very, very poor

However, care must be taken when using density indices to evaluate the flow of powders. This is because for some very poor flowing and highly cohesive powders, the energy applied from tapping is insufficient to disrupt the relatively strong inter-particle interactions between adjacent particles (see below) [74]. Consequently, there is little change between the initial density (bulk density) and final density (tapped density), thus providing misleadingly small Carr indices and Hausner ratios which can be misinterpreted as good flowing powders.

As mentioned earlier, the United States Pharmacopeia (USP38-NF33 Chapter 616) [71] provides guidelines to measure both the bulk and tapped densities. However, because these guidelines recommend either the use of relatively large amounts of

sample, at least 100 g, or to fill relatively large containers, the smallest of which is 25 cm³, these guidelines may not be readily suitable for applications where only relatively small amounts of samples are available such as when investigating novel pharmaceutical systems.

To overcome such hurdles, some have developed modified methods for measuring the densities of powders [14, 75-78]. For example, Hughes *et al.*, 2015 [78] compared the bulk density (measured through the method outlined in the United States Pharmacopeia (USP36-NF31 Chapter 616) [79]) and the “conditioned bulk density” (CBD) from a commercially available powder rheometer (see below). The authors of [78] concluded that the CBD from the powder rheometer was comparable to the USP standard methods and would be suitable for early development of APIs (active pharmaceutical ingredient).

Additionally, Thalberg *et al.*, 2004 [75], used a “compressed density” of dry powder inhaler (DPI) formulations in place of the traditionally measured tapped density. This was achieved by compressing a known mass of powder with a known force. The authors of [75] claimed that there were no significant differences between the “compressed density” and the traditionally measured tapped density when investigating carrier particles alone. This was not true, however, when measuring ordered mixtures as the new method resulted in slightly higher density values than the traditionally measured tapped density [75]. The authors of [75] attributed this to the fact that the new method used a piston to compress the powder and thus was able to compress the entire length of the powder bed, while in the traditional method of measuring the tapped density there is a pressure gradient along the powder bed as a result of the weight of powder above.

Interestingly, methods such as the one described by Thalberg *et al.*, 2004 [75] may be useful in overcoming the limitations of the density indices, specifically in regards to evaluating very poor flowing highly cohesive powders where tapping may not provide sufficient energy to consolidate the powder bed. In cases where a mechanical force is exerted to induce compression of powder beds, these methods of flow assessments

can be considered examples of indirect measurements of confined mechanical flow. The advantages of these methods are: they are relatively simple methods to assess flow and they are able to assess the flowability of highly cohesive powders that are very poor flowing. The limitation of compressibility measurements is that these measurements also are not able to account for the consolidation effect on powder flow.

1.8.2. Powder Avalanche

Measuring powder avalanching is most commonly carried out in a rotating cylinder type apparatus with either a photocell array behind the rotating cylinder or a digital camera to detect avalanches [80, 81], while some novel apparatus use a load cell located underneath the rotating cylinder to detect each avalanche [82]. Examples of such instruments include the Revolution Powder Analyser by Mercury Scientific Inc., USA, the AeroFlow by TSI Inc., USA and the GranuDruM by APTIS, Belgium.

In the ideal scenario when a constant volume of powder is placed in a sealed cylinder and rotated (see Figure 1-5) the powder is transported upwards and will reach a stage where it can just maintain its structure (see Figure 1-5b). The angle of the free surface of the powder structure to the horizontal is known as the maximum angle of stability, α_s , sometimes referred to as the avalanche angle. Upon further rotation of the cylinder, the powder will avalanche under gravitational forces to create a new stable surface, sometimes referred to as the post avalanche position (see Figure 1-5c) [83]. As the cylinder continues to rotate this process repeats until the end of the experiment.

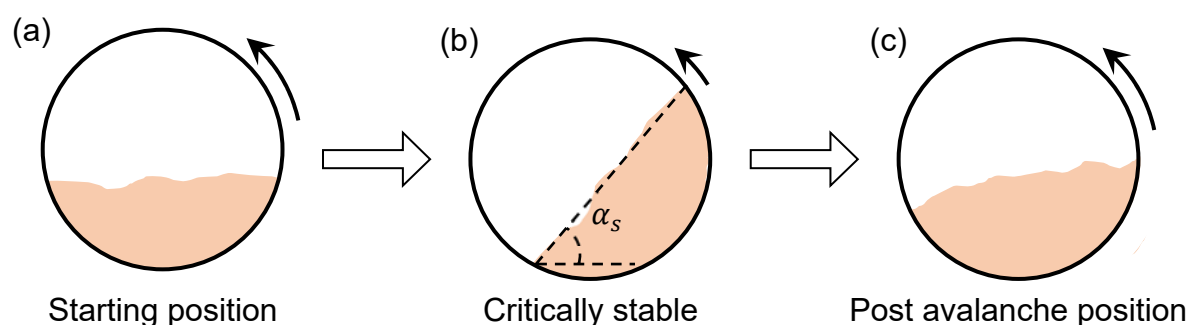


Figure 1-5: Ideal stages of a powder avalanching experiment.

However, in reality there are a number of possible flow patterns a powder can have within a rotating cylinder: slipping, slumping, rolling, cascading and cataracting which are depicted in Figure 1-6 [84, 85].

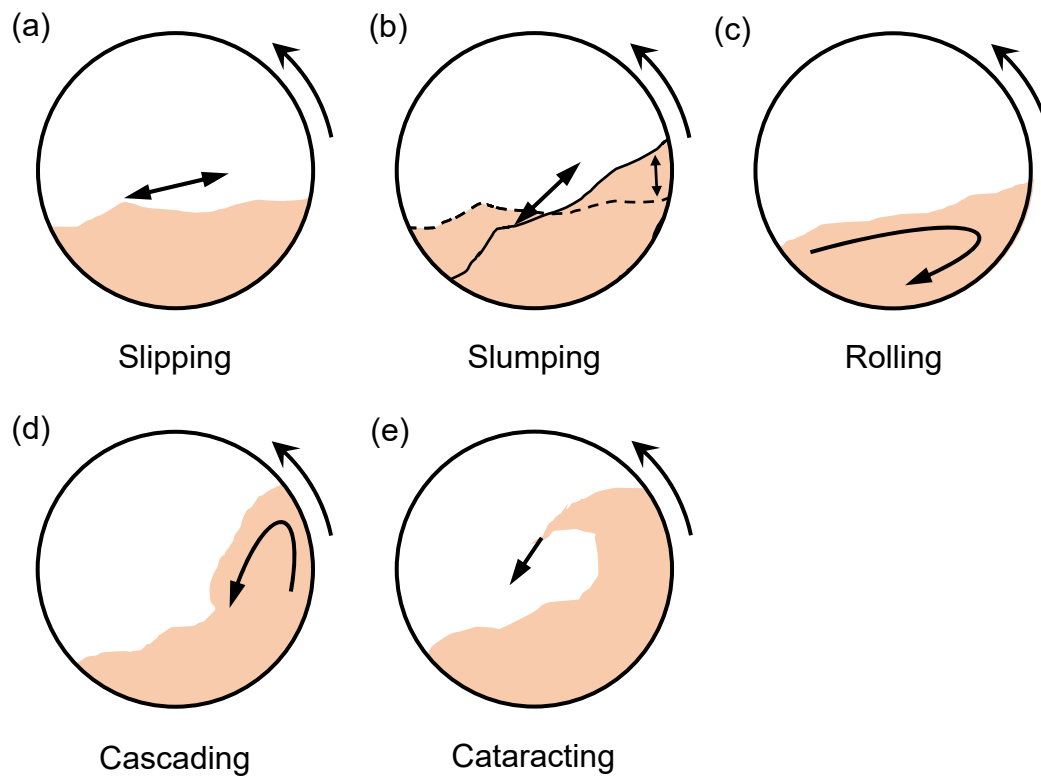


Figure 1-6: Possible flow behaviours of a powder within a rotating cylinder. Adapted from Boateng *et al.*, 1996 [85].

The slipping flow pattern occurs when the powder bed, as a whole, slips along the contacting wall of the rotating cylinder. The slumping flow pattern occurs when the powder bed is transported upwards along the rotating wall and becomes unstable, fails and slips, or “slumps” down the wall. Both of these flow patterns indicate that the inter-particle interactions within the powder are greater than the wall friction of the contacting surface of the cylinder. Therefore, neither of these flow patterns are useful in evaluating powder flow. This can, however, be remedied by increasing the contacting wall friction by, for instance, applying a metal sieve-like mesh or sand paper on the inner wall of the rotating cylinder [75]. The rolling flow pattern, in contrast, is an indication of very good powder flow and is also a desirable flow pattern for blending

as this pattern promotes good particle mixing [85]. The cascading and cataracting flow patterns are both signs of poor powder flow.

Due to the chaotic nature of avalanching, it is not possible to predict the magnitude of each avalanche. Instead, the time (or weight) of each avalanche is, like with many chaotic processes, often presented as the so-called “strange attractor plot”, where t_n (or W_n) forms the abscissa, while t_{n+1} (or W_{n+1}) forms the ordinate as depicted in Figure 1-7. Here, the points for the time (or mass) of consecutive avalanches are recorded and joined together until the end of the experiment ($[t_1, t_2]$, $[t_2, t_3]$, $[t_3, t_4] \dots [t_n, t_{n+1}]$) [80].

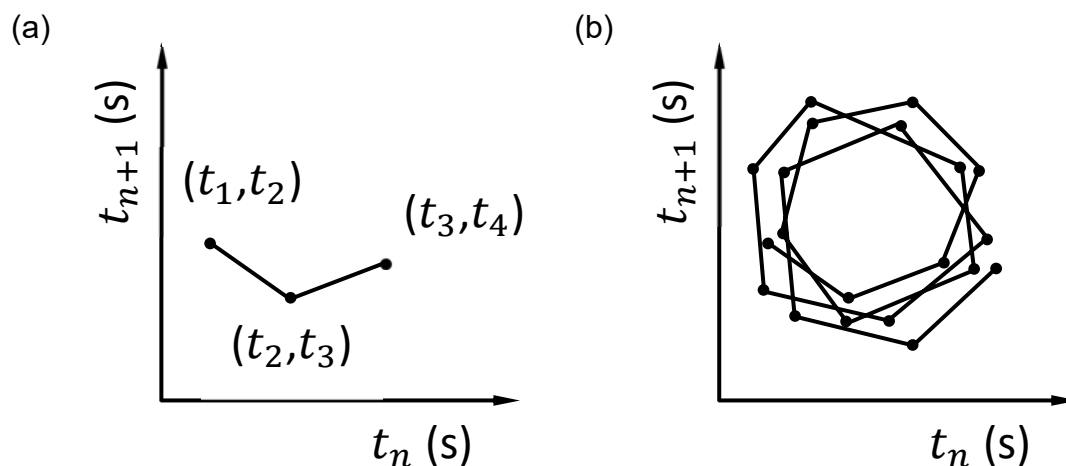


Figure 1-7: Simplified representation of the construction of a strange attractor plot during an avalanching experiment where the time of each avalanche is recorded. (a) Shows the construction of the first three data points of a strange attractor plot and (b) strange attractor plot of twenty avalanches. Adapted from Kaye *et al.*, 1995 [80].

In such a plot, the centroid of the plot is equivalent to the Mean Time to Avalanche (MTA), sometimes referred to as the avalanche time, while the two-dimensional scatter of the plot represents the regularity of the powder flow behaviour, which may be represented as a so-called “avalanche standard deviation”. The flowability of a powder is therefore described by both the MTA and the “deviation” of the strange attractor plot. Generally, for a good flowing powder, a small scatter along with a small MTA value is

obtained, while the opposite is true for poor flowing powders where a large MTA value and a large deviation is obtained.

However, such simplistic analysis of powder flow behaviour from powder avalanching can be misleading. For example, powder flow behaviours that involve slipping or slumping may produce low MTA values and low deviation values and thus can be misinterpreted as good, consistent flow behaviour. To resolve this, Lee *et al.*, 2000 [86] proposed a dual approach to evaluating powder flow via avalanching by taking both the numerical data and factoring the type of powder flow pattern that was observed during the avalanching experiment. As powder avalanching does not result in significant powder consolidation and avalanches occur from gravitational forces, the avalanching method can be considered an example of indirect measurements of unconfined gravitational flow. Limitations of the avalanching method are that the flow pattern of powders in a revolving cylinder can be influenced by the rate of revolution of the cylinder, the powder is susceptible to segregation and agglomeration and aeration can occur which can potentially alter the flow behaviour of the powder. The advantage of the powder avalanche method is that it is able to identify a range of powder flow behaviours in a dynamic manner.

1.8.3. Angle of Repose

Imagine pouring a powder from a height onto a flat horizontal surface resulting in a cone-like “pile” as depicted in Figure 1-8. The angle of repose (AOR), sometimes referred to as the “repose angle”, is defined as the inner angle measured from the horizontal to the free sloping edge of the cone-like pile [70]. There are a number of different experimental methods with which to measure the angle of repose [87]. These can be loosely categorised into two types: static and dynamic.

The static angle of repose is so named due to the static nature of the experiment. Perhaps, the most commonly used static methods are the “fixed funnel and free-standing cone” method and the “fixed base cone” method which are recommended in the United States Pharmacopeia (USP38-NF33 Chapter 1174) (see Figure 1-8) [69].

In the “fixed funnel and free-standing cone” method, the powder is poured through a funnel that is at a fixed height above the surface. The pile is built up until its apex just reaches the bottom of the funnel. The base of the pile is free to spread horizontally across the flat surface. Alternatively, in the “fixed base cone” method, the powder is poured through a funnel that is raised as the apex of the pile builds up to its maximum height. The pile base is fixed as a result of a lipped horizontal surface. In both cases, the internal angle of the free sloping edge to the horizontal surface is known as the angle of repose, α , and can be calculated from Equation (1.7):

$$\tan \alpha = \frac{h}{r} \quad (1.7)$$

where h is the vertical distance between the base of the pile to the apex and r is the radius of the base of the pile.

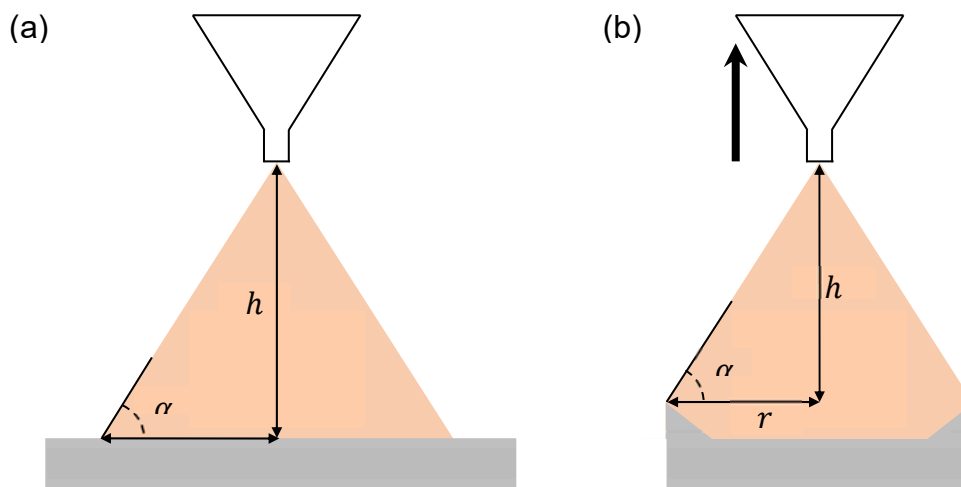


Figure 1-8: Schematic of a pile of powder on a flat surface. (a) The “fixed and free-standing cone” method and (b) the “fixed bed cone” method.

As the angle of repose is the angle of the free sloping edge of a pile, significant powder consolidation does not occur. Consequently, the angle of repose can be considered an example of indirect measurements of unconfined gravitational flow. The angle of repose is also an indirect indicator of the relative strength of competing forces—those that promote the flow of powders and thus the collapse of the powder pile, namely gravity, and those that prevent powder flow, that is the inter-particle interactions [2]. In

other words, it is related to the powder's resistance to movement between adjacent particles. Therefore, in general, a smaller angle of repose is associated with free-flowing powders, while a larger angle of repose is associated with poor-flowing cohesive powders [27, 54, 69, 87]. Table 1-2 provides a qualitative description of powder flowability as measured by the angle of repose [70].

Table 1-2: Qualitative description of the flow property of powders as measured by angle of repose.

Flow property	Angle of repose (°)
Excellent	25-30
Good	31-35
Fair (aid not needed)	36-40
Passable (material may hang up)	41-45
Poor (must agitate, vibrate)	46-55
Very poor	56-65
Very, very poor	>66

However, in spite of the different methods to measure the angle of repose, they all suffer from the same limitations, in particular, they may not be suitable for measuring highly cohesive powders with very poor flow [69]. The angle of repose also does not take into consideration the consolidation effect on powder flow [27] and segregation can result, especially for samples with a wide particle size distribution.

The angle of repose is likely to be dependent on factors such as the experimental setup, operator and method. Consequently, the reproducibility of such measurements is poor [87, 88] and difficulties may also arise when comparing data as they are highly-dependent on manual handling and slight variation in experimental setups [89]. Brown, 1961 [90] showed that the flow of powders through different apertures can be highly different and thus incomparable. However, with the introduction of standard methods, for example ASTM D6393-14: Standard Test Method for Bulk Solids Characterization by Carr indices, and instruments designed to conform to such standards, these limitations may be mitigated. Examples of such instruments that are manufactured to

comply with standards include the Micron Powder Characteristics Tester by Hosokawa Micron Corp., Japan and the Flowability Tester BEP2, Copley Scientific Ltd., UK [91, 92].

The “dynamic angle of repose” is so named due to the dynamic nature of the experiment. Perhaps the most common of these dynamic methods is through powder avalanching (see above) measured by the “rotating cylinder” method (see Figure 1-5). Upon further rotation of the cylinder beyond the critically stable position (see Figure 1-5b), the critically stable powder will avalanche to create a new stable surface (see Figure 1-5c) [83]. As the cylinder continues to rotate, the angle of the new surface of the powder structure to the horizontal will change (see Figure 1-5c), this angle is then defined as the dynamic angle of repose, α_d . Thus, measurements of powder flow via powder avalanching is regarded as dynamic measurements of flow [83].

The advantages of the angle of repose are it is one of the quickest, easiest and most cost-effective method to evaluate the flow of powders and thus is commonly used to differentiate between powders [89, 93-95]. The limitation of this method is its inability to account for the consolidation effect on the flow of powders.

1.8.4. Flow Through an Orifice and the Critical Orifice Diameter

Within the pharmaceutical industry there are many examples where powders are required to flow through an orifice such as flow out of hoppers and into feed mechanisms of tableting or capsule filling machines [54]. Flow through an orifice was traditionally measured discretely by measuring either the time required for a given mass/volume of powder to flow through an orifice or the mass/volume of powder to flow through an orifice in a given time period [96, 97]. The mean flow rate can then be calculated either as mass or volume per unit time. The greatest limitation of such measurements is the inability to profile any inconsistent flow patterns of the powder [98]. To rectify this, Gold *et al.* in 1966 [98] proposed the use of an electronic powder flowmeter which utilized a calibrated electronic strain gauge connected to a chart recorder. This is the basis of several modern apparatus. However, today, such

apparatus utilise an electronic balance to register the mass of powder flowing through the orifice. From this the mean flow rate can also be calculated. Examples of such apparatus include the Granulate Flow Tester by Erweka GmbH, Germany and the Flowability Tester BEP2 by Copley Scientific Ltd., UK [92, 99].

Advantages of this method are that it can be a quick and simple experiment to conduct and it usually requires very little training. Additionally, this method can be a more sensitive measurement of flow for powder and lubricant and/or glidant mixtures than other methods to evaluate powder flow, for example the angle of repose [88, 100]. However, care must be taken as the flow of powders through an orifice is highly dependent on a number of factors which not only includes the particles themselves but also the setup. Factors such as orifice geometry (size and shape), geometry of the container used (eg. funnel, hopper, cylinder *etc.*), as well as the material it is constructed of need to be considered. This being the case, there are two main ways in which flow through an orifice experiment can be conducted. The first is utilising a standardized setup. For instance, the United States Pharmacopeia (USP38-NF33 Chapter 1174) [69] recommends a flat bottom cylindrical shaped container with a circular orifice with a diameter at least six times greater than the particle diameter while the diameter of the cylinder is at least twice the diameter of the orifice. The second way is to use a setup which closely simulates the real-world application where the powder flow will occur. For example, if a tablet blend is to be dispensed from a stainless steel hopper into a tablet feed mechanism, it may be useful to conduct the flow through an orifice experiment with a hopper constructed of the same material as the processing equipment and with similar geometries [54, 69]. The data provided from such a setup can be quite useful as the flow rate of the powder through a specific diameter orifice may be a useful guide for various processes, for instance, filling a specific capsule size or producing specific tablet sizes at a specified rate [54].

Due to the dependency on the setup of powder flow through an orifice, comparisons between different setups can be difficult [69, 90]. Additionally, the use of this method, like the angle of repose, does not take the consolidation effect on powder flow into consideration and is also limited to relatively free-flowing powders [69] despite there

being a range of setups such as the use of vibrating hoppers to aid in the flow of cohesive powders [98]. When gravity is the force inducing flow, measurements of flow rate can be considered examples direct measurements of unconfined gravitational flow. The advantages of the flow through an orifice method includes it being a simple and quick method to assess powder flow. Limitations of this method include it not being suitable for highly cohesive powders and the effect of consolidation on powder flow cannot be accounted for [101].

To aid in continuously measuring the flow of cohesive powders directly, a Finnish group, Intelligent Pharmaceuticals Oy, recently released the FlowPro (Intelligent Pharmaceuticals Oy, Finland). It consists of an inbuilt analytical balance interfaced to a computer for data acquisition and a motor to vertically tap a flat bottomed cylindrical stainless steel cuvette with a circular orifice diameter of 3.0 mm. The vertical tapping is believed to provide sufficient energy to break the cohesive inter-particle interactions of the cohesive powder and thus promote the flow of the powder [102]. What distinguishes the FlowPro from other related instruments is that it is possible to measure the flow of poor flowing cohesive powders with only a small amount of powder [102-105]. This is helpful in scenarios where only small amounts of sample are available.

With the availability of hoppers with various sized apertures, the determination of the critical orifice diameter—the minimum orifice diameter required for satisfactory powder flow through the orifice—can be measured. Such apparatus, for example the Flodex™ by Hanson Research Corp., USA, consist of a container with interchangeable bases with a hole in the centre of various sizes [106]. Unlike the flow through an orifice method, the critical orifice diameter is not a direct measure of powder flow; rather it is a measure of the cohesive and adhesive forces of the bulk powder and the ability of the powder to form an arch. That is, the minimum orifice diameter is a direct measure of the overall attractive forces found in the bulk powder [26, 54, 107].

1.8.5. Powder Rheometer

A number of dynamic systems claim to measure the apparent “rheological” properties of powders. These increasingly popular systems are known as “powder rheometers”. Since their introduction, the concept of measuring the rheological properties of powders has gained much interest [108-112]. Rheological measurements on powders were conducted as early as the mid-1900s on fluidised powder systems [113-116]. These measurements were performed on fluidised powder systems so that the powder was more likely to behave with fluid-like properties where a “resistance to flow” exists [117]. This “resistance to flow” is the result of inter-particle interactions and resembles the concept of viscosity when describing the rheology of liquids [113-116].

This measured “resistance to flow” was extended to powders in the condensed state (non-fluidized powders) [118]. Here, Cole [118], used a propeller-shaped stirrer blade to measure the cohesiveness of powders by measuring the resistance of the powder bed to the rotating blade. Automated commercial powder rheometers such as the Powder Flow Analyser by Stable Micro Systems, UK and the FT4 Powder Rheometer® by Freeman Technology, UK are now available. Such instruments essentially consist of a vessel and a propeller type blade attached to a motor which is capable of rotating the blade in either direction (clockwise or counter-clockwise) whilst also lowering or raising the blade—all movements at a controlled rate.

In the example of the FT4 Powder Rheometer®, a helical blade is used. The instrument continuously measures the required torque to rotate the blade at a constant rate as the blade is moved through the powder either in the downward or upward direction. In general, the more cohesive the powder, the more torque is required to continuously rotate the blade at a constant rate through the powder. This is because cohesive powders contain stronger inter-particle interactions between adjacent particles; ergo, the powder provides more resistance to flow. The opposite is true for free-flowing powders. That is, free-flowing powders have weaker inter-particles forces between adjacent particles and thus require less torque to cause the powder to flow.

Rotating the blade in either the downward and upward direction allows the instrument to measure the behaviour of the powder flowing in a confined space or an unconfined space. In the downward direction, the rotating blade has a bulldozing-like effect on the powder, pushing it downwards into a confined space, thereby consolidating the powder. As it does so, it is expected that the work required to rotate the blade at a constant rate will increase. This required work is referred to as the “basic flowability energy” (BFE) [119] and can be considered an example of indirect measurements of confined mechanical flow. Conversely, in the upward direction, the rotating blade lifts the powder into an open space; therefore, it is expected that the work required to rotate the blade at a constant rate reduces. This is referred to as the “specific energy” (SE) [119] and can be considered an example of indirect measurements of unconfined mechanical flow. Additionally, as the powder is being lifted upwards, there is a resulting effect on the powder bed, an aeration effect, which acts to condition the powder to remove previous powder history and consolidation [119]. These two tests together measure powder flow in a dynamic manner.

One of the advantages claimed for the FT4 system is the automated pre-conditioning of the sample prior to testing [119] in which the movement and vessel design allows for the reproducible formation of a powder bed. As the pre-conditioning stage of the measurement is intended to remove sample history and to allow for uniform packing and consolidation of the sample powder, a significant source of variability is reported to be eliminated [119].

In attempts to address the complexity of powders and their flow behaviours [119, 120], powder rheometer systems can be supplied with a wide variety of different attachments intended to support a variety of measurements designed to probe the different aspects of powder flow. For example, if one is interested in the stability of powder flow when the powder is continuously made to flow, the rheometer is capable of repeatedly testing the sample powder during a number of test cycles [119]. This may be of interest, for instance, from a quality control perspective where there may be difficulty in producing acceptable quality products. Tests also include quantitative investigation of the compressibility and air permeability of the sample powder.

The advantage of such instruments is they are capable of dynamically measuring a range of bulk powder flow behaviours in a repeated and continuous fashion. The limitation of such instruments is their lack of standardisation and thus difficulties may arise when comparing differing powders unless all measurements were conducted on the same instrument using the same method. Additionally, a common criticism of powder rheometers, in general, is the empirical nature of the measurements [121]. That is, the stresses applied to powders during measurements are not defined and are poorly understood and so a range of measurements are performed empirically [121]. Although, it should be noted that attempts to understand the stress fields of loosely packed powders when agitated by a rotating blade are ongoing [122-124] and these may provide valuable insights into the dynamic measurements that are performed by powder rheometers.

Nonetheless, it appears that powder rheometers are filling a growing need to measure the bulk properties of powders in a dynamic manner and so can be an invaluable instrument to powder technologists and scientists alike.

1.8.6. Shear Cells

Jenike recognised the importance of the consolidation effect on powder flow and also the lack of flow measurements that took such considerations into account. To remedy this, Jenike in 1961 [27, 125] developed a translational shear cell (now known as the Jenike shear cell) to characterise the mechanical properties of powder flow from a consolidated state. The shear cell essentially consists of three main parts: a stationary well which forms the base of the shear cell, a shear ring which sits directly above the base to complete a split cell system and the last component is a lid upon which carrier weights can be loaded to produce a known normal stress, as depicted in Figure 1-9. This forms the benchmark for all other shear testers [126].

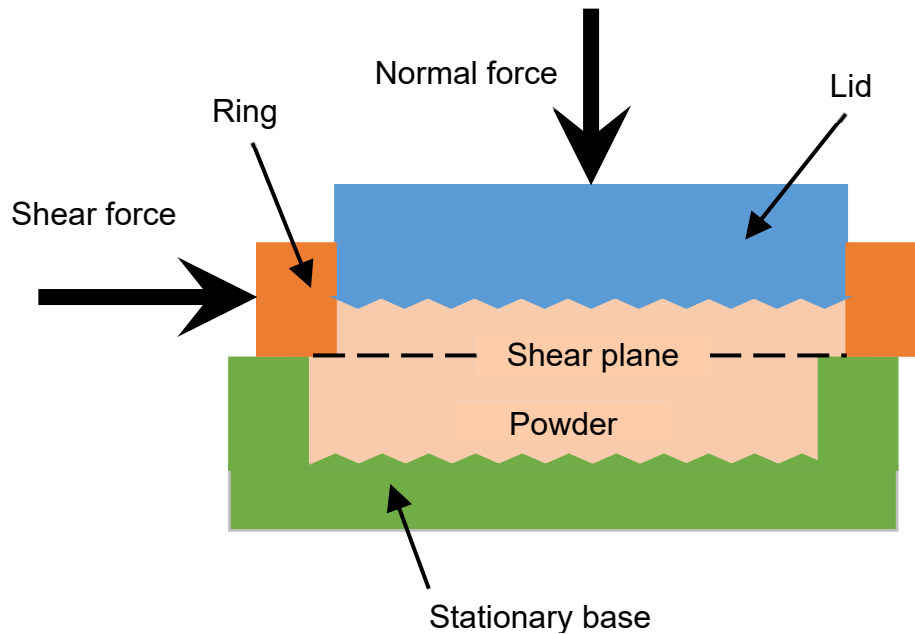


Figure 1-9: Translational shear cell.

The base with the shear ring is filled with the test powder and the lid is put in place. A known weight is added to the lid to consolidate the test powder. The minimum force required to translate the upper portion of the shear cell horizontally is recorded. The experiment is then repeated for a number of different normal stresses. Unfortunately, such translational shear cells are generally challenging and labour-intensive to operate and require a large amount of sample as fresh sample must be used for each measurement [107].

Over the years there have been a number of different shear cells developed such as the annular shear cell, ring shear cell, uniaxial, biaxial and triaxial testers [127-132], all of which work on the same principle. For a comprehensive description of such testers, the reader is invited to read Schwedes, 2003 [133]. Only the rotational type shear testers will be covered in this chapter.

Some rotational type shear testers such as the annular shear cell, for example the Schulze ring shear tester, the Powder Flow Tester by Brookfield Engineering, USA or the FT4 Powder Rheometer® by Freeman Technology, UK with a shear head attachment are reported to be easier to operate than translational shear cells. The principal advantage of the rotational shear testers over the translational shear testers

is that the shear displacement is not limited by the apparatus (as the displacement is in a circular path) [132, 134]. Consequently, the need for fresh sample is greatly reduced as all shear tests at each normal stress can be performed on the one sample. These testers work by measuring the amount of torque required to shear the powder for a given set of normal stresses to give a complete yield locus on a normal stress versus shear stress plot (see Figure 1-10) [131, 132]. From this plot, parameters to quantify powder flow (flow function, cohesion coefficient and angle of internal friction) can be determined, refer to Figure 1-10 [134, 135].

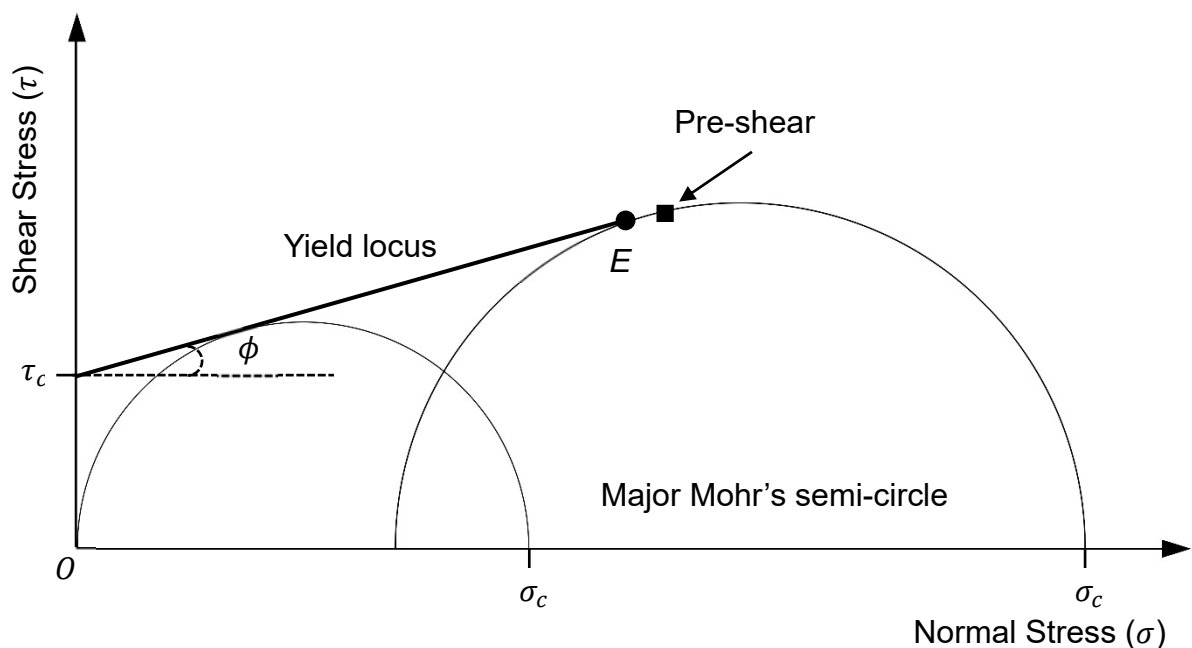


Figure 1-10: Typical normal stress versus shear stress plot of a cohesive powder showing the definition of failure properties. O is the origin, τ_c is the cohesion, ϕ is the angle of internal friction, σ_c is the unconfined yield strength, σ_1 is the major principal stress and point E is the end-point of the yield locus. Adapted from Thomson, 1997 [136].

The flow function, ff_c , is defined as the ratio of the major principal stress, σ_1 , to the unconfined yield strength, σ_c , refer to Equation (1.8).

$$ff_c = \frac{\sigma_1}{\sigma_c} \quad (1.8)$$

The flow function can be used as a measure of powder flowability where larger values corresponds to easier flowing powders with the general guide as follows: $ff_c < 1$ = non-flowing, $1 < ff_c < 2$ = very cohesive, $2 < ff_c < 4$ = cohesive, $4 < ff_c < 10$ = easy flowing and $ff_c > 10$ = free flowing [14, 27, 137, 138]. The cohesion coefficient, τ_c , sometimes referred to as the cohesion, is the shear stress intercept (τ -axis) of the yield locus. As the cohesion coefficient is the intercept of the τ -axis of a σ, τ plot, that is $\sigma = 0$, the cohesion coefficient can be thought of as the minimum amount of shearing stress required to cause a powder to flow in a hypothetical zero consolidating stress environment. A larger cohesion coefficient would represent a poorer flowing powder and vice versa [136]. The angle of internal friction (AIF), ϕ , Figure 1-10 is the angle of the yield locus to the horizontal and represents the strength of the inter-particle interactions of the powder under consolidation [134, 139]. For poorer flowing powders, the angle of internal friction tends to be higher [135, 136]. Parameters derived from shear cell testing can be considered as examples of indirect measurements of consolidated flow as pre-shearing is performed prior to each shear measurement.

An advantage of recent shear tester designs [140-143] is that the shear testing stage and the pre-shearing stage can be automated. This may help in reducing the overall time needed to perform an experiment. However, criticisms of rotational type shear testers are that, in general, a relatively large amount of sample is still required and due to the high dependency of powder flow on the state of consolidation/aeration of the powder and the fact that moderate to large consolidating pressures are used, the bulk performance of the sample may have been altered. Consequently, samples that have undergone shear testing are not recommended to be re-used. Additionally, there is a realistic lower limit to how little consolidation shear testers can apply during shear testing [144, 145]. In the ideal case, the lower limit of the shear cell would go down to 0 Pa so that an accurate cohesion value, for example, can be determined. Furthermore, at low consolidation shear testing, results may be prone to higher degrees of errors [144].

Nevertheless, despite the complexity of the theory or the shear testers themselves, users should not avoid such a test because shear cells provide valuable data on the

properties of a powder, specifically shear cell measurements provide information on the flow of powders under the effects of consolidation. With these data, specifically designed equipment such as hoppers and silos is possible; thus, these tests are said to be far more useful and informative to engineers for real world applications than tests such as angle of repose [27].

1.9. Improving the Flow of Powders

The poor flow of fine powders can often present significant challenges to optimal pharmaceutical manufacturing, thus leading to economic loss [2, 3, 7, 8]. To alleviate some of the complications faced with working with cohesive fine powders, a number of strategies to improve the flow of powders have been developed.

A widely used method to improve flow is through size enlargement such as granulation, especially in the case of low-dose oral solid dosage forms [146]. Granulation is a process where small particles are formed into substantially larger masses (granules) whilst keeping the initial particles identifiable [147]. As the particles are formed into substantially larger masses, the flow promoting force is substantially increased. Therefore, the flow of the bulk material is improved making it easier to handle [100, 148, 149]. Although effective in improving flowability, granulation can be a complex multistep process that can be time consuming and costly, especially wet granulation [150-152]. Alternatively, formulation strategies where cohesive fine powders are blended with excipients such as lubricants or flow aids, for instance, magnesium stearate (MgSt) and fumed silica, have been shown to be effective in improving the flow of fine powders [97, 100, 153-155]. However, for highly cohesive powders, blending may not be effective in improving flow as the blending process may not be sufficiently energetic to overcome the relatively strong inter-particle interactions. Therefore, blending may not effectively mix the excipients with the fine powder [12].

1.9.1. Surface Modification

An alternate route to improve the flow of fine powders is through particle engineering. As explained above, the surfaces of fine powders are intimately linked to the flow behaviour of fine powders [29], therefore, modification of the surfaces appears to be a logical approach to improve flowability. Solvent based coating methods such as spray drying, fluid bed coating or pan coating are commonly used to modify the surfaces of powders [156-159]. However, as these methods are typically time consuming and costly (due to the need for a drying step) and may also require the use of organic solvents that could be harmful to the environment, solvent based coating may not always be suitable [159, 160].

1.9.1.1. Intensive Mechanical Dry Coating

In contrast to solvent based surface modification, dry coating offers the ability to modify the surfaces of powders without the use of liquids. There are various systems available to modify the surfaces of powders via dry coating such as the mechanofusion system (Hosokawa Micron Powder Systems, Japan), the Nara Hybridization System (NHS) (Nara Machinery Co., Ltd., Japan), the Magnetically Assisted Impact Coater (MAIC) (Aveka, Inc., USA) and the theta composer (Tokuju Corp., Japan) as well as processes that subject powders to high stresses, such as co-milling and high shear blending [159-162]. The dry coating method that is of particular interest to this study is the mechanofusion system as it offers the ability to modify the surfaces of powders without significantly affecting other aspects of the powder, for instance particle size and size distribution which may otherwise alter the flow of the powder [10, 14, 163].

Surface modification through mechanofusion (dry coating) is achieved by subjecting both a host powder (powder of interest) and a guest powder (surface modifier) to high shear and compaction stresses [14, 164]. Guest powders are typically smaller and/or softer than the host powder. The high stresses can be sufficiently energetic to deagglomerate both the host and guest powders as well as delaminate, smear and/or spread the softer guest powders such as MgSt on the host particles [14, 15, 165, 166]. In doing so, mechanofusion is able to coat host particles with guest particle, see Figure 1-11, more effectively than processes such as traditional blending, thereby enabling a greater portion of the host particles to be coated [12].

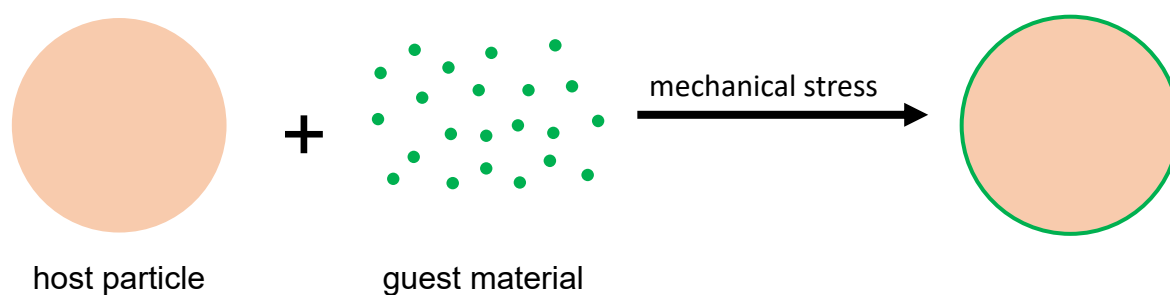


Figure 1-11: Schematic of dry coating a host powder with a guest powder to coat the host particles with the guest powder.

The flow of cohesive fine powders has been shown to improve after dry coating [9-13]. For instance, dry coating 20 μm α -lactose with 1% w/w MgSt was effective in improving the flow of the lactose, while the flow of 7 μm salbutamol sulphate was improved after dry coating with 5% w/w MgSt and the flow of 43 μm ibuprofen was also observed to have improved after dry coating with 1% w/w MgSt [14-16].

The improvement in the flow of fine powders dry coated with MgSt has largely been attributed to the very thin MgSt coating altering the surface energy of the powder [157, 166-169]. Indeed, as discussed in Chapter 1: Section 1.5.1.1, a reduction in the surface energy is likely to result in lowering the pull-off force required to break the cohesive contacts between contacting particles, thereby enhancing powder flow. However, other mechanisms may also contribute to the improved flow of MgSt coated powders. For instance, the hydrophobicity of the host powder may increase. Consequently, as discussed in Chapter 1: Section 1.5.2, the magnitude of the capillary force could decrease, thus lowering the magnitude of the inter-particle interaction. Overall, the mechanisms of how surface coatings such as MgSt alter the flow of surface modified powders remain relatively poorly understood and deserve further investigation.

1.10. Surface Property Measurements

As discussed in Chapter 1: Section 1.5, both surface energy and wettability (or hydrophilicity/hydrophobicity when referring to water) can affect the magnitude of inter-particle interactions. The wettability of powders is characterised by the contact angle liquid makes on the surfaces of the particles. A poorly wettable (or hydrophobic) surface is characterised by a large contact angle.

1.10.1. Wettability Measurement

1.10.1.1. Liquid Intrusion

The liquid intrusion method is commonly used to measure the wettability of powders. The method takes advantage of the natural intrusion of a liquid into a bed of a powder, provided that the liquid makes a contact angle less than 90°. The principal attraction

of this method is that the powder does not require modifying, it remains in its bulk powder form as opposed to being compressed to form compacts or adhered to a scaffold with adhesives. In addition, especially with the introduction of automated instruments, the liquid intrusion method is relatively quick and simple to perform.

Collectively, voids within powder beds act as small capillaries that liquids can intrude. The intrusion rate of liquids into powder beds is related to the contact angle of the liquid as described by Washburn in 1921 [170].

$$l^2 = \frac{r_c \gamma_L \cos \theta}{2\eta} t \quad (1.9)$$

where l is the intruded distance of the liquid front at time, t ; γ_L is the surface tension of the liquid, r_c is the effective capillary radius of the powder bed, θ is the contact angle of the liquid and η is the viscosity of the liquid.

However, due to difficulties in accurately visualising the liquid front as the experiment progresses, it is often more convenient to measure the mass of the intruded liquid rather than the intruded distance. For a cylindrical powder bed, the relationship between the mass of the intruded liquid and the distance of the liquid is given by [171]:

$$m = \pi R_c^2 l \rho \varepsilon \quad (1.10)$$

where m is the mass of the intruded liquid, R_c is the internal radius of the cylindrical column, ρ is the density of the liquid and ε is the porosity of the powder bed.

Substituting Equation (1.10) into Equation (1.9) gives the “modified” Washburn equation:

$$m^2 = \frac{C\rho^2\gamma_L \cos \theta}{\eta} t \quad (1.11)$$

where $C = \frac{r_c}{2} (\pi R_c^2 \varepsilon)^2$ and is termed the *material constant*. This parameter reflects the packing geometry of the particles in the powder bed. As can be noted, a plot of mass squared versus time would result in a straight line. The gradient of this line can be used to determine the contact angle of the liquid.

However, as there are two unknown variables in Equation (1.11)—the material constant, C , and the contact angle, θ —the contact angle of the liquid cannot be determined directly with one liquid only. Consequently, another liquid must be used to determine the material constant. This is achieved by using a perfectly wetting liquid, which means having a contact angle of 0° to the powder, to act as the reference liquid, indicated by subscript r . Thus, Equation (1.11) can be reduced to:

$$\frac{m_r^2}{t_r} = \frac{C_r \rho_r^2 \gamma_{Lr}}{\eta_r} \quad (1.11a)$$

where $\cos \theta_r = 1$ as $\theta_r = 0^\circ$.

For a probe liquid, indicated by subscript p , it follows that:

$$\frac{m_p^2}{t_p} = \frac{C_p \rho_p^2 \gamma_{Lp} \cos \theta_p}{\eta_p} \quad (1.11b)$$

As liquid intrusion experiments require the powder bed to be completely wetted by the liquid, powder beds can only be used once. Therefore, additional powder beds must be prepared for each liquid. If the powder beds consist of the same powder material and are prepared by a standardised packing procedure, it is usually assumed that the material constants of the powder beds are identical—that is, $C_p = C_r$ [172-177]. Therefore, substituting Equation (1.11a) into Equation (1.11b) gives:

$$\cos \theta_p = \frac{\rho_r^2 \gamma_{Lr} \eta_p}{\rho_p^2 \gamma_{Lp} \eta_r} \cdot \frac{m_p^2 t_r}{m_r^2 t_p} \quad (1.12)$$

which can be simplified to the following equation:

$$\cos \theta_p = F_l \cdot \frac{\text{Gradient}_p}{\text{Gradient}_r} \quad (1.13)$$

where $F_l = \frac{\rho_r^2 \gamma_{Lr} \eta_p}{\rho_p^2 \gamma_p \eta_r}$ and is termed the *liquid factor*.

Also, as powders must come in contact with the probe and reference liquids during liquid intrusion experiments, powders may potentially dissolve, thereby altering the surfaces of the constituting particles (even if only a small amount of the powder dissolves). Consequently, the liquid intrusion method is only suitable for powders that do not dissolve in both the probe and reference liquids.

1.11. Surface Energy Measurements

As discussed earlier (Chapter 1: Section 1.5.1.1), the surface energy of powders affects the adhesive/cohesive forces that exist between two surfaces. Consequently, the ability to measure the surface energy of pharmaceutical powders is of great interest. Here, two methods are discussed on how this can be achieved: the contact angle method and inverse gas chromatography (IGC).

1.11.1. Contact Angles

The contact angle of liquids is governed, in part, by the surface energy of the solid, as described by Young's equation [178, 179]. Thus, a selection of liquids can be used to probe powders to determine their surface energies. To determine the dispersive component, a completely apolar liquid should be used, while polar liquids need to be used to determine the polar component. With the contact angles of these different liquids known, the surface energy can be determined through one of the following methods:

1.11.1.1. Zisman's Method: the Critical Surface Tension

Fox and Zisman introduced the concept of the critical surface tension, γ_c , for wetting of solids, where liquids with surface tensions greater than γ_c will not wet the solid surface [180]. By determining the contact angle of a range of liquids on the solid sample surface, Zisman and co-workers showed that a plot of $\cos \theta$ vs. γ_L fell close to a linear line or within a narrow rectangular band [181]. The corresponding γ_L value that intercepts the $\cos \theta = 1$ line is noted as the critical surface tension [181]. However, Zisman cautioned the use of critical surface tensions as a measure of surface energies as γ_c is only an empirical value [180]. Nevertheless, γ_c provides useful information regarding the wetting of liquids and the energetics of solids [181].

Although Zisman's method appears to be relatively simple and straight forward, this method is better suited for non-polar liquids wetting low-energy solids [180, 182, 183]. The critical surface tension only describes the dispersive component of the surface energy of a solid surface [184].

1.11.1.2. Fowkes' Method

In 1964, Fowkes [37] used the geometric mean method, first proposed by Girifalco and Good [45], to split the different components of the interfacial tension between two surfaces and proposed the following equation:

$$\gamma_{SL} = \gamma_S + \gamma_L - 2\sqrt{\gamma_S^D \gamma_L^D} \quad (1.14)$$

By substituting Young's equation into Equation (1.14), the following equation is known as the Young-Fowkes equation:

$$\cos \theta = -1 + 2\sqrt{\gamma_S^D} \left(\sqrt{\frac{\gamma_L^D}{\gamma_L}} \right) \quad (1.15)$$

The dispersive component of the surface energy, γ_S^D , can then be calculated through the transposition of Equation (1.15). As can be seen, the use of the Young-Fowkes equation also only applies to systems where only non-polar interactions occur. It should be stated that the Fowkes method is better suited for high surface tension liquids on low-energy solids such as polymers [37].

1.11.1.3. Owens-Wendt: the Two Components Method

Following on from Fowkes, Owens and Wendt [46] added a polar component to give the following Owens-Wendt equation:

$$1 + \cos \theta = 2\sqrt{\gamma_S^D} \left(\sqrt{\frac{\gamma_L^D}{\gamma_L}} \right) + 2\sqrt{\gamma_S^P} \left(\sqrt{\frac{\gamma_L^P}{\gamma_L}} \right) \quad (1.16)$$

In order to determine the dispersive component, γ_S^D , and the polar component, γ_S^P , of the surface energy, two probe liquids with known dispersive and polar surface tensions, that is, known values for γ_L^D and γ_L^P , must be used. The values of γ_S^D and γ_S^P can then be determined. The total surface energy, γ_S^T , is then found through the summation of γ_S^D and γ_S^P .

1.11.1.4. Wu's Harmonic Mean Method

In 1971, Wu proposed an alternative method for determining the surface energy of surfaces [185]. Instead of utilising the geometric mean approach originally proposed by Girifalco and Good [45], Wu utilised a harmonic mean approach to give the following equation:

$$\gamma_L(1 + \cos \theta) = \frac{4\gamma_S^D\gamma_L^D}{\gamma_S^D + \gamma_L^D} + \frac{4\gamma_S^P\gamma_L^P}{\gamma_S^P + \gamma_L^P} \quad (1.17)$$

It should be noted that in Wu's method two possible values can be obtained for γ_S^D and γ_S^P . Determining which of the two values is the real surface energy can often be difficult

but may simply involve logical thinking, especially if a negative number is obtained [186].

1.11.1.5. Good-van Oss: the Three Components Method

The approach that Good, van Oss and Chaudhury took is to split surface energy into three components—a dispersive interaction, γ^D , an acidic interaction, γ_S^+ , and a basic interaction, γ_S^- [44, 187-189]. These acid-base interactions are otherwise referred to as “polar” or “specific” interactions [61, 173, 190-192]. The authors proposed the following which is known as the Good-van Oss equation:

$$\gamma_L(1 + \cos \theta) = 2 \left(\sqrt{\gamma_S^D \gamma_L^D} + \sqrt{\gamma_S^+ \gamma_L^-} + \sqrt{\gamma_S^- \gamma_L^+} \right) \quad (1.18)$$

where, γ_S^+ and γ_S^- are the Lewis acid and Lewis base parameters of surface energy, respectively, while γ_L^+ and γ_L^- are the Lewis acid and Lewis base parameters of surface tension, respectively.

In order to determine the values of γ_S^D , γ_S^+ and γ_S^- , three probe liquids with known γ_L^D , γ_L^- and γ_L^+ must be used. This forms three equations which can be solved simultaneously to determine the surface energy of the sample where the specific energy, γ^P , of the sample is determined with the following equation [44]:

$$\gamma_S^P = 2\sqrt{\gamma_S^+ \gamma_S^-} \quad (1.19)$$

The total surface energy, γ_S^T , can then be calculated by the summation of γ_S^D and γ_S^P .

1.11.2. Inverse Gas Chromatography

In the late 1960's, the development of a chromatographic method provided material scientists with the ability to measure the surface energy of solids [193]. This method is known as inverse gas chromatography (IGC). Similar to conventional gas chromatography (GC), IGC employs a stationary phase and a mobile phase. However,

in IGC, the stationary phase of an IGC is the sample of interest such as a powder, while the mobile phase comprises a series of known vapour probes [194, 195].

IGC can be performed under infinite dilution conditions, or “zero surface coverage”, where very small amounts of vapour probes are introduced to the stationary phase. Hence, Henry’s Law is obeyed and the so-called probe-probe interactions are considered to be negligible, thereby leaving only the probe-sample interactions present [195, 196]. Vapour probes introduced to the stationary phase will predominantly interact with certain sites on the surface of the sample. That is, dispersive probes, such as *n*-alkanes, predominantly interact with non-polar sites on the surface through dispersive interactions. Lewis acid and Lewis base vapour probes predominantly interact with basic and acidic sites on the surface, respectively, predominantly through specific interactions (electron-acceptor/donor interactions) and, to a lesser extent, through dispersive interactions as these interactions are innate [43].

The affinity of the vapour probes to these sites determines the retention volume of the probe (the volume of mobile phase required to elute the probe through the stationary phase). The net retention volume (the retention volume minus the hold-up volume), V_N , of the dispersive probe is related to the free energy of desorption and adsorption, and the dispersive energy component of the total surface energy by [197]:

$$\Delta G_D^0 = -\Delta G_A^0 = RT \ln V_N + C = 2N_A \sqrt{\gamma_S^D} a \sqrt{\gamma_L^D} + K \quad (1.20)$$

where ΔG_D^0 and ΔG_A^0 are the free energy of desorption and adsorption, respectively, R is the ideal gas constant, T is the temperature in Kelvin, a is the cross-sectional area of the vapour probe molecule, N_A is Avogadro's number, γ_S^D is the dispersive energy component of the solid, γ_L^D is the dispersive energy component of the probe in the liquid state and K is a constant

If a plot of $RT \ln V_N$ versus $a\sqrt{\gamma_L^D}$ is constructed for the dispersive probes, the n -alkanes, a straight line is obtained, termed the alkane line (see Figure 1-12). From this, the slope of the alkane line can be used to determine γ_S^D :

$$\gamma_S^D = \left(\frac{\text{slope}}{2N_A}\right)^2 \quad (1.21)$$

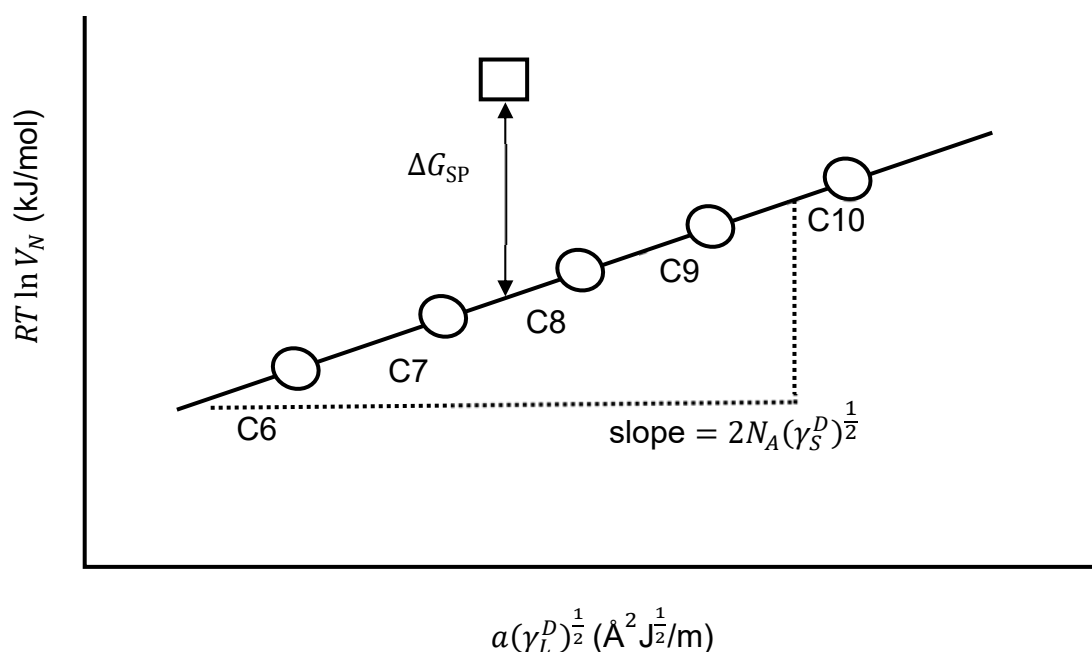


Figure 1-12: Typical plot of $RT \ln V_N$ vs. $a(\gamma_L^D)^{\frac{1}{2}}$ where data from the dispersive probes (\circ) falls within a straight line, while data from specific probes (\square) lies above the alkane line. Image adapted from [197].

Because polar probes interact with both specific and dispersive interactions and the two interactions are additive, data from these probes will lie above the alkane line (see Figure 1-12) [44, 197]. The difference of ordinates between the alkane line and the data point corresponding to the given polar probe is known as the specific free energy, ΔG_{SP} , and is given by the left hand side of Equation (1.22) [197]. This value provides a measure of the strength of the interaction between the specific probe and the surface of the sample. However, the specific free energy is in units of energy per mole (kJ/mol), while the dispersive energy component, γ_S^D , is in units of energy per square meter

(mJ/m²). This not only makes it difficult to directly compare the two quantities but it is also difficult to obtain the overall surface energy of the surface. In order to rectify this, harmonization of the units is achieved through the use of Avogadro's number and the cross-sectional area of the vapour probe molecule. The specific free energy is related to the polar components of the surface energy by the equation proposed by Good-van Oss [188] (right hand side of Equation (1.22)):

$$RT \ln \frac{V_N}{V_N^{ref}} = \Delta G_{SP} = 2a N_A [\sqrt{\gamma_L^+ \gamma_S^-} + \sqrt{\gamma_L^- \gamma_S^+}] \quad (1.22)$$

where V_N^{ref} is the retention volume corresponding to a dispersive probe, γ_L^+ is the electron-acceptor parameter of the acidic probe molecule, γ_S^- is the electron-donor parameter (basic site) of the solid's surface, γ_L^- is the electron-donor parameter of the basic probe molecule and γ_S^+ is the electron-acceptor parameter (acidic site) of the solid's surface

In order to determine the values of γ_S^+ and γ_S^- for the sample material, it is necessary to utilise a Lewis base and a Lewis acid with known values of γ_L^- and γ_L^+ for each probe. The polar component of the surface energy, γ_S^P , can then be calculated with Equation (1.19).

However, criticism of infinite dilution measurements arises from the fact that only very low concentrations of the vapour probes are used [198]. Therefore, according to gas adsorption theories [199, 200], the frequency of occupancy of vapour probes are much more prevalent on higher energy sites than sites with lower surface energies. That is, only the highest surface energy sites are probed, which is estimated to be less than 0.1% of the total surface [201]. The disadvantage of measurements at infinite dilution is obvious, they are unlikely to provide a complete representation of the entire energetics of the total surface of the sample.

Alternatively, IGC can also be performed under finite concentration conditions where higher amounts of probe vapour are introduced to the stationary phase. By doing so, a larger portion of the surface may be probed, thus allowing for a distribution of surface

energies to be measured [198, 202]. Although IGC at finite concentration may provide more information about the distribution of the surface energies of the sample, it is, however, less well defined as the probe-probe interactions may become increasingly prominent at higher probe concentrations.

1.12. Thesis Statement

Dry coating, such as mechanofusion, is an attractive approach to improve the flow of fine powders by altering the surfaces of the powders. Although dry coating fine powders with MgSt via mechanofusion has been shown to be effective in improving the flow of fine powders, the mechanism of how flow is improved remains relatively poorly understood. The improvement has largely been attributed to the MgSt coating decreasing the surface energy of the powder, thereby lowering the pull-off force to break the cohesive contacts. However, as the powders are now coated with a hydrophobic material, the contact angle of water to the surface modified powders may have also increased. With larger contact angles, the magnitude of capillary forces within the powders are expected to decrease, which may contribute to the improvement in the flow of the fine powders. To date, there has been little research exploring the influence of the MgSt coating on the hydrophobicity of MgSt coated powders and its contribution to the improved flow of the powders. This thesis aims to provide further insights into the mechanisms involved in the improvement of powder flow as a result of dry coating cohesive fine powders with the pharmaceutical lubricant MgSt.

1.13. Aims and Objectives

1. To modify the surfaces of a fine powder with magnesium stearate through mechanofusion.
2. To measure the flowability of the fine powder as well as the surface modified powder.
3. To measure the surface energy of the fine powder as well as the surface modified powder.

4. To measure the surface hydrophobicity of the fine powder as well as the surface modified powder.
5. To evaluate the relationship of the surface energy and hydrophobicity of the powders to the flowability of the powders.

1.14. References

- [1] Knowlton TM, Carson JW, Klinzing GE, Yang WC, The importance of storage, transfer and collection, *Chem Eng Prog.* 90(1994) 44-54.
- [2] Pietsch WB, Adhesion and agglomeration of solids during storage, flow and handling - A survey, *J Eng Ind.* 91(1969) 435-49.
- [3] Prescott JK, Barnum RA, On powder flowability, *Pharm Technol.* 24(2000) 60.
- [4] Armstrong NA, Tablet manufacture, *Encyclopedia of pharmaceutical technology*, 3rd ed., Informa Healthcare, NY, USA, 2007, 3653-71.
- [5] Yaginuma Y, Ozeki Y, Kakizawa M, Gomi SI, Watanabe Y, Effects of powder flowability on die-fill properties in rotary compression, *J Drug Deliv Sci Technol.* 17(2007) 205-10.
- [6] Juliano P, Barbosa-Canovas GV, Food powders flowability characterization: Theory, methods and applications, *Annu Rev Food Sci Technol*, Annual Reviews, CA, USA, 2010, 211-39.
- [7] Baxter T, Barnum R, Prescott JK, Flow: General principles of bulk solids handling, in: Augsburger LL, Hoag SW (Eds.), *Pharmaceutical dosage forms - Tablets: Unit operations and mechanical properties*, 3rd ed., Informa Healthcare, NY, USA, 2008, 75-110.
- [8] Ganesan V, Rosentrater KA, Muthukumarappan K, Flowability and handling characteristics of bulk solids and powders – a review with implications for DDGS, *Biosystems Engineering.* 101(2008) 425-35.
- [9] Zhou Q, Qu L, Larson I, Stewart PJ, Morton DAV, Effect of mechanical dry particle coating on the improvement of powder flowability for lactose monohydrate: A model cohesive pharmaceutical powder, *Powder Technol.* 207(2011) 414-21.
- [10] Zhou QT, Qu L, Larson I, Stewart PJ, Morton DAV, Improving aerosolization of drug powders by reducing powder intrinsic cohesion via a mechanical dry coating approach, *Int J Pharm.* 394(2010) 50-9.
- [11] Begat P, Morton D, Shur J, Kippax P, Staniforth J, Price R, The role of force control agents in high-dose dry powder inhaler formulations, *J Pharm Sci.* 98(2009) 2770-83.
- [12] Zhou Q, Qu L, Gengenbach T, Denman JA, Larson I, Stewart PJ, et al., Investigation of the extent of surface coating via mechanofusion with varying additive levels and the influences on bulk powder flow properties, *Int J Pharm.* 413(2011) 36-43.
- [13] Paw R, Goggin P, Bajwa G, Feasibility study to investigate the application of mechanofusion to improve flow properties of a cohesive API, *J Pharm Pharmacol.* 62(2010) 1435-6.
- [14] Zhou Q, Armstrong B, Larson I, Stewart PJ, Morton DAV, Improving powder flow properties of a cohesive lactose monohydrate powder by intensive mechanical dry coating, *J Pharm Sci.* 99(2010) 969-81.

- [15] Zhou QT, Qu L, Gengenbach T, Larson I, Stewart PJ, Morton DAV, Effect of surface coating with magnesium stearate via mechanical dry powder coating approach on the aerosol performance of micronized drug powders from dry powder inhalers, *AAPS PharmSciTech*. 14(2013) 38-44.
- [16] Qu L, Zhou Q, Gengenbach T, Denman JA, Stewart PJ, Hapgood KP, et al., Investigation of the potential for direct compaction of a fine ibuprofen powder dry-coated with magnesium stearate, *Drug Dev Ind Pharm*. 41(2015) 825-37.
- [17] Huang Z, Kunnath KT, Han X, Deng X, Chen L, Davé RN, Ultra-fine dispersible powders coated with L-Leucine via two-step co-milling, *Adv Powder Technol*. 29(2018) 2957-65.
- [18] Peleg M, Flowability of food powders and methods for its evaluation — A review, *J Food Process Eng*. 1(1977) 303-28.
- [19] Igwe GJI, Powder technology and multiphase systems: Gas permeametry and surface area measurement, Ellis Horwood, NY, USA, 1991.
- [20] Tomas J, Assessment of mechanical properties of cohesive particulate solids. Part 1: Particle contact constitutive model, *Particulate Science and Technology*. 19(2001) 95-110.
- [21] Molerus O, Effect of interparticle cohesive forces on the flow behaviour of powders, *Powder Technol*. 20(1978) 161-75.
- [22] Sutton H, Flow properties of powders and the role of surface character, in: Parfitt G, Sing K (Eds.), *Characterization of powder surfaces*, Academic Press, NY, USA, 1976, 107-58.
- [23] Tomas J, Fundamentals of cohesive powder consolidation and flow, *Granular matter*. 6(2004) 75-86.
- [24] Ashton MD, Cheng DCH, Farley R, Valentin FHH, Some investigations into the strength and flow properties of powders, *Rheologica Acta*. 4(1965) 206-18.
- [25] Molerus O, Theory of yield of cohesive powders, *Powder Technol*. 12(1975) 259-75.
- [26] Kruyt NP, Results of Jenike's (1987) radial stress field theory for the flow of granular materials in conical hoppers: Flow regimes and flow factors, *Powder Technol*. 76(1993) 109-12.
- [27] Jenike AW, *Storage and flow of solids*, University of Utah, Utah, USA, 1964.
- [28] Jenike AW, A theory of flow of particulate solids in converging and diverging channels based on a conical yield function, *Powder Technol*. 50(1987) 229-36.
- [29] Orband JLR, Geldart D, Direct measurement of powder cohesion using a torsional device, *Powder Technol*. 92(1997) 25-33.
- [30] Stewart PJ, Particle interaction in pharmaceutical systems, *Pharm Int*. 7(1986) 146-9.
- [31] Aulton ME, (Ed.) *Pharmaceutics: The science of dosage form design*. 2nd ed., Churchill Livingstone, Edinburgh, UK, 2002.
- [32] Keesom WH, On Waal's cohesion forces, *Phys Z*. 22(1921) 129-41.
- [33] Debye P, The van der Waals cohesion forces, *Phys Z*. 21(1920) 178-87.
- [34] London F, On the theory and systematic of molecular forces, *Z Phys*. 63(1930) 245-79.
- [35] Hamaker HC, The London--van der Waals attraction between spherical particles, *Physica*. 4(1937) 1058-72.
- [36] Butt H-J, Kappl M, *Van der Waals forces, Surface and interfacial forces*, Wiley-VCH, Weinheim, Germany, 2010, 5-53.

- [37] Fowkes FM, Attractive forces at interfaces, *Ind Eng Chem.* 56(1964) 40-52.
- [38] Johnson KL, Kendall K, Roberts AD, Surface energy and the contact of elastic solids, *Proc R Soc Lond A.* 324(1971) 301-13.
- [39] Derjaguin BV, Muller VM, Toporov YP, Effect of contact deformations on the adhesion of particles, *J Colloid Interface Sci.* 53(1975) 314-26.
- [40] Xu DW, Liechti KM, Ravi-Chandar K, On the modified Tabor parameter for the JKR-DMT transition in the presence of a liquid meniscus, *J Colloid Interface Sci.* 315(2007) 772-85.
- [41] Muller VM, Derjaguin BV, Toporov YP, On two methods of calculation of the force of sticking of an elastic sphere to a rigid plane, *Colloids Surf.* 7(1983) 251-9.
- [42] Fowkes FM, Determination of interfacial tensions, contact angles, and dispersion forces in surfaces by assuming additivity of intermolecular interactions in surfaces, *The Journal of Physical Chemistry.* 66(1962) 382-.
- [43] van Oss CJ, Acid—base interfacial interactions in aqueous media, *Colloids Surf, A.* 78(1993) 1-49.
- [44] van Oss CJ, Good RJ, Chaudhury MK, Additive and nonadditive surface tension components and the interpretation of contact angles, *Langmuir.* 4(1988) 884-91.
- [45] Girifalco LA, Good RJ, A theory for the estimation of surface and interfacial energies: 1. Derivation and application to interfacial tension, *J Phys Chem.* 61(1957) 904-9.
- [46] Owens DK, Wendt RC, Estimation of the surface free energy of polymers, *J Appl Polym Sci.* 13(1969) 1741-7.
- [47] Thomson W, On the equilibrium of vapour at a curved surface of liquid. *Proc R Soc Edinb;* 1870; Edinburgh, UK; 1870. p. 63-8.
- [48] Zimon AD, Adhesion of dust and powder, 2nd ed., Consultants Bureau, NY, USA, 1982.
- [49] Cross NL, Picknett RG, Particle adhesion in the presence of a liquid film. in: Johnson HR, Littler DJ, (Eds.), *The mechanism of corrosion by fuel impurities;* 1963; Marchwood, UK: Butterworths; 1963. p. 383-90.
- [50] Das S, Larson I, Young P, Stewart P, Influence of storage relative humidity on the dispersion of salmeterol xinafoate powders for inhalation, *J Pharm Sci.* 98(2009) 1015-27.
- [51] Staniforth JN, Rees JE, Electrostatic charge interactions in ordered powder mixes, *J Pharm Pharmacol.* 34(1982) 69-76.
- [52] Zeng XM, Martin G, Marriott C, Particulate interactions in dry powder formulations of inhalation, Taylor & Francis, NY, USA, 2000.
- [53] Podczeczek F, Mia Y, The influence of particle size and shape on the angle of internal friction and the flow factor of unlubricated and lubricated powders, *Int J Pharm.* 144(1996) 187-94.
- [54] Staniforth JN, Powder flow, in: Aulton ME (Ed.) *Pharmaceutics: The science of dosage form design,* 2nd ed., Churchill Livingstone, Edinburgh, UK, 2002, 197-211.
- [55] Hou H, Sun CC, Quantifying effects of particulate properties on powder flow properties using a ring shear tester, *J Pharm Sci.* 97(2008) 4030-9.
- [56] Liu L, Marziano I, Bentham A, Litster J, White E, Howes T, Effect of particle properties on the flowability of ibuprofen powders, *Int J Pharm.* 362(2008) 109-17.
- [57] Danish FQ, Parrott EL, Flow rates of solid particulate pharmaceuticals, *J Pharm Sci.* 60(1971) 548-54.

- [58] Israelachvili JN, Intermolecular and surface forces, 3rd ed., Academic Press, MA, USA, 2011.
- [59] Rietema K, The dynamics of fine powders, Elsevier Applied Science, London, UK, 1991.
- [60] Augenstein DA, Hogg R, An experimental study of the flow of dry powders over inclined surfaces, Powder Technol. 19(1978) 205-15.
- [61] Das S, Larson I, Young P, Stewart P, Understanding lactose behaviour during storage by monitoring surface energy change using inverse gas chromatography, Dairy Science & Technology. 90(2010) 271-85.
- [62] Newell HE, Buckton G, Butler DA, Thielmann F, Williams DR, The use of inverse phase gas chromatography to study the change of surface energy of amorphous lactose as a function of relative humidity and the processes of collapse and crystallisation, Int J Pharm. 217(2001) 45-56.
- [63] Butt H-J, Kappl M, Normal capillary forces, Adv Colloid Interface Sci. 146(2009) 48-60.
- [64] Iida K, Otsuka A, Danjo K, Sunada H, Measurement of adhesive force between particles and polymer films, Chem Pharm Bull. 40(1992) 189-92.
- [65] Homola AM, Israelachvili JN, Gee ML, McGuiggan PM, Measurements of and relation between the adhesion and friction of two surfaces separated by molecularly thin liquid films, J Tribology. 111(1989) 675-82.
- [66] Kim T-G, Yoo Y-S, Lee S-H, Park J-G, Effects of size, humidity, and aging on particle removal from Si wafers, Microelectron Eng. 86(2009) 145-9.
- [67] Xu Z, Mansour HM, Hickey AJ, Particle interactions in dry powder inhaler unit processes: A review, J Adhes Sci Technol. 25(2011) 451-82.
- [68] Hausner H, Friction conditions in a mass of metal powder, Int J Powder Metall. 3(1967) 7-13.
- [69] Powder flow, United States Pharmacopeia, US Pharmacopial Convention, MD, USA, 2015, 1326-30.
- [70] Carr RL, Evaluating flow properties of solids, Chem Eng. 72(1965) 163-8.
- [71] Bulk density and tapped density of powders, United States Pharmacopeia, US Pharmacopial Convention, MD, USA, 2015, 420-4.
- [72] Quantachrome Instruments, Tapped density analyzers. [internet] c2013-2015 2015 [cited 2015 Apr 19]; Available from: <http://www.quantachrome.com/density/autotap.html>
- [73] Copley Scientific, Tapped density. [internet] c2015 2015 [cited 2015 Apr 15]; Available from: <http://www.copleyscientific.com/home/pharmaceutical-testing/powder-testing/powder-density-testers/tapped-density>
- [74] Kulkarni PA, Berry RJ, Bradley MSA, Review of the flowability measuring techniques for powder metallurgy industry, Proc Inst Mech Eng Part E-J Process Mech Eng. 224(2010) 159-68.
- [75] Thalberg K, Lindholm D, Axelsson A, Comparison of different flowability tests for powders for inhalation, Powder Technol. 146(2004) 206-13.
- [76] Lee T, Hsu FB, A cross-performance relationship between Carr's index and dissolution rate constant: The study of acetaminophen batches, Drug Dev Ind Pharm. 33(2007) 1273-84.
- [77] Borini GB, Andrade TC, Freitas LAP, Hot melt granulation of coarse pharmaceutical powders in a spouted bed, Powder Technol. 189(2009) 520-7.

- [78] Hughes H, Leane M, Tobyn M, Gamble J, Munoz S, Musembi P, Development of a material sparing bulk density test comparable to a standard USP method for use in early development of API's, *AAPS PharmSciTech.* 16(2015) 165-70.
- [79] Bulk density and tapped density of powders, *United States Pharmacopeia, US Pharmacopial Convention, MD, USA, 2013, 264-7.*
- [80] Kaye BH, Gratton-Liimatainen J, Faddis N, Studying the avalanching behaviour of a powder in a rotating disc, *Part Part Syst Charact.* 12(1995) 232-6.
- [81] Lumay G, Boschini F, Traina K, Bontempi S, Remy JC, Cloots R, et al., Measuring the flowing properties of powders and grains, *Powder Technol.* 224(2012) 19-27.
- [82] Faqih A, Chaudhuri B, Alexander AW, Davies C, Muzzio FJ, Silvina Tomassone M, An experimental/computational approach for examining unconfined cohesive powder flow, *Int J Pharm.* 324(2006) 116-27.
- [83] Soh JLP, Liew CV, Heng PWS, New indices to characterize powder flow based on their avalanching behavior, *Pharm Dev Technol.* 11(2006) 93-102.
- [84] Henein H, Brimacombe JK, Watkinson AP, An experimental study of segregation in rotary kilns, *Meter Trans B.* 16(1985) 763-74.
- [85] Boateng AA, Barr PV, Modelling of particle mixing and segregation in the transverse plane of a rotary kiln, *Chem Eng Sci.* 51(1996) 4167-81.
- [86] Lee YSL, Poynter R, Podcizek F, Newton JM, Development of a dual approach to assess powder flow from avalanching behavior, *AAPS PharmSciTech.* 1(2000) 44-52.
- [87] Train D, Some aspects of the property of angle of repose of powders, *J Pharm Pharmacol.* 10(1958) T127-T35.
- [88] Gold G, Duvall RN, Palermo BT, Slater JG, Powder flow studies II: Effect of glidants on flow rate and angle of repose, *J Pharm Sci.* 55(1966) 1291-5.
- [89] Wouters IMF, Geldart D, Characterising semi-cohesive powders using angle of repose, *Part Part Syst Charact.* 13(1996) 254-9.
- [90] Brown RL, Minimum energy theorem for flow of dry granules through apertures, *Nature.* 191(1961) 458-61.
- [91] HosokawaMicronCorp., Micron powder characteristics tester. [internet] c2015 2015 [cited 2015 Apr 19]; Available from: <http://www.hmicronpowder.com/products/hosokawa-powder-characteristics-tester-pt-x>
- [92] CopleyScientific, Powders, Quality solutions for the testing of pharmaceuticals, 2013 Edition ed., Copley Scientific Ltd., Nottingham, UK, 2013, 53-7.
- [93] Jonat S, Albers P, Gray A, Schmidt PC, Investigation of the glidant properties of compacted colloidal silicon dioxide by angle of repose and X-ray photoelectron spectroscopy, *Eur J Pharm Biopharm.* 63(2006) 356-9.
- [94] Sarraguça MC, Cruz AV, Soares SO, Amaral HR, Costa PC, Lopes JA, Determination of flow properties of pharmaceutical powders by near infrared spectroscopy, *J Pharm Biomed Anal.* 52(2010) 484-92.
- [95] Kumar S, Gupta S, Effect of excipients on dissolution enhancement of aceclofenac solid dispersions studied using response surface methodology: A technical note, *Archives of Pharmacal Research.* 37(2014) 340-51.
- [96] Hammerness FC, Thompson HO, A study of the effect of lubricant and fines on a tablet granulation, *J Am Pharm Assoc.* 47(1958) 58-61.
- [97] Chowhan ZT, Yang IC, Powder flow studies IV. Tensile strength and orifice flow rate relationships of binary mixtures, *Int J Pharm.* 14(1983) 231-42.

- [98] Gold G, Duvall RN, Palermo BT, Powder flow studies I: Instrumentation and application, *J Pharm Sci.* 55(1966) 1133-6.
- [99] Erweka, Granulate flow testers. [Internet] 2015 2015 [cited 2015 Apr 18]; Available from: <http://www.erweka.com/products/item/granulate-flow/gt.html>
- [100] Gold G, Duvall RN, Palermo BT, Slater JG, Powder flow studies III: Factors affecting flow of lactose granules, *J Pharm Sci.* 57(1968) 667-71.
- [101] Powder flow, United States Pharmacopeia, US Pharmacopial Convention, MA, USA, 2011, 723-6.
- [102] Genina N, Räikkönen H, Ehlers H, Heinämäki J, Veski P, Yliruusi J, Thin-coating as an alternative approach to improve flow properties of ibuprofen powder, *Int J Pharm.* 387(2010) 65-70.
- [103] Soppela I, Airaksinen S, Murtomaa M, Tenho M, Hatara J, Räikkönen H, et al., Investigation of the powder flow behaviour of binary mixtures of microcrystalline celluloses and paracetamol, *Journal of Excipients and Food Chemicals.* 1(2010) 55-67.
- [104] Sandler N, Reiche K, Heinämäki J, Yliruusi J, Effect of moisture on powder flow properties of theophylline, *Pharmaceutics.* 2(2010) 275-90.
- [105] Seppälä K, Heinämäki J, Hatara J, Seppälä L, Yliruusi J, Development of a new method to get a reliable powder flow characteristics using only 1 to 2 g of powder, *AAPS PharmSciTech.* 11(2010) 402-8.
- [106] HansonResearchCorp., Physical testing. [internet] [cited 2015 Apr 18]; Available from: <http://hansonresearch.com/physical-testing/flodex-2/>
- [107] Podczeczek F, Particle-particle adhesion in pharmaceutical powder handling, Imperial College Press, London, UK, 1998.
- [108] Han X, Ghoroi C, To D, Chen Y, Davé R, Simultaneous micronization and surface modification for improvement of flow and dissolution of drug particles, *Int J Pharm.* 415(2011) 185-95.
- [109] Pitchayajittipong C, Price R, Shur J, Kaerger JS, Edge S, Characterisation and functionality of inhalation anhydrous lactose, *Int J Pharm.* 390(2010) 134-41.
- [110] Shur J, Harris H, Jones M, Kaerger JS, Price R, The role of fines in the modification of the fluidization and dispersion mechanism within dry powder inhaler formulations, *Pharm Res.* 25(2008) 1931-40.
- [111] Lindberg NO, Palsson M, Pihl AC, Freeman R, Freeman T, Flowability measurements of pharmaceutical powder mixtures with poor flow using five different techniques, *Drug Dev Ind Pharm.* 30(2004) 785-91.
- [112] Bruni G, Colafigli A, Lettieri P, Elson T, Torque measurements in aerated powders using a mechanically stirred fluidized bed rheometer (msFBR), *Chem Eng Res Des.* 83(2005) 1311-8.
- [113] Matheson GL, Herbst WA, Holt PH, Characteristics of fluid-solid systems, *Ind Eng Chem.* 41(1949) 1098-104.
- [114] Hagyard T, Sacerdote AM, Viscosity of suspensions of gas-fluidized spheres, *Ind Eng Chem Res.* 5(1966) 500-8.
- [115] Grace JR, The viscosity of fluidized beds, *Can J Chem Eng.* 48(1970) 30-3.
- [116] Ashwin BS, Hagyard T, Saunders ICB, Young TE, Viscometers having damped torsional oscillation, *J Sci Instrum.* 37(1960) 480.
- [117] Rietema K, Rheology of fluidized powders, The dynamics of fine powders, Elsevier Applied Science, London, UK, 1991, 162-86.

- [118] Cole GC, Powder characteristics for capsule filling, in: Ridgway K (Ed.) *Hard capsules: Development and technology*, The Pharmaceutical Press, London, UK, 1987, 80-6.
- [119] Freeman R, Measuring the flow properties of consolidated, conditioned and aerated powders — A comparative study using a powder rheometer and a rotational shear cell, *Powder Technol.* 174(2007) 25-33.
- [120] Freeman RE, The flowability of powders - an empirical approach, *From Powder to Bulk.* 2000(2000) 545-56.
- [121] Patel H, Please explain- difference between 'Powder Flow Characterization (performed by -Rheometer) and Rheology' ? [Forum] 2013 [cited 2015 Apr 20]; Available from: http://www.linkedin.com/groupItem?view=&qid=2302430&type=member&item=5804260238005649411&commentID=-1&trk=groups_guest_item_detail-b-jump_last#lastComment
- [122] Hare CL, Ghadiri M, Dennehy R, Collier A, Particle breakage in agitated dryers, *AIP Conf Proc.* 1145(2009) 851-4.
- [123] Hare C, Ghadiri M, Prediction of bulk particle breakage due to naturally formed shear bands, *AIP Conf Proc.* 1542(2013) 487-90.
- [124] Hare C, Zafar U, Ghadiri M, Freeman T, Clayton J, Murtagh M, Analysis of the dynamics of the FT4 powder rheometer. *Powder Technol.* 2015.
- [125] Jenike AW, Gravity flow of bulk solids, University of Utah, Utah, USA, 1961.
- [126] Jonhanson JR, The Johanson indicizer system versus the Jenike shear tester, *Bulk Solids Handling.* 12(1992) 237-40.
- [127] Kuentz M, Schirg P, Powder flow in an automated uniaxial tester and an annular shear cell: a study of pharmaceutical excipients and analytical data comparison, *Drug Dev Ind Pharm.* 39(2013) 1476-83.
- [128] Arthur JRF, Dunstan T, Enstad GG, Determination of the flow function by means of a cubic plane strain tester, *International journal of bulk solids storage in silos.* 1(1985) 7-10.
- [129] Scarlett B, Todd AC, A split ring annular shear cell for the determination of the shear strength of a powder, *J Phys E.* 1(1968) 655.
- [130] Bishop AW, Henkel DJ, The measurement of soil properties in the triaxial test, 2nd ed., Edward Arnold, London, UK, 1962.
- [131] Kamath S, Puri VM, Manbeck HB, Hogg R, Flow properties of powders using four testers — measurement, comparison and assessment, *Powder Technol.* 76(1993) 277-89.
- [132] Carr JF, Walker DM, An annular shear cell for granular materials, *Powder Technol.* 1(1968) 369-73.
- [133] Schwedes J, Review on testers for measuring flow properties of bulk solids (based on an IFPRI-Report 1999), *Granular matter.* 5(2003) 1-43.
- [134] Svarovsky L, *Powder testing guide: methods of measuring the physical properties of bulk powders*, Elsevier Applied Science, London, UK, 1987.
- [135] Schulze D, *Silo design for flow, Powders and bulk solids: Behavior, characterization, storage and flow*, Springer, Berlin, Germany, 2008, 291-317.
- [136] Thomson FM, Storage and flow of particulate solids, in: Fayed ME, Otten L (Eds.), *Handbook of powder science & technology*, Springer, NY, USA, 1997, 389-486.

- [137] Ghoroi C, Gurumurthy L, McDaniel DJ, Jallo LJ, Davé RN, Multi-faceted characterization of pharmaceutical powders to discern the influence of surface modification, *Powder Technol.* 236(2013) 63-74.
- [138] Yu WL, Muteki K, Zhang L, Kim G, Prediction of bulk powder flow performance using comprehensive particle size and particle shape distributions, *J Pharm Sci.* 100(2011) 284-93.
- [139] Schulze D, *Powders and bulk solids: Behavior, characterization, storage and flow*, Springer, Berlin, Germany, 2008.
- [140] BrookfieldEngineeringLaboratories, Powder flow tester. [internet] c2005-2015 2015 [cited 2015 Apr 17]; Available from: <http://www.brookfieldengineering.com/products/pft/powder-flow-tester.asp>
- [141] Sci-TecInc., ShearScan flowability tester. [internet] c2005 2005 [cited 2015 Apr 20]; Available from: <http://www.sci-tec-inc.com/shearscan/index.html>
- [142] MercuryScientificInc., Volution powder flow tester. [internet] c2010-2012 2012 [cited 2015 Apr 11]; Available from: <http://www.mercuryscientific.com/instruments/volution-powder-flow-tester>
- [143] FreemanTechnology, About the FT4 powder rheometer. [internet] c2015 2015 [cited 2015 Apr 20]; Available from: <http://www.freemantech.co.uk/powders/?pt=About%20the%20FT4%20Page&p=MQ>
- ≡
- [144] Søggaard SV, Pedersen T, Allesø M, Garnaes J, Rantanen J, Evaluation of ring shear testing as a characterization method for powder flow in small-scale powder processing equipment, *Int J Pharm.* 475(2014) 315-23.
- [145] Schulze D, *A more detailed look at properties of bulk solids, Powders and bulk solids: Behavior, characterization, storage and flow*, Springer, Berlin, Germany, 2008, 113-61.
- [146] Zheng J, (Ed.) *Formulation and analytical development for low-dose oral drug products*, John Wiley & Sons, NJ USA, 2009.
- [147] Perry RH, Green DW, (Eds.), *Perry's chemical engineers' handbook*. 7th ed., McGraw-Hill, NY, USA, 1997.
- [148] Watano S, Imada Y, Hamada K, Wakamatsu Y, Tanabe Y, Dave RN, et al., Microgranulation of fine powders by a novel rotating fluidized bed granulator, *Powder Technol.* 131(2003) 250-5.
- [149] Pitt K, Sinka C, *Tabletting*, in: Salman AD, Hounslow MJ, Seville JPK (Eds.), *Handbook of powder technology*, Elsevier Science B.V., Amsterdam, The Netherlands, 2007, 735-78.
- [150] Mirani AG, Patankar SP, Borole VS, Pawar AS, Kadam VJ, Direct compression high functionality excipient using coprocessing technique: A brief review, *Current Drug Delivery.* 8(2011) 426-35.
- [151] Morris KR, Griesser UJ, Eckhardt CJ, Stowell JG, Theoretical approaches to physical transformations of active pharmaceutical ingredients during manufacturing processes, *Advanced Drug Delivery Reviews.* 48(2001) 91-114.
- [152] Terashita K, Imamura K, Preparation of antipyretic analgesic by direct compression and its evaluation, *Chem Pharm Bull.* 50(2002) 1542-9.
- [153] Waimer F, Krumme M, Danz P, Tenter U, Schmidt PC, A novel method for the detection of sticking of tablets, *Pharm Dev Technol.* 4(1999) 359-67.
- [154] Lee J, Intrinsic adhesion force of lubricants to steel surface, *J Pharm Sci.* 93(2004) 2310-8.

- [155] Jonat S, Hasenzahl S, Gray A, Schmidt PC, Mechanism of glidants: Investigation of the effect of different colloidal silicon dioxide types on powder flow by atomic force and scanning electron microscopy, *J Pharm Sci.* 93(2004) 2635-44.
- [156] Mangal S, Meiser F, Tan G, Gengenbach T, Denman J, Rowles MR, et al., Relationship between surface concentration of l-leucine and bulk powder properties in spray dried formulations, *Eur J Pharm Biopharm.* 94(2015) 160-9.
- [157] Jong T, Li J, Morton DAV, Zhou Q, Larson I, Investigation of the changes in aerosolization behavior between the jet-milled and spray-dried colistin powders through surface energy characterization, *J Pharm Sci.* 105(2016) 1156-63.
- [158] Dahlberg C, Millqvist-Fureby A, Schuleit M, Surface composition and contact angle relationships for differently prepared solid dispersions, *Eur J Pharm Biopharm.* 70(2008) 478-85.
- [159] Pfeffer R, Dave RN, Wei D, Ramlakhan M, Synthesis of engineered particulates with tailored properties using dry particle coating, *Powder Technol.* 117(2001) 40-67.
- [160] Manoj G, Vikas AS, Mahesh K, Vipin K, Mechanical methods for dry particle coating processes and their applications in drug delivery and development, *Recent Patents on Drug Delivery & Formulation.* 4(2010) 58-81.
- [161] Wei G, Mangal S, Denman J, Gengenbach T, Lee Bonar K, Khan RI, et al., Effects of coating materials and processing conditions on flow enhancement of cohesive acetaminophen powders by high-shear processing with pharmaceutical lubricants, *J Pharm Sci.* 106(2017) 3022-32.
- [162] Lau M, Young PM, Traini D, Investigation into the manufacture and properties of inhalable high-dose dry powders produced by comilling API and lactose with magnesium stearate, *AAPS PharmSciTech.* 18(2017) 2248-59.
- [163] Koskela J, Morton DAV, Stewart PJ, Juppo AM, Lakio S, The effect of mechanical dry coating with magnesium stearate on flowability and compactibility of plastically deforming microcrystalline cellulose powders, *Int J Pharm.* 537(2018) 64-72.
- [164] Alonso M, Satoh M, Miyunami K, Mechanism of the combined coating-mechanofusion processing of powders, *Powder Technol.* 59(1989) 45-52.
- [165] Stank K, Steckel H, Physico-chemical characterisation of surface modified particles for inhalation, *Int J Pharm.* 448(2013) 9-18.
- [166] Zhou Q, Denman JA, Gengenbach T, Das S, Qu L, Zhang HL, et al., Characterization of the surface properties of a model pharmaceutical fine powder modified with a pharmaceutical lubricant to improve flow via a mechanical dry coating approach, *J Pharm Sci.* 100(2011) 3421-30.
- [167] Han X, Jallo L, To D, Ghoroi C, Davé R, Passivation of high-surface-energy sites of milled ibuprofen crystals via dry coating for reduced cohesion and improved flowability, *J Pharm Sci.* 102(2013) 2282-96.
- [168] Jallo LJ, Schoenitz M, Dreizin EL, Dave RN, Johnson CE, The effect of surface modification of aluminum powder on its flowability, combustion and reactivity, *Powder Technol.* 204(2010) 63-70.
- [169] Chen L, Ding X, He Z, Fan S, Kunnath KT, Zheng K, et al., Surface engineered excipients: II. Simultaneous milling and dry coating for preparation of fine-grade microcrystalline cellulose with enhanced properties, *Int J Pharm.* 546(2018) 125-36.
- [170] Washburn EW, The dynamics of capillary flow, *Physical Review.* 17(1921) 273-83.

- [171] Grundke K, Boerner M, Jacobasch HJ, Characterization of fillers and fibres by wetting and electrokinetic measurements, *Colloids Surf.* 58(1991) 47-59.
- [172] Studebaker ML, Snow CW, The influence of ultimate composition upon the wettability of carbon blacks, *The Journal of Physical Chemistry.* 59(1955) 973-6.
- [173] Shi Q, Gardner DJ, Wang JZ, Surface properties of polymeric automobile fluff particles characterized by inverse gas chromatography and contact angle analysis. Fourth International Conference on Woodfiber-Plastic Composites; 1997; WI, USA: Forest Products Society; 1997. p. 245-56.
- [174] Teipel U, Mikonsaari I, Determining contact angles of powders by liquid penetration, *Part Part Syst Charact.* 21(2004) 255-60.
- [175] Galet L, Patry S, Dodds J, Determination of the wettability of powders by the Washburn capillary rise method with bed preparation by a centrifugal packing technique, *J Colloid Interface Sci.* 346(2010) 470-5.
- [176] Chen M, Wu S, Tang W, Gong J, Caking and adhesion free energy of maltitol: Studying of mechanism in adhesion process, *Powder Technol.* 272(2015) 235-40.
- [177] Hammes MV, Englert AH, Noreña CPZ, Cardozo NSM, Effect of water activity and gaseous phase relative humidity on microcrystalline cellulose water contact angle measured by the Washburn technique, *Colloids Surf, A.* 500(2016) 118-26.
- [178] Young T, An essay on the cohesion of fluids, *Philos Trans R Soc Lond.* 95(1805) 6587.
- [179] *Surface science techniques*, Springer, Berlin, Germany, 2013.
- [180] Fox HW, Zisman WA, The spreading of liquids on low energy surfaces: I. polytetrafluoroethylene, *J Colloid Sci.* 5(1950) 514-31.
- [181] Zisman WA, Relation of the equilibrium contact angle to liquid and solid constitution, *Contact Angle, Wettability, and Adhesion*, American Chemical Society, Washington DC, USA, 1964, 1-51.
- [182] Fox HW, Hare EF, Zisman WA, The spreading of liquids on low-energy surfaces: VI. Branched-chain monolayers, aromatic surfaces, and thin liquid films, *J Colloid Sci.* 8(1953) 194-203.
- [183] Erbil HY, *Surface chemistry of solid and liquid interfaces*, Blackwell, Oxford, UK, 2006.
- [184] van Oss CJ, *Interfacial forces in aqueous media*, 2 ed., CRC Press, Boca Raton, USA, 2006.
- [185] Wu S, Calculation of interfacial tension in polymer systems, *J Poly Sci C.* 34(1971) 19-30.
- [186] Kiesvaara J, Yliruusi J, Ahomäki E, Contact angles and surface free energies of theophylline and salicylic acid powders determined by the Washburn method, *Int J Pharm.* 97(1993) 101-9.
- [187] van Oss CJ, Good RJ, Chaudhury MK, The role of van der Waals forces and hydrogen bonds in "hydrophobic interactions" between biopolymers and low energy surfaces, *J Colloid Interface Sci.* 111(1986) 378-90.
- [188] van Oss CJ, Chaudhury MK, Good RJ, Monopolar surfaces, *Adv Colloid Interface Sci.* 28(1987) 35-64.
- [189] van Oss CJ, Good RJ, Chaudhury MK, Mechanism of DNA (southern) and protein (western) blotting on cellulose nitrate and other membranes, *J Chromatogr A.* 391(1987) 53-65.

- [190] Dove JW, Buckton G, Doherty C, A comparison of two contact angle measurement methods and inverse gas chromatography to assess the surface energies of theophylline and caffeine, *Int J Pharm.* 138(1996) 199-206.
- [191] Cline D, Dalby R, Predicting the quality of powders for inhalation from surface energy and area, *Pharm Res.* 19(2002) 1274-7.
- [192] Steele DF, Moreton RC, Staniforth J, Young P, Tobyn M, Surface energy of microcrystalline cellulose determined by capillary intrusion and inverse gas chromatography, *The AAPS journal.* 10(2008) 494-503.
- [193] Lloyd DR, Ward TC, Schreiber HP, Pizaña CC, (Eds.), *Inverse gas chromatography: Characterization of polymers and other materials*, American Chemical Society, Washington DC, USA, 1989.
- [194] Braun J-M, Guillet J, *Study of polymers by inverse gas chromatography, Mechanisms of Polyreactions-Polymer Characterization*, Springer, Berlin, Germany, 1976, 107-45.
- [195] Belgacem MN, Gandini A, Inverse gas chromatography as a tool to characterize dispersive and acid-base properties of the surface of fibers and powders, in: Pefferkorn E (Ed.) *Interfacial Phenomena In Chromatography*, Marcel Dekker Inc., NY, USA, 1999, 41-124.
- [196] Dorris GM, Gray DG, Adsorption of *n*-alkanes at zero surface coverage on cellulose paper and wood fibers, *J Colloid Interface Sci.* 77(1980) 353-62.
- [197] Schultz J, Lavielle L, Martin C, The role of the interface in carbon fibre-epoxy composites, *J Adhesion.* 23(1987) 45-60.
- [198] Das SC, Larson I, Morton DAV, Stewart PJ, Determination of the polar and total surface energy distributions of particulates by inverse gas chromatography, *Langmuir.* 27(2011) 521-3.
- [199] Sircar S, Role of adsorbent heterogeneity on mixed gas adsorption, *Ind Eng Chem Res.* 30(1991) 1032-9.
- [200] Do DD, Dynamics of adsorption in heterogeneous solids, in: Rudziński W, Steele WA, Zgrablich G (Eds.), *Equilibria and dynamics of gas adsorption on heterogeneous solid surfaces*, Elsevier, Amsterdam, The Netherlands, 1997, 777-835.
- [201] Yla-Maihaniemi P, Heng J, Thielmann F, Williams D, Inverse gas chromatographic method for measuring the dispersive surface energy distribution for particulates, *Langmuir.* 24(2008) 9551-7.
- [202] Das SC, Zhou Q, Morton DAV, Larson I, Stewart PJ, Use of surface energy distributions by inverse gas chromatography to understand mechanofusion processing and functionality of lactose coated with magnesium stearate, *Eur J Pharm Sci.* 43(2011) 325-33.

Chapter 2: Surface Modification and Physical Characterisation of a Model Pharmaceutical Powder

Geoffrey Tan

Bachelor of Pharmaceutical Sciences (Honours)

Drug Delivery, Disposition and Dynamics, Monash Institute of Pharmaceutical
Sciences. 381 Royal Parade, Parkville, VIC, 3052, Australia

Chapter 2: Surface Modification and Physical Characterisation of a Model Pharmaceutical Powder

2.1. Commentary

A core objective of this thesis was to measure the hydrophobicity of powders (thesis objective 4). This can be achieved by measuring the contact angle of water to the powder via the liquid intrusion method. However, as this method requires the powder to come in contact with both water and a reference liquid, the powder may potentially dissolve which would likely alter the surfaces of the powder. To overcome this challenge, micron-sized glass beads (MGB) were selected to be a model pharmaceutical powder as they were not likely to dissolve in water or liquids that may be used as the reference liquid. Furthermore, an additional advantage of using MGB as a model pharmaceutical powder is that it is possible to alter the surfaces of the powder whilst keeping other aspects of the powder, such as its morphology, particle size and size distribution, unchanged. Consequently, any changes to the flowability of the engineered powders would be due to their modified surfaces.

The method of coating the surfaces of MGB with magnesium stearate using mechanofusion is described in this chapter. Also included is the physical characterisation of the dry coated powder.

2.2. Materials

Micron-sized glass beads (Cospheric LLC, CA, USA) were used as a model pharmaceutical powder. Magnesium stearate NF (MgSt), was obtained from Mallinckrodt Baker Inc. (NJ, USA). Milli-Q water was produced from a Direct-Q® 3 UV Water Purification System (Merck KGaA, Hesse, Germany). All materials were used as received.

2.3. Methods

2.3.1. Particle Engineering via Dry Coating

Dry coating of MGB with MgSt was achieved with an AMS-Mini mechanofusion system (Hosokawa Micron Powder Systems, Osaka, Japan). Prior to dry coating, approximately 20 g of MGB with varying levels of MgSt (0.05, 0.1, 0.175, 0.25, 0.5, 0.75, 1 and 2% w/w) was blended in a tumble mixer (Turbula[®] T2F, Glen Mills Inc., NJ, USA) at 101 rpm (revolutions per minute) for 10 mins. The blended samples were then dry coated at 500 rpm for 2 mins and then 3000 rpm for another 10 mins with a Nobilta angled blade process head. Water (22±2° C) was circulated through the built-in water jacket to prevent the temperature within the processing chamber from exceeding 25° C. The dry coated samples were noted as M-MGB-X, where X is the weight percentage of the MgSt level.

2.3.2. Laser Diffraction

The particle size and size distribution of the samples were measured via laser diffraction (Mastersizer[®] 2000, Malvern Instruments, Worcestershire, UK) equipped with a sample dispersion unit (Hydro 2000S, Malvern Instruments, Worcestershire, UK). Approximately 100 mg of sample powder was sonicated in approximately 10 ml of Milli-Q water for 10 mins prior to particle sizing. Sample dispersion was achieved with a stirrer speed of 2000 rpm and ultrasound at 100% with an obscuration range of 5-10%. Particle size analysis was calculated with a reference refractive index of 1.33 for Milli-Q water and 1.51 for the sample powders (Cospheric LLC, CA, USA) [1]. The particle size distribution was described by the volume median diameter (VMD), d_{10} (diameter at 10% under size), d_{50} (diameter at 50% under size) and d_{90} (diameter at 90% under size). Averages were calculated from replicates of three.

2.3.3. Scanning Electron Microscopy

The morphology of the powders was investigated via scanning electron microscopy (SEM) (Phenom™, Phenom-World, Eindhoven, The Netherlands). Each sample was prepared by slowly pouring a small amount of powder onto double-sided carbon tape mounted on a sample holder. Any excess powder not adhered to the tape was gently blown off with a stream of compressed air. Samples were sputter coated with gold (Emitech K550X, Quorum Technologies Ltd., Kent, UK) with a coating current of 25 mA for 6 minutes.

2.3.4. Statistical Analysis

Statistical analysis was achieved with a one-way analysis of variance (ANOVA) with a Tukey's *post hoc* analysis where a significant difference was obtained if $p < 0.05$ (IBM SPSS Statistics v23, IBM Corp., NY, USA).

2.4. Results

2.4.1. Observations

Visual observations of MGB readily showed that the powder typically existed as relatively large agglomerates. M-MGB-0.05, however, typically formed substantially smaller agglomerates. Samples dry coated with higher levels of MgSt no longer showed obvious signs of agglomerate structures.

2.4.2. Particle Size Analysis

The data obtained from the laser diffraction investigation, presented in Figure 2-1 and Table 2-1, shows that the uncoated glass powders had a d_{50} of approximately 10 μm with a d_{10} and a d_{90} of approximately 6 μm and 17 μm , respectively. Furthermore, it is also observed that dry coating the glass particles with different amounts of MgSt does not significantly ($p > 0.05$) alter the particle size nor the size distribution of the powder.

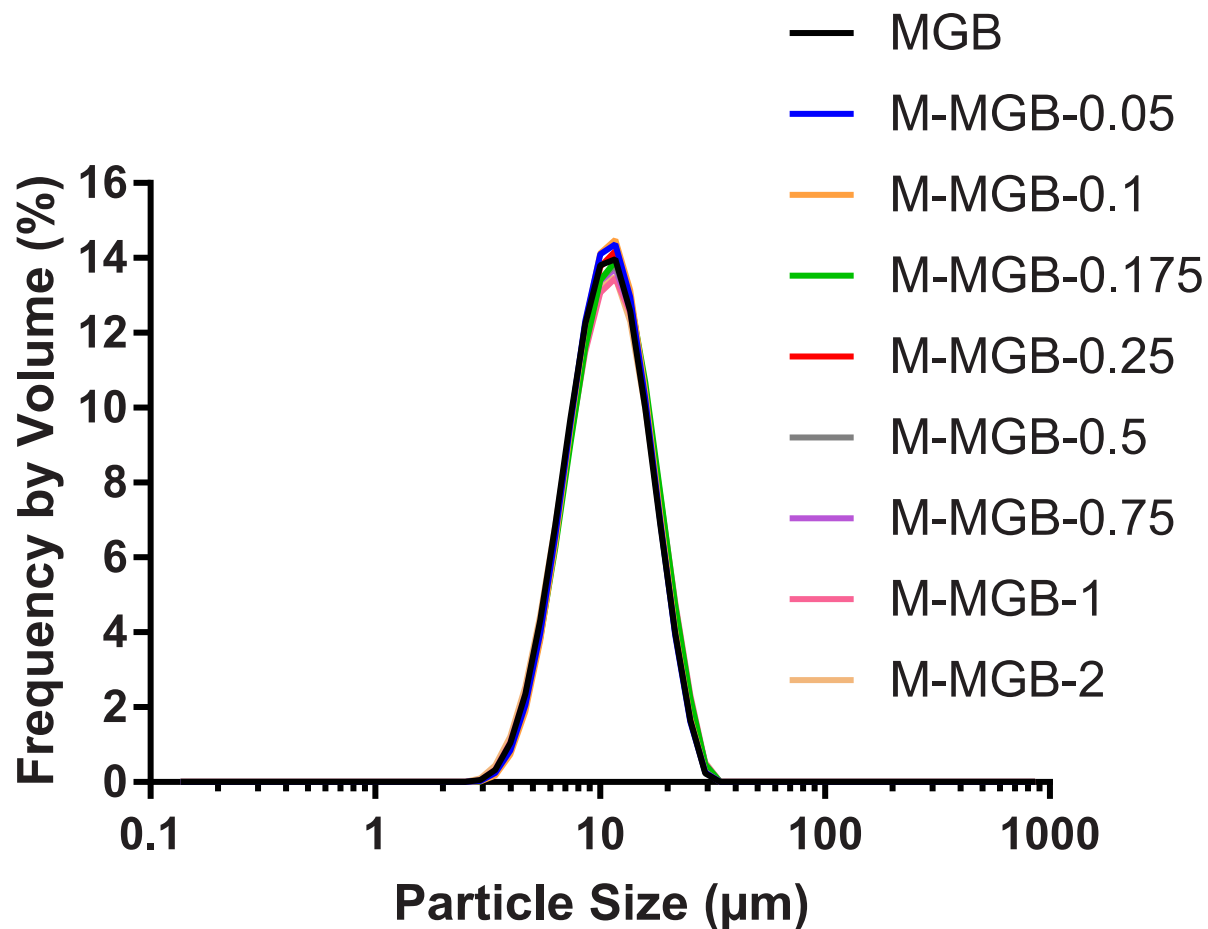


Figure 2-1: Average particle size distribution of uncoated and coated MGB. $n = 3$.

Table 2-1: Particle size distribution of MGB and M-MGB-X. Parenthesis represent standard deviation. $n = 3$.

Sample	Particle size (μm)			Span
	d_{10}	d_{50}	d_{90}	
MGB	5.7 (0.1)	9.9 (0.1)	16.7 (0.4)	1.1 (0.04)
M-MGB-0.05	5.9 (0.3)	10.0 (0.4)	16.4 (0.7)	1.0 (0.04)
M-MGB-0.1	5.9 (0.3)	10.0 (0.5)	16.7 (0.8)	1.1 (0.01)
M-MGB-0.175	5.9 (0.1)	10.1 (0.1)	16.8 (0.1)	1.1 (0.01)
M-MGB-0.25	5.9 (0.2)	10.3 (0.01)	17.5 (0.3)	1.1 (0.04)
M-MGB-0.5	5.9 (0.3)	10.2 (0.3)	17.1 (0.4)	1.1 (0.1)
M-MGB-0.75	5.8 (0.1)	10.2 (0.1)	17.3 (0.5)	1.1 (0.04)
M-MGB-1	5.7 (0.1)	10.2 (0.3)	17.3 (0.8)	1.1 (0.04)
M-MGB-2	5.7 (0.1)	10.2 (0.1)	17.5 (0.2)	1.2 (0.003)

2.4.3. Powder Morphology

Representative SEM images of the samples are presented in Figure 2-2. It can be observed that the uncoated glass particles were spherical. Additionally, it was also observed that dry coating the glass powders does not alter their morphology.

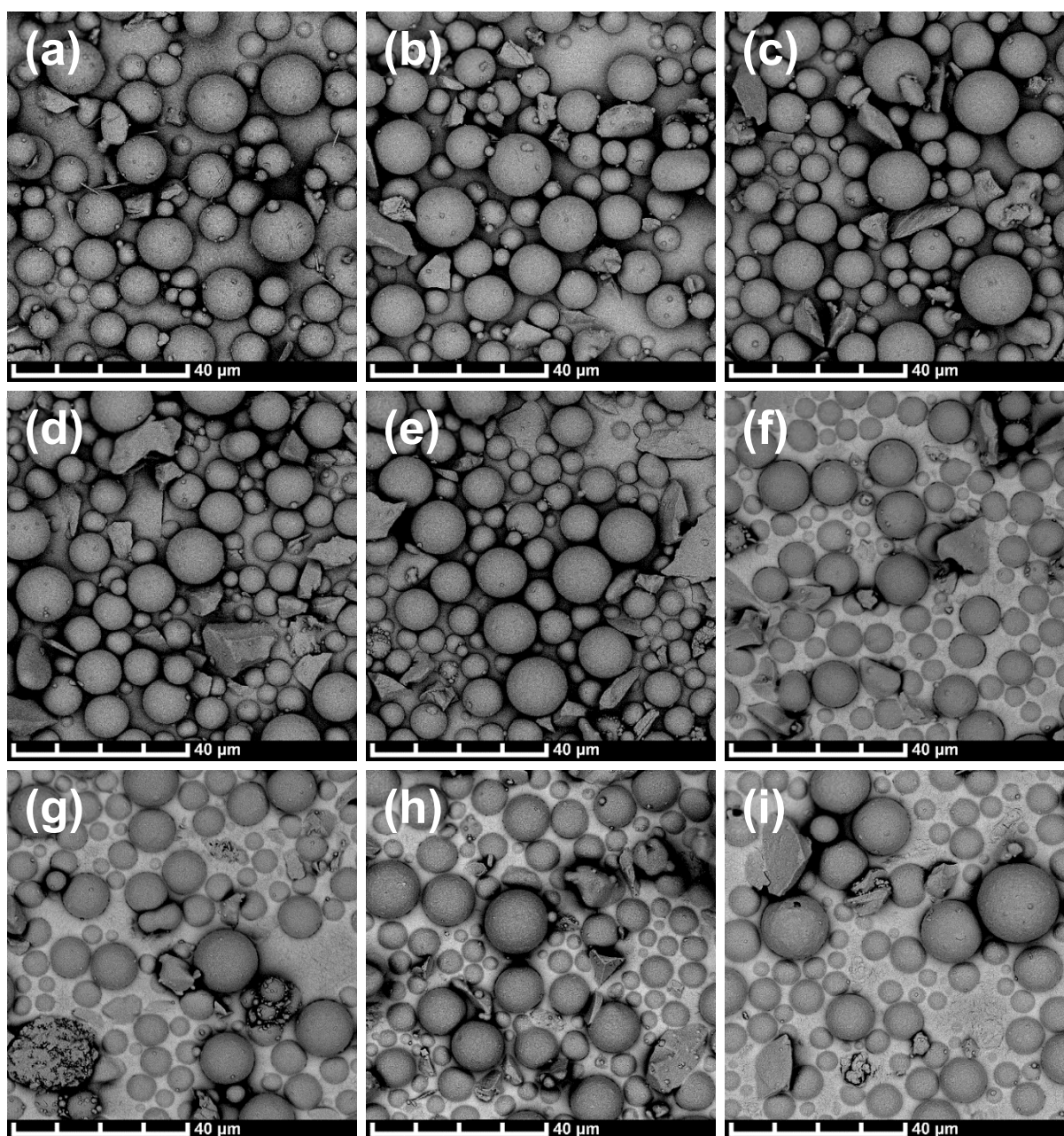


Figure 2-2: Representative SEM of: (a) MGB, (b) M-MGB-0.05, (c) M-MGB-0.1, (d) M-MGB-0.175, (e) M-MGB-0.25, (f) M-MGB-0.5, (g) M-MGB-0.75, (h) M-MGB-1 and (i) M-MGB-2. All images are at 3000x magnification.

2.5. Conclusions

Surface modification of micron-sized glass beads (MGB) with a d_{50} of approximately 10 µm was achieved by dry coating MGB with varying amounts of magnesium stearate (MgSt) via mechanofusion. Particle size analysis showed that dry coating MGB with

MgSt did not significantly alter the particle size or size distribution of the engineered powders, while SEM analysis showed that the morphology of the host powder was spherical.

2.6. References

[1] 2011 [cited 09/04/2013]; Available from: http://www.cospheric-microspheres.com/P2011SL_Solid_Glass_Spheres_d90_8um_25g_p/p2011sl%20-%2025g.htm

Chapter 3: Development of New Experimental Methods

Geoffrey Tan

Bachelor of Pharmaceutical Sciences (Honours)

Drug Delivery, Disposition and Dynamics, Monash Institute of Pharmaceutical
Sciences. 381 Royal Parade, Parkville, VIC, 3052, Australia

Chapter 3: Development of New Experimental Methods

3.1. Commentary

One of the core objectives of this thesis was to evaluate the importance of both the surface energy and hydrophobicity of engineered powders (Thesis Objective 3 and Thesis Objective 4, respectively). The surface energies of the samples were measured by inverse gas chromatography. However, when using MGB that had been dry coated with MgSt, the inverse gas chromatography over-pressured which prevented the surface energy of the samples to be measured. To resolve this, a new method was developed to decrease the pressure drop across the stationary phase of the inverse gas chromatography system, thereby allowing the surface energy to be measured. The first part of this chapter presents a publication detailing this new method [1].

The hydrophobicity of the samples was measured via the liquid intrusion method. For this method, two liquids are required: the probe liquid (in this case water) and a perfectly wetting liquid as a reference liquid. The standard approach of selecting the reference liquid is selecting a liquid with a low surface tension and assume that this liquid will perfectly wet the samples. However, this assumption does not always hold true. Additionally, the analysis of data obtained from the liquid intrusion method requires division of a set of intrusion rates of the probe liquid with a set of intrusion rates of the reference liquid. However, from the literature, there does not appear to be a standardised way of doing this. The second part of this chapter presents a publication that proposes a new experimental approach for the selection of a reference liquid [2]. It also describes ways to divide the rates of intrusion of the probe liquid with the rates of intrusion of the reference liquid.

This chapter was published in: *Tan G, Qu L, Morton DAV, Larson I, A strategy to evaluate the surface energy of high packing efficiency fine powders via inverse gas chromatography, Powder Technol. 320(2017) 470-3* and *Tan G, Morton DAV, Larson I, Strategies to analyse data obtained from liquid intrusion experiments of loose porous materials, J Pharm Biomed Anal. 145(2017) 711-7.*

3.2. Part I: A Strategy to Evaluate the Surface Energy of High Packing Efficiency Fine Powders via Inverse Gas Chromatography

3.2.1. Introduction

Determination of the surface energy of a fine powder is of particular interest to many material applications, as this energy is directly related to their cohesive inter-particulate interactions. Thus, the surface energy can influence the bulk performances of powders, such as powder flow out of a hopper and into a tablet die during pharmaceutical tablet manufacturing [3-7]. One of the most common methods to measure the surface energy of bulk powders is through inverse gas chromatography (IGC) [8-14]. Similar to conventional gas chromatography (GC), IGC consists of a stationary phase and a mobile phase. However, unlike GC methods, the stationary phase of IGC is the sample of interest, in this case a powder, while the mobile phase comprises a series of known vapours [15, 16]. However, not all powders are suitable for IGC analysis. For example, the porosity or the packing efficiency of a powder bed can be a critical factor in determining whether the powder is suitable to form the stationary phase of an IGC.

Generally, powders that either consist of relatively large particle sizes or that are highly cohesive tend to have packing efficiencies that are likely to produce appropriately porous powder beds [7]. Accordingly, the pressure drop across the stationary phase is likely to be within measurable limits and thus over-pressuring of the system is unlikely. Conversely, powders with high packing efficiencies, for instance free-flowing fine powders, are likely to produce powder beds with low porosity [7]. The mobile phase can then experience a much higher resistance while passing through the stationary phase; thus, the pressure drop across the stationary phase can exceed the upper measurable limit: the system over-pressures. This can be problematic to surface energy determination as accurate retention volumes for the vapour probes cannot be determined, where the compression of the mobile phase within the column cannot be corrected for [17]. Clearly, a robust methodology to determine the surface energy of high packing efficiency powders which otherwise produce over-pressuring is required.

Anecdotal evidence suggests that blending free-flowing fine powders with large carrier particles may aid in increasing the porosity of the resultant powder bed; thus, in theory, reduce the likelihood of the system over-pressuring. However, the concern here is that a foreign surface is introduced. This may, therefore, influence the surface energy determination as the vapour probes could potentially probe the surface of the carrier particles instead of the sample of interest and thus provide misleading surface energy data. However, this could be resolved for carrier particles with silanized surfaces, for instance larger-sized silanized glass powders, as their surface energy is expected to be low. Consequently, as the probes are assumed to interact primarily with the highest energy sites [18-21], it is expected that the surface of such carrier particles can be considered inert. Additionally, because the carrier particles are much larger than the powders of interest, the total surface area presented by the carrier particles would be significantly smaller than the surface area of the powder of interest. Thus, in theory, the large carrier particles should not interfere to any meaningful extent with the surface energy analysis.

The purpose of this paper is to evaluate the suitability of blending larger-sized silanized glass particles with free-flowing fine powders to reduce the pressure drop across the stationary phase, thereby decreasing the likelihood of over-pressuring the system. Additionally, this paper aims to determine whether the introduction of carrier particles influences the measurement of the surface energy (including its components) of a fine powder.

3.2.2. Materials and Methods

3.2.2.1. *Materials*

The model pharmaceutical active used for surface energy measurements was micron-sized glass beads (MGB), $d_{50} = 10 \mu\text{m}$, which was procured from Cospheric LLC (CA, USA). Magnesium stearate NF (MgSt) was obtained from Mallinckrodt Baker Inc. (NJ, USA). The carrier particles used were commercially available 250 μm pre-silanized glass beads, which were obtained from Sigma-Aldrich Co. LLC. (MO, USA). All

silanized glass wool and pre-silanized glass columns were purchased from Surface Measurement Systems Ltd. (London, UK). GC grade decane, nonane, octane, heptane, hexane, dichloromethane and toluene were obtained from Sigma-Aldrich Co. LLC. (MO, USA). All materials were used as received.

3.2.2.2. Dry Coating

Dry coating of MGB with MgSt was achieved in an AMS-Mini mechanofusion system (Hosokawa Micron Corp., Osaka, Japan). Prior to dry coating, approximately 20 g of MGB with 0.1% w/w MgSt was blended in a tumble mixer (Turbula® T2F, Glen Mills Inc., NJ, USA) at 101 rpm (revolutions per minute) for 10 mins. The blended samples were then dry coated at 500 rpm for 2 mins and then 3000 rpm for another 10 mins with a Nobilta angled blade process head. Water ($22\pm 2^\circ\text{C}$) was circulated through the built-in water jacket to prevent the temperature within the processing chamber from exceeding 25°C . The dry coated samples are noted as M-MGB-0.1.

3.2.2.3. Blending Fine Powders with Carrier Particles

Blends of MGB with carrier glass beads (CGB) and M-MGB-0.1 with CGB was achieved by gentle agitation using a smooth-surface mortar and pestle for approximately 2 mins with MGB:CGB and M-MGB-0.1:CGB proportions as described in Table 3-1.

Table 3-1: Mass and blend proportion of MGB and CGB.

Sample ID	Mass of MGB (g)	%CGB (w/w)	Estimated Relative Surface Area (MGB:CGB) [‡]
MGB_0.2-0	0.2	0	
MGB_0.6-0	0.6	0	
MGB_0.7-0	0.7	0	
MGB_1.2-0	1.2	0	
MGB_1.5-0	1.5	0	
MGB_2.3-0	2.3	0	
M-MGB-0.1_1.2-0	1.2	0	
MGB_0.2-95	0.2	95	822
MGB_1.5-50	1.5	50	15625
MGB_0.7-50	0.7	50	15625
MGB_0.7-70	0.7	70	6696
MGB_0.7-80	0.7	80	3906
M-MGB-0.1_1.2-70	1.2	70	6696

[‡]Calculation based on monodisperse spherical particles with a diameter of 250 μm for CGB and 10 μm for both MGB and M-MGB-0.1.

3.2.2.4. Surface Energy Measurements

The surface energy of MGB and M-MGB-0.1 was determined with the use of an inverse gas chromatography instrument (iGC 2000, Surface Measurement Systems Ltd., London, UK) at infinite dilution.

The powder samples and blended samples (see Table 3-1) were packed into pre-silanized glass columns (300 x 4 mm ID). Both ends of the column were loosely stoppered with silanized glass wool to prevent sample movement. Packed columns were then gently tapped manually until no visible signs of voids, cracks, or channels.

Prior to surface energy measurements, the samples were first pre-conditioned with a stream of helium at a flow rate of 10 sccm (standard cubic centimetre per minute) for

a period of 120 mins at 303.15 K and 0% RH (relative humidity). To measure the surface energy, helium at 10 sccm was used to carry a series of *n*-alkane probes (GC grade decane, nonane, octane, heptane and hexane) and specific probes (dichloromethane and toluene) through the stationary phase to determine the dispersive surface energy, γ_S^D , and the specific free energy, ΔG^{SP} , respectively. The concentration used for all probes was at 0.03 p/p_0 (where p is the partial pressure and p_0 is the saturation vapour pressure) and the system was kept at 303.15 K and 0% RH. Dead volumes were based on the elution time of methane gas at 0.03 p/p_0 ; detection of the probes was achieved with a flame ionization detector (FID). Results were analysed via SMS-iGC analysis software v1.3 (Surface Measurement Systems Ltd., London, UK). Replicates of 3 were conducted for all samples.

γ_S^D of the sample and ΔG^{SP} of both dichloromethane and toluene was calculated with the Schultz method [22]. However, through this method, ΔG^{SP} is obtained in units of energy per mole (kJ/mol), while γ_S^D is in units of energy per area (mJ/m²). The harmonization of these units was achieved through the use of Avogadro's number and the cross-sectional area of the vapour probe (refer to Table 3-2) [9, 17, 23, 24]. ΔG^{SP} is related to the polar surface energy through the concept presented by Good-van Oss [25], Equation (3.1):

$$\Delta G^{SP} = 2aN_A(\sqrt{\gamma_L^+\gamma_S^-} + \sqrt{\gamma_L^-\gamma_S^+}) \quad (3.1)$$

where a is the cross-sectional area of the probe, N_A is Avogadro's number, γ_L^+ is the electron-acceptor parameter of the acidic probe, γ_S^- is the electron-donor parameter of the sample surface (basic site), γ_L^- is the electron-donor parameter of the basic probe and γ_S^+ is the electron-acceptor parameter of the sample surface (acidic site).

Table 3-2: The electron-acceptor parameter, γ_L^+ ; electron-donor parameter, γ_L^- ; and cross-sectional area, a , of dichloromethane and toluene (Surface Measurement Systems Ltd., London, UK).

Probe	γ_L^+ (mJ/m ²)	γ_L^- (mJ/m ²)	a (x10 ⁻¹⁹ m ²)
Dichloromethane	5.20	0	2.45
Toluene	0	2.30	4.60

As described in the work presented by van Oss *et al.*, 1998 [26], the polar surface energy, γ_S^P , was calculated with Equation (3.2):

$$\gamma_S^P = 2\sqrt{\gamma_S^+ \gamma_S^-} \quad (3.2)$$

The total surface energy, γ_S^T , of the sample is the additive components of γ_S^D and γ_S^P [26].

3.2.2.5. Statistical Analysis

Statistical analysis was achieved with a one-way analysis of variance (ANOVA) with a Tukey's *post hoc* analysis where a significant difference was obtained if $p < 0.05$ (IBM SPSS Statistics v23, IBM Corp., NY, USA).

3.2.3. Results and Discussions

To understand the effect of sample mass on the measurement of surface energy, varying masses of MGB were analysed. The results are presented in Figure 3-1.

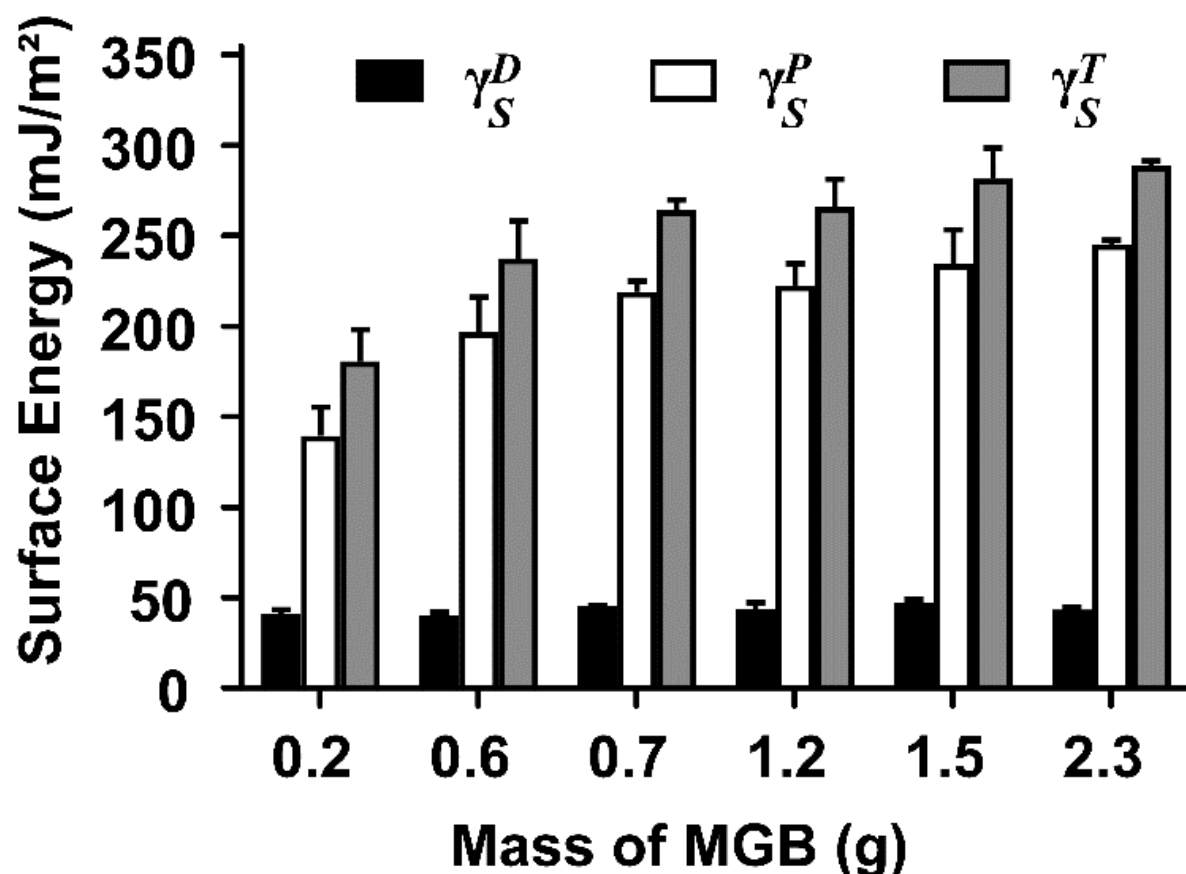


Figure 3-1: Surface energy of MGB with varying amount of MGB. $n = 3$, error bars represent SD.

It appears that the sample mass can have an effect on the measurement of surface energy. At the lowest amount tested, approximately 0.2 g, the total surface energy was measured to be approximately 181 ± 17 mJ/m². With 0.6 g of MGB, however, the surface energy increased significantly ($p < 0.05$) to approximately 238 ± 20 mJ/m². However, once the sample mass was at 0.7 g or above, it appears that the sample mass no longer influence the measurement of surface energy with no significant differences ($p > 0.05$) with increasing sample mass.

To further analyse the effect sample mass had on surface energy measurements, the surface energy was split into its components—the dispersive, γ_S^D , and the specific (or polar), γ_S^P (refer to Figure 3-1). It appears that the dispersive surface energy of MGB is only slightly influenced by the sample mass as the only significantly different ($p < 0.05$) samples found were between MGB_1.5 and the two lowest sample masses (0.2

and 0.6 g), respectively, where the difference, however, was only very minor. All other samples were not significantly different ($p > 0.05$) from one another.

The polar surface energy, in contrast, appears to be affected by the amount of sample present. Increasing the mass of MGB from 0.2 g to 0.6 g, increased the polar surface energy from 140 ± 16 mJ/m² to 197 ± 19 mJ/m². However, with larger amounts of MGB (with at least 0.7 g of MGB), the sample mass did not give significantly different ($p > 0.05$) values in the measurement of the surface energy. Therefore, this work demonstrates the importance of having sufficient sample within the IGC column, which appears logical as the sample forms the stationary phase in an IGC system. Increasing the amount of sample beyond a critical amount would ensure there is sufficient surface area for the IGC probes to interact with. For this specific case, the critical mass of sample required was found to be 0.7 g of MGB (for convenience, the 'mass' was used even though the critical amount of sample actually depends on surface area).

To determine what effect the introduction of large carrier particles, in the form of 250 μ m silanized glass beads, has on the determination of the surface energy of a powder, varying amounts of MGB:CGB were prepared and analysed with an IGC. The results are presented in Figure 3-2.

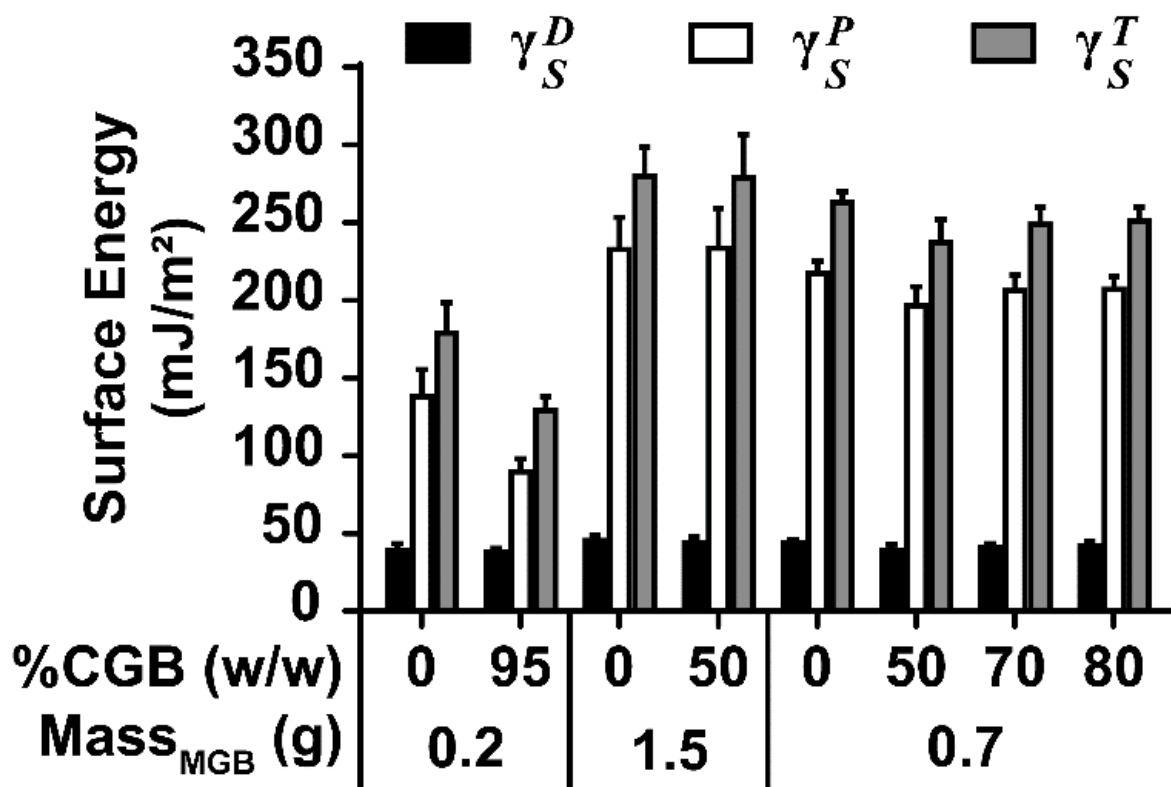


Figure 3-2: Surface energy of different masses of MGB and different proportion of CGB. $n = 3$, error bars represents SD.

Consistent with the results presented above, the change in the total surface energy was largely the result of a change in the polar surface energy, while the dispersive surface energy was not observed to significantly change ($p > 0.05$) with the addition of CGB. As observed, the introduction of 250 μm silanized glass beads can influence the surface energy determination of the sample of interest (MGB), where the surface energy was underestimated. This only occurred with the lowest amount of sample powder, 0.2 g of MGB, where the polar surface energy decreased significantly from $140 \pm 16 \text{ mJ/m}^2$ with no CGB to $91 \pm 7 \text{ mJ/m}^2$ with 95% w/w CGB.

However, increasing the MGB mass to 1.5 g, the addition of 50% w/w CGB did not significantly influence ($p > 0.05$) the measurement of the surface energy of MGB. Moreover, even when the MGB mass was decreased to 0.7 g, blending MGB with varying proportions of CGB did not significantly alter ($p > 0.05$) the measured surface energy, even with the addition of 80% w/w CGB. This may suggest that the actual sample mass within the column, or more specifically, the surface area of the sample

in the column, is more a critical factor than the amount of carrier particles. These results are in good agreement with the findings of Hadjittofis *et al.*, 2017 [27].

To investigate the effect of CGB on the pressure drop across a stationary phase composed of free-flowing fine powder, the pressure drop across columns packed with MGB and M-MGB-0.1 with and without CGB, respectively, was measured, and is reported in Figure 3-3.

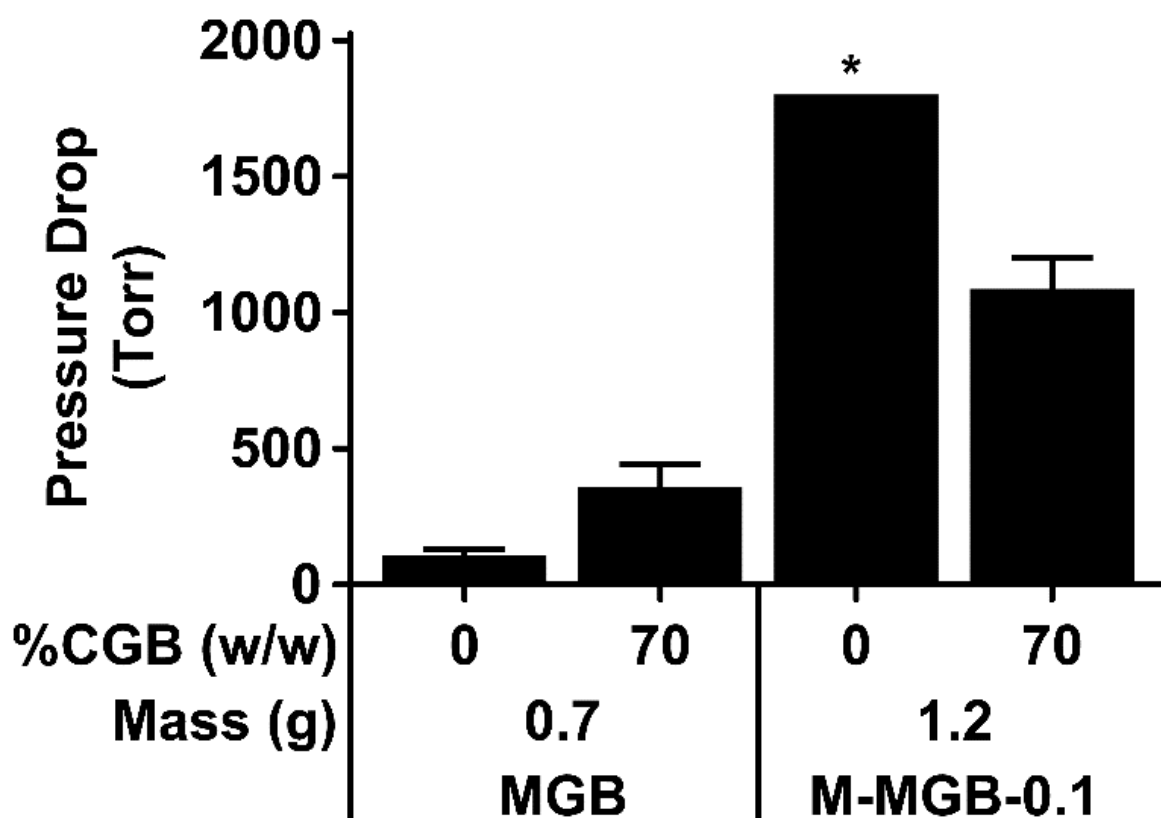


Figure 3-3: Pressure drop across the stationary phase composed of MGB:CGB and M-MGB-0.1:CGB. $n = 3$, error bars represents SD. *The pressure drop across the stationary phase composed of 1.2 g of M-MGB-0.1 with no CGB was too high to be measured (above 1800 Torr, which is the upper measurable limit on the instrument).

The pressure drop across columns packed with MGB alone was approximately 107 ± 23 Torr—within the measurable limit. Interestingly, blending 70% w/w CGB with MGB increased the pressure drop across the columns to approximately 355 ± 88 Torr. The observed increase in pressure drop was likely due to the tighter packing of the

MGB:CGB blends within the 4 mm ID column. As the bulk volume of the MGB:CGB blend was relatively large (compared to the volume of the IGC column), it was necessary to tap the column more frequently so that the entire sample would fit within the column. Despite the slight increase in the pressure drop across these columns, however, it is important to note that the pressure drop across these columns remained within the measurable limit. Consequently, the small increase in the pressure drop is not expected to influence the measurement of the surface energy.

Alternatively, not surprisingly, columns packed with M-MGB-0.1 alone over-pressured during IGC analysis (the pressure drop was above 1800 Torr, which is the upper measurable limit of the iGC 2000). However, blending 1.2 g of M-MGB-0.1 with 70% w/w CGB decreased the pressure drop to measurable limits where it was approximately 1086 ± 114 Torr—thus successfully preventing the system from over-pressuring.

3.2.4. Conclusions

Measurements of the surface energy of powders with high packing efficiencies through inverse gas chromatographic methods can be challenging as excessive pressure build up can occur. To alleviate this, the powder can be blended with large carrier particles such as 250 μm silanized glass beads. The results presented here show that the mass of the sample within the stationary phase is more important than the amount of silanized glass carrier particles added. Therefore, provided that the sample mass is above the critical mass required, the addition of large silanized glass carrier particles does not significantly interfere with the measurement of the surface energy of the sample powder. Additionally, blending free-flowing fine powder (M-MGB-0.1) with 70% w/w 250 μm silanized glass beads was successful in preventing over-pressuring of the system. Therefore, blending larger-sized carrier particles with powders with high packing efficiencies may be a quick and simple solution to overcome excessive pressure build up during surface energy analysis with inverse gas chromatography.

Although this paper specifically focused on the suitability of blending fine powders with large silanized carrier particles for the measurement of the surface energy via IGC at infinite dilution, future research extending to varying surface coverages could provide significant insights to a complementary side of IGC analysis, especially for the measurement of the surface energetics of powders with high packing efficiencies.

3.2.5. Acknowledgements

GT is thankful for the financial support of Graduate Research, Monash University, for providing a Monash Equity Scholarship.

3.2.6. References

- [1] Tan G, Qu L, Morton DAV, Larson I, A strategy to evaluate the surface energy of high packing efficiency fine powders via inverse gas chromatography, *Powder Technol.* 320(2017) 470-3.
- [2] Tan G, Morton DAV, Larson I, Strategies to analyse data obtained from liquid intrusion experiments of loose porous materials, *J Pharm Biomed Anal.* 145(2017) 711-7.
- [3] Johnson KL, Kendall K, Roberts AD, Surface energy and the contact of elastic solids, *Proc R Soc Lond A.* 324(1971) 301-13.
- [4] Derjaguin BV, Muller VM, Toporov YP, Effect of contact deformations on the adhesion of particles, *J Colloid Interface Sci.* 53(1975) 314-26.
- [5] Maugis D, Adhesion of spheres: The JKR-DMT transition using a dugdale model, *J Colloid Interface Sci.* 150(1992) 243-69.
- [6] Butt H-J, Kappl M, Contact mechanics and adhesion, Surface and interfacial forces, Wiley-VCH, Weinheim, Germany, 2010, 219-50.
- [7] Aulton ME, (Ed.) *Pharmaceutics: The science of dosage form design.* 2nd ed., Churchill Livingstone, Edinburgh, UK, 2002.
- [8] Hadjar H, Balard H, Papirer E, An inverse gas chromatography study of crystalline and amorphous silicas, *Colloids Surf, A.* 99(1995) 45-51.
- [9] Traini D, Young PM, Thielmann F, Acharya M, The influence of lactose pseudopolymorphic form on salbutamol sulfate–lactose interactions in DPI formulations, *Drug Dev Ind Pharm.* 34(2008) 992-1001.
- [10] Zhou Q, Denman JA, Gengenbach T, Das S, Qu L, Zhang HL, et al., Characterization of the surface properties of a model pharmaceutical fine powder modified with a pharmaceutical lubricant to improve flow via a mechanical dry coating approach, *J Pharm Sci.* 100(2011) 3421-30.
- [11] Ali SSM, Heng JYY, Nikolaev AA, Waters KE, Introducing inverse gas chromatography as a method of determining the surface heterogeneity of minerals for flotation, *Powder Technol.* 249(2013) 373-7.

- [12] Shah UV, Olusanmi D, Narang AS, Hussain MA, Gamble JF, Tobby MJ, et al., Effect of crystal habits on the surface energy and cohesion of crystalline powders, *Int J Pharm.* 472(2014) 140-7.
- [13] Mangal S, Meiser F, Tan G, Gengenbach T, Denman J, Rowles MR, et al., Relationship between surface concentration of l-leucine and bulk powder properties in spray dried formulations, *Eur J Pharm Biopharm.* 94(2015) 160-9.
- [14] Jong T, Li J, Morton DAV, Zhou Q, Larson I, Investigation of the changes in aerosolization behavior between the jet-milled and spray-dried colistin powders through surface energy characterization, *J Pharm Sci.* 105(2016) 1156-63.
- [15] Braun J-M, Guillet J, Study of polymers by inverse gas chromatography, *Mechanisms of Polyreactions-Polymer Characterization*, Springer, Berlin, Germany, 1976, 107-45.
- [16] Belgacem MN, Gandini A, Inverse gas chromatography as a tool to characterize dispersive and acid-base properties of the surface of fibers and powders, in: Pefferkorn E (Ed.) *Interfacial Phenomena In Chromatography*, Marcel Dekker Inc., NY, USA, 1999, 41-124.
- [17] Thielmann F, Naderi M, Burnett D, Jervis H, Investigation of the acid-base properties of an MCM-supported ruthenium oxide catalyst by inverse gas chromatography and dynamic gravimetric vapour sorption, in: Jackson SD, Hargreaves JSJ, Lennon D (Eds.), *Catalysis in Application*, The Royal Society of Chemistry, Cambridge, UK, 2003, 233-9.
- [18] Sircar S, Role of adsorbent heterogeneity on mixed gas adsorption, *Ind Eng Chem Res.* 30(1991) 1032-9.
- [19] Do DD, Dynamics of adsorption in heterogeneous solids, in: Rudziński W, Steele WA, Zgrablich G (Eds.), *Equilibria and dynamics of gas adsorption on heterogeneous solid surfaces*, Elsevier, Amsterdam, The Netherlands, 1997, 777-835.
- [20] Yla-Maihaniemi P, Heng J, Thielmann F, Williams D, Inverse gas chromatographic method for measuring the dispersive surface energy distribution for particulates, *Langmuir.* 24(2008) 9551-7.
- [21] Mohammadi-Jam S, Waters KE, Inverse gas chromatography applications: A review, *Adv Colloid Interface Sci.* 212(2014) 21-44.
- [22] Schultz J, Lavielle L, Martin C, The role of the interface in carbon fibre-epoxy composites, *J Adhesion.* 23(1987) 45-60.
- [23] Cline D, Dalby R, Predicting the quality of powders for inhalation from surface energy and area, *Pharm Res.* 19(2002) 1274-7.
- [24] Das SC, Behara SRB, Bulitta JB, Morton DAV, Larson I, Stewart PJ, Powder strength distributions for understanding de-agglomeration of lactose powders, *Pharm Res.* 29(2012) 2926-35.
- [25] van Oss CJ, Chaudhury MK, Good RJ, Monopolar surfaces, *Adv Colloid Interface Sci.* 28(1987) 35-64.
- [26] van Oss CJ, Good RJ, Chaudhury MK, Additive and nonadditive surface tension components and the interpretation of contact angles, *Langmuir.* 4(1988) 884-91.
- [27] Hadjitofis E, Zhang GGZ, Heng JYY, Influence of sample preparation on IGC measurements: the cases of silanised glass wool and packing structure, *RSC Advances.* 7(2017) 12194-200.

3.3. Part II: Strategies to Analyse Data Obtained from Liquid Intrusion Experiments of Loose Porous Materials

3.3.1. Introduction

The characterization and understanding of how liquids wet powders has significant importance to many processes within a range of industries. The contact angle, θ , is often used as a measure of wettability [1]. For example, within the pharmaceutical industry, wet granulation is a commonly used unit operation to prepare powders for tableting [2]. This process involves the addition of a liquid to the powder material to aid in the formation of agglomerates. The contact angle of the liquid to the powder can affect the granulation process and the overall quality of the granules and thus may affect the overall quality and production of pharmaceutical tablets [3, 4].

Additionally, with the dissolution of fine powders, the contact angle of the dissolution media to the powder plays a critical role as the initial stages of dissolution (wetting of the powder by the liquid and subsequent liquid penetration into the powder) are highly influenced by the contact angle [5]. In such cases, smaller contact angles may aid in the dissolution of the powder [6].

Furthermore, as the contact angle represents the equilibrium of energies at the solid-liquid-vapour interface, information regarding the surface energy of a solid can be obtained from contact angle data [1, 7].

3.3.1.1. Measurement of Contact Angles

Although there are numerous methods to measure the contact angle of liquids to smooth, flat surfaces [8, 9], the methods available for the measurement of contact angles of liquids to powders is, however, limited and typically fraught with challenges [10].

To overcome the challenges, some researchers have compressed powders to form dense compacts with relatively flat surfaces [11, 12]. Sessile drops on these compacts are used to measure the contact angle. Alternatively, the powder can be compacted into thin rectangular plates, which are used as Wilhelmy plates [13]. However, the use of compacted powders suffers from a number of recognised limitations. One of which is that in order to form a compact, the powder must undergo some change, such as plastic deformation, that may alter the properties of the powder [9, 12, 14]. In addition, as reported by Neumann and Good, 1979 [8], capillaries could exist in the compacts which may lead to unstable sessile drops as the liquid penetrates into the compact.

To bypass the need to form compacts, some researchers have adhered a thin layer of powder onto thin solid supports (with the use of adhesives), which can then be used as Wilhelmy plates [15]. The major limitation in this approach is the potential for the adhesive to spread over the particles and thus come in contact with the liquid, thereby affecting the measured contact angle [15].

3.3.1.1.1. Liquid Intrusion

The liquid intrusion method is a commonly used method to measure the contact angle of liquids to powders. The method takes advantage of the natural intrusion of a liquid into a bed of a powder, provided that the liquid makes a contact angle less than 90° . The principal attraction of this method is that the sample does not require modifying: it remains as its bulk powder form. In addition, especially with the introduction of automated instruments, the liquid intrusion method is a relatively quick and simple method to perform.

3.3.2. Background

Within a bed of powders, there are voids. Collectively, these voids act as a bundle of small capillaries that liquids can intrude. The rate at which a liquid intrudes into a powder bed is related to the contact angle of the liquid as described by Washburn in 1921 [16].

$$l^2 = \frac{r_c \gamma_L \cos \theta}{2\eta} t \quad (3.3)$$

where l is the intruded distance of the liquid front at time, t ; γ_L is the surface tension of the liquid, r_c is the effective capillary radius of the powder bed, θ is the contact angle of the liquid and η is the viscosity of the liquid.

However, due to difficulties in accurately visualising the liquid front as the experiment progresses, it is often more convenient to measure the mass of the intruded liquid rather than the intruded distance. For a cylindrical powder bed, the relationship between the intruded liquid mass and the distance of the liquid is given by [17]:

$$m = \pi R_c^2 l \rho \varepsilon \quad (3.4)$$

where m is the mass of the intruded liquid, R_c is the internal radius of the cylindrical column, ρ is the density of the liquid and ε is the porosity of the powder bed.

Substituting Equation (3.4) into Equation (3.3) gives the “modified” Washburn equation:

$$m^2 = \frac{C \rho^2 \gamma_L \cos \theta}{\eta} t \quad (3.5)$$

where $C = \frac{r_c}{2} (\pi R_c^2 \varepsilon)^2$ and is termed the *material constant*. This parameter reflects the packing geometry of the particles in the powder bed. As can be noted, a plot of mass squared versus time would result in a straight line. The gradient of this line can be used to determine the contact angle of the liquid.

However, as there are two unknown variables in Equation (3.5)—the material constant, C , and the contact angle, θ —the contact angle of the liquid cannot be determined directly with one liquid only. Consequently, another liquid must be used to determine the material constant. This is achieved by using a reference liquid, indicated

by subscript r , that is “perfectly wetting”, which means having a contact angle of 0° to the powder. Thus, Equation (3.5) can be reduced to:

$$\frac{m_r^2}{t_r} = \frac{C_r \rho_r^2 \gamma_{Lr}}{\eta_r} \quad (3.5a)$$

where $\cos \theta_r = 1$ as $\theta_r = 0^\circ$.

For a probe liquid, indicated by subscript p , it follows that:

$$\frac{m_p^2}{t_p} = \frac{C_p \rho_p^2 \gamma_{Lp} \cos \theta_p}{\eta_p} \quad (3.5b)$$

As liquid intrusion experiments require the powder bed to be completely wetted by the liquid, powder beds can only be used once. Therefore, additional powder beds must be prepared for each liquid. If the powder beds consists of the same powder material and are prepared by a standardised packing procedure, it is often assumed that the material constant of each powder bed are identical—that is, $C_p = C_r$ [18-23]. Therefore, substituting Equation (3.5a) into Equation (3.5b) gives:

$$\cos \theta_p = \frac{\rho_r^2 \gamma_{Lr} \eta_p}{\rho_p^2 \gamma_{Lp} \eta_r} \cdot \frac{m_p^2 t_r}{m_r^2 t_p} \quad (3.6)$$

which can be simplified to the following equation:

$$\cos \theta_p = F_l \cdot \frac{\text{Gradient}_p}{\text{Gradient}_r} \quad (3.6a)$$

where $F_l = \frac{\rho_r^2 \gamma_{Lr} \eta_p}{\rho_p^2 \gamma_{Lp} \eta_r}$ and is termed the *liquid factor*.

This is the current established approach for determining the contact angle of a liquid to a powder sample [18].

3.3.2.1. The Reference Liquid

In theory, the reference liquid must be a perfectly wetting liquid with a contact angle of 0° to the powder, thereby making it possible to determine the material constant of the powder bed. However, in reality, it is often a major challenge to demonstrate that a liquid shows a contact angle of 0° [24]. Instead, in practice, it is common to use a low surface tension liquid and assume its contact angle to the powder is 0° [25, 26]. If the reference liquid does not, in practice, make a contact angle of 0° with the powder, the calculated contact angle for the probe liquid will be incorrect.

Consequently, it is important for the selected reference liquid to possess a contact angle as close to zero as possible (if not exactly zero) to improve the accuracy of the calculated contact angle of a probe liquid. This may be achieved by the use of a low surface tension liquid, thereby increasing the likelihood of the liquid spreading over the surface of the powder. Historically, a liquid with a low surface tension commonly used is *n*-hexane [17, 20, 25]. Other commonly used reference liquids include: cyclohexane, short chain alcohols and other short chain *n*-alkanes [7, 10, 26, 27]. The choice of a low surface tension liquid may be justified by the spreading coefficient, S , [28]:

$$S = \gamma_S - (\gamma_{SL} + \gamma_L) \quad (3.7)$$

where γ_S is the surface energy of the solid and γ_{SL} is the interfacial energy of the solid/liquid interface. Spreading of the liquid occurs when $S \geq 0$ —in other words, a liquid is more likely to spread over a surface when the surface tension of the liquid is lower than the surface energy of the solid [1].

However, in practice, a lower surface tension liquid may not necessarily be a better wetting liquid, perhaps due to the chemistry of the liquid and surface of the solid. Therefore, as noted by Buckton *et al.*, 1985 [29], the choice of the reference liquid should preferably be based on experimental evidence.

3.3.2.2. Analysis of Multiple Measurements

Despite the use of the same standard packing procedure to prepare each powder bed, it is unlikely that different powder beds will possess identical material constants [17, 18]. Thus, in reality, the liquid intrusion method when studying powders is not a perfectly *matched* system. In other words, the material constant of the powder beds used with the probe liquid, C_p , and those used with the reference liquid, C_r , are not identical—that is, in reality $C_p \neq C_r$. The non-identical nature of C_p and C_r can be a source of error in the calculated contact angle of the probe liquid.

This is further complicated if replicate experiments are performed for the probe liquid and another set of replicate experiments for the reference liquid. As the material constant of the powder beds for the two liquids are not perfectly matched, there is no established methodology to *pair* the probe gradient with the reference gradient. In other words, there are multiple ways to divide the gradient of the probe liquid with the gradient of the reference liquid. Consequently, this provides a lack of control in data analysis as there are multiple combinations in which the data can be analysed. The simplest approach is to average the gradients of the probe liquid and the gradients of the reference liquid, Equation (3.6a) can then be used to calculate the contact angle of the probe liquid. However, the problem with that approach is that only a single value of the contact angle is obtained. Thus, to determine the variability in the obtained average contact angle, the variability of both the average gradients of the probe and reference liquid must be propagated through to the average contact angle, which is most likely to be a conservative estimate of the variability of the contact angle. This paper is targeted at this limitation and to the search for a more robust approach.

This paper aims to address some of the limitations of liquid intrusion experiments:

1. Selecting the most appropriate reference liquid and
2. Analysing multiple sets of reference and probe liquid data for which the material constant of each powder bed may not, necessarily, be identical.

3.3.3. Materials and Methods

3.3.3.1. Materials

Glass beads ($d_{50} = 10 \mu\text{m}$ with a span of 1.1 ± 0.04) were used as a model pharmaceutical active which was obtained from Cospheric LLC (CA, USA). *n*-Hexane (GC grade), absolute ethanol and acetone were purchased from Merck KGaA, Hesse, Germany. Milli-Q water was produced from a Direct-Q® 3 UV Water Purification System (Merck KGaA, Hesse, Germany). All materials were used as received.

3.3.3.2. Selecting the Most Appropriate Reference Liquid

For the case of two different liquids, indicated by subscript A and subscript B, intruding into a powder bed where the theory presented by Washburn (1921) [16] holds true, the rate of liquid intrusion by the two liquids can be expressed as Equation (3.5c) and Equation (3.5d), respectively:

$$\frac{m_A^2}{t_A} = \frac{C_A \rho_A^2 \gamma_{LA} \cos \theta_A}{\eta_A} \quad (3.5c)$$

$$\frac{m_B^2}{t_B} = \frac{C_B \rho_B^2 \gamma_{LB} \cos \theta_B}{\eta_B} \quad (3.5d)$$

For the case where the material constant of the powder beds are identical (or assumed to be identical), the division of Equation (3.5c) and Equation (3.5d) gives:

$$\frac{\text{Gradient}_A}{\text{Gradient}_B} = F_l \cdot \frac{\cos \theta_A}{\cos \theta_B} \quad (3.8)$$

For the specific case where both liquids wet the solid to the same extent—that is, when $\theta_A = \theta_B$ —Equation (3.8) can be simplified to:

$$Q_{AB} = F_l \quad (3.8a)$$

where $Q_{AB} = \frac{\text{Gradient A}}{\text{Gradient B}}$

Thus, for any case where $Q_{AB} \neq F_l$, it naturally follows that both liquids do not wet the solid to the same extent: one of the two liquids (either liquid A or liquid B) must be a poorer wetting liquid, hence having a larger contact angle compared to the other liquid. That is, if $Q_{AB} > F_l$, then liquid B must be the poorer wetting liquid with a larger contact angle (when compared to liquid A), while if $Q_{AB} < F_l$, then liquid A must be the poorer wetting liquid with a larger contact angle (when compared to liquid B). Therefore, the liquid with the lower contact angle should be used as the reference liquid.

To determine whether the calculated Q_{AB} values are significantly different from the F_l value, an appropriate statistical analysis, such as a one-sample t -test, can be performed.

3.3.3.3. Analysing Multiple Sets of Reference and Probe Liquid Data

Table 3-3 presents intrusion rates for both the probe and the reference liquid. Three possible methods of analysing data from multiple sets of probe and reference liquid intrusion rates are presented below:

Table 3-3: Example of five intrusion rates for a reference liquid and five intrusion rates for a probe liquid. The magnitude of the gradients' corresponding material constant, denoted by superscript (A-E), is ranked in order of: $A > B > C > D > E$.

Collection Order	Gradient	
	Reference (Liquid A)	Probe (Liquid B)
1	R_1^B	P_1^A
2	R_2^D	P_2^B
3	R_3^E	P_3^E
4	R_4^A	P_4^D
5	R_5^C	P_5^C
Average	$\bar{R} = \frac{R_1+R_2+\dots+R_5}{5}$	$\bar{P} = \frac{P_1+P_2+\dots+P_5}{5}$
Standard Deviation	$\sigma_R = \sqrt{\frac{1}{4} \sum_{i=1}^5 (R_i - \bar{R})^2}$	$\sigma_P = \sqrt{\frac{1}{4} \sum_{i=1}^5 (P_i - \bar{P})^2}$

Method 1 – Averaged Gradients:

The contact angle of the probe liquid is calculated based on the averaged gradients of both the probe liquid, \bar{P} , and the reference liquid, \bar{R} .

1. Average the gradients of the probe liquid and the gradients of the reference liquid.
2. Calculate the standard deviation of the gradients of both the probe and the reference liquid.
3. From the averaged gradients of the probe, \bar{P} , and reference, \bar{R} , liquid, calculate the contact angle of the probe liquid with Equation (3.6a) or Q_{AB} with Equation (3.8).
4. Estimate the error of the calculated averaged contact angle or Q_{AB} through Propagation of Error Theory, Equation (3.9) and Equation (3.10), respectively:

$$\sigma_{\theta} = \frac{\sqrt{\left(-\frac{F_L \bar{P}}{R^2} \sigma_R\right)^2 + \left(\frac{F_L}{R} \sigma_P\right)^2}}{\sqrt{1 - \left(\frac{F_L \bar{P}}{R}\right)^2}} \quad (3.9)$$

$$\sigma_{Q_{AB}} = |Q_{AB}| \sqrt{\left(\frac{\sigma_A}{\bar{A}}\right)^2 + \left(\frac{\sigma_B}{\bar{B}}\right)^2} \quad (3.10)$$

Method 2 – Data Collection Order:

The pairing of the intrusion rate of the probe liquid to the intrusion rate of the reference liquid is based on the sequence the data was collected.

1. Calculate the Q_{AB} for each replicate with Equation (3.8) or divide the gradient of the probe liquid by the gradient of the reference liquid based on the order the data was collected ($P_1/R_1, P_2/R_2, \dots, P_5/R_5$).
2. Calculate the contact angle of the probe liquid of each quotient with Equation (3.6a).
3. Calculate the average contact angle of the probe liquid or the Q_{AB} .

Method 3 – Rank of the Material Constants:

To minimise the error associated with the non-identical nature of C_p and C_r , the division of the gradient of the probe liquid by the gradient of the reference liquid should be done in such a way that the pore structure of the respective powder beds are as closely matched as possible. That is, to pair the probe gradient with the reference gradient based on their respective material constants. This can be achieved through the rank order of the material constants; thereby, the powder beds with the largest pore structure are more likely to be paired together, while powder beds with the smallest pore structure are more likely to be paired together.

1. To obtain the rank order of the material constant of the powder beds used with the probe liquid, C_p , first calculate C_p by fixing the contact angle of the probe liquid, θ_p , to an arbitrarily value between 0° and 90° . Use Equation (3.5b). Rank C_p from smallest to largest.
2. Sort the gradients of the probe liquid based on the rank order of C_p (smallest to largest).
3. Calculate the material constant of the powder beds, C_r , used with the reference liquid with an assumed $\theta_r = 0^\circ$. Use Equation (3.5a). Rank C_r from smallest to largest.

- Sort the gradients of the reference liquid based on the rank order of C_r (smallest to largest).
- Calculate Q_{AB} with Equation (3.8) or divide the gradient of the probe liquid by the gradient of the reference liquid based on the new order (P_3^E/R_3^E , P_4^D/R_2^D , ..., P_1^A/R_4^A).
- Calculate the contact angle of the probe liquid of each quotient with Equation (3.6a).
- Calculate the average contact angle of the probe liquid or the average Q_{AB} .

3.3.3.4. Case Study

Liquid intrusion studies were performed with an automated tensiometer (Sigma 700, Attension, Biolin Scientific, Stockholm, Sweden), refer to Figure 3-4 for details.

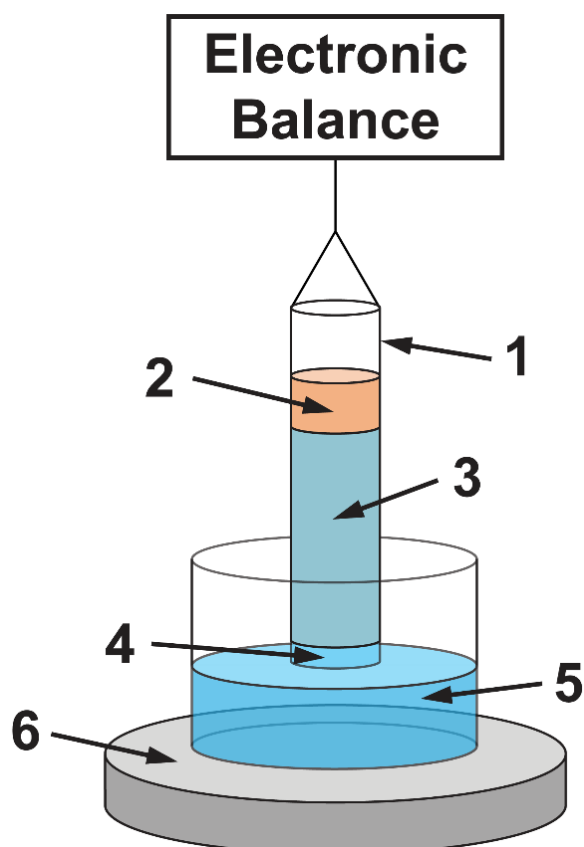


Figure 3-4: Schematic of a liquid intrusion setup. 1. Glass column, 2. Powder bed (un-wetted), 3. Powder bed (wetted), 4. Glass frit, 5. Liquid reservoir and 6. Mobile stage.

Powder beds were prepared by pouring approximately 1.24 g of glass beads through a funnel at a fixed height into a custom made borosilicate glass column (50 mm x 10 mm ID) with a POR 2 borosilicate sintered glass frit (pore size of 40-100 μm) as a base to retain the powder (Monash Scientific, Melbourne, Australia). In order to ensure the integrity of the glass frit, 1 layer of filter paper (pre-cut 10 mm diameter Whatman Grade 1 filter paper, Whatman PLC., Kent, UK) was placed in the column prior to loading of the sample. The column was cleaned prior to each experiment by washing and rinsing with Milli-Q water, ethanol and acetone. The column was then dried with a stream of dry compressed air.

Packing of the powder beds were achieved by tapping the filled columns 200 times with an automatic tapping instrument (AUTOTAP™, Quantachrome Instruments, FL, USA). The tapper operated with a 3.18 mm vertical tap at a tapping speed of 260 taps/min.

Tapped columns were suspended over the liquid reservoir and the liquid was raised until it just contacted the base of the column. All liquid intrusion studies were performed at $25\pm 2^\circ\text{C}$ with freshly packed powder beds. Replicates of five were performed for all samples with all liquids. Table 2 presents the liquid properties (density, viscosity and surface tension) of all liquids used at 25°C .

Table 3-4: Liquid properties of *n*-hexane, ethanol and water at 25°C [30].

Liquid	Density (kg/m^3)	Viscosity ($\text{Pa}\cdot\text{s}$)	Surface tension (N/m)
<i>n</i> -Hexane	654.466	0.000300	0.01789
Ethanol	784.855	0.001074	0.02197
Water	997.047	0.000890	0.07199

After the construction of the mass squared versus time plots, the linear region of interest (LROI) was identified. To ensure robust data analysis, a simple guideline was developed to identify the LROI of mass squared versus time plots. The LROI was identified as the linear region before the plateau, refer to Figure 3-5.

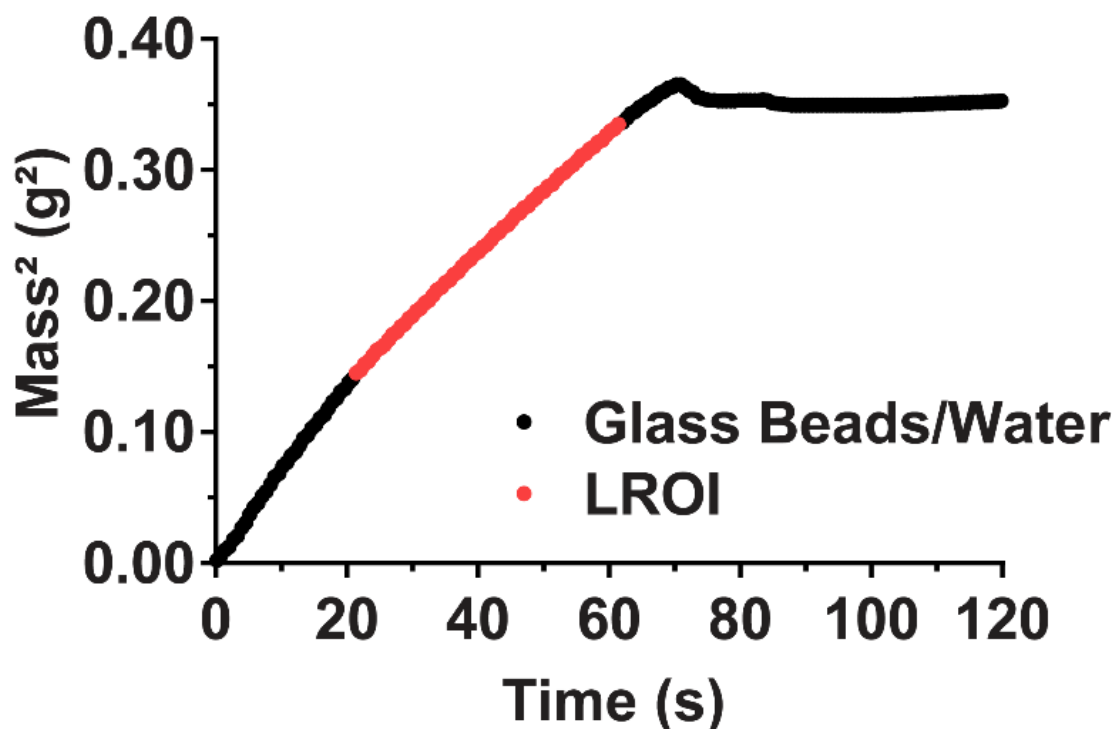


Figure 3-5: Mass squared versus time plot for water intruding into a powder bed of glass beads with the LROI highlighted.

The contact angle of the probe liquid was then calculated according to the methods described in Chapter 3: Section 3.3.3.3.

3.3.3.5. Statistical Analysis

To determine whether Q_{AB} is significantly different from F_l , statistical analysis was achieved with a one-sample t -test where a significant difference was obtained if $p < 0.05$ (IBM SPSS Statistics v23.0, IBM Corp., NY, USA). A normal distribution was assumed for all cases.

3.3.4. Results and Discussions

Table 3-5 presents the intrusion rates of all test liquids intruding into fresh powder beds of glass beads.

Table 3-5: Intrusion rates of *n*-hexane, ethanol and water intruding into powder beds of glass beads at 25±2° C. The data is presented in the order of collection.

<i>n</i>	Gradient (g ² /s)		
	<i>n</i> -Hexane	Ethanol	Water
1	0.00557	0.00415	0.00473
2	0.00699	0.00434	0.00441
3	0.00974	0.00396	0.00493
4	0.00613	0.00468	0.00514
5	0.00774	0.00482	0.00474
Average	0.00724	0.00439	0.00479
SD	0.00163	0.000362	0.000272
RSD	22.5	8.2	5.7

SD = Standard deviation, RSD = Relative standard deviation

It is worth noting the large variation in the intrusion rate of *n*-hexane into powder beds of the glass beads: at approximately 20%. The reason for such a large variation is perhaps related to the properties of the liquid, specifically the highly volatile nature of *n*-hexane, though further investigation is needed to provide a more complete understanding. Nonetheless, such data is worth including as it reflects some of the possible outcomes of liquid intrusion studies.

As can be noted from Table 3-5, *n*-hexane has a faster intrusion rate than ethanol, which, when coupled with the fact that it also has a lower surface tension compared to ethanol [30], may suggest that *n*-hexane is the better wetting liquid with a smaller contact angle. However, it is important to note that the intrusion rate of a liquid is dependent on three factors—the contact angle of the liquid to the powder, θ ; the pore structure of the powder bed, C ; and the liquid properties, $\rho^2\gamma_l/\eta$. Consequently, to determine which of the two liquids is, in fact, the better wetting liquid, both the intrusion rate and the liquid parameters must be taken into account.

Table A.1 (Appendix) present the Q_{AB} values for *n*-hexane to ethanol calculated according to Method 1 and Method 2, while the Q_{AB} value for Method 3 is presented

in Table A.2 (Appendix). Table A.3 (Appendix) presents the contact angle of water to the glass beads, calculated based on Method 1 and Method 2, while the contact angle calculated based on Method 3 is presented in Table A.4 (Appendix).

When Q_{AB} was calculated according to Method 1, a value of 1.648 ± 0.394 was obtained. However, when Method 2 was used, a value of 1.666 ± 0.467 was obtained, which is not significantly different to a F_l value of 2.028 (*n*-hexane to ethanol at 25° C)—suggesting that both *n*-hexane and ethanol wetted the glass beads to the same extent. In contrast, when calculated according to Method 3, the Q_{AB} value was 1.634 ± 0.237 , which is significantly different to a F_l value of 2.028. This suggests that ethanol is the better wetting liquid for the system used. Given that ethanol is expected to wet the glass beads just as well as *n*-hexane, or better, and the associated health risks associated with *n*-hexane, ethanol was selected as the reference liquid. As observed in Table A.3 (Appendix), the contact angle of water when Method 1 was used was $80.2 \pm 0.02^\circ$. When Method 2 was used, the contact angle was found to be $80.1 \pm 1.0^\circ$, while calculated through Method 3, a contact angle of $80.1 \pm 0.3^\circ$ was obtained.

However, it is worth noting that the three methods used to analyse the liquid intrusion data produced similar average Q_{AB} values and contact angles. This is not surprising as the calculation of Q_{AB} and contact angles was performed with the same set of intrusion rates of *n*-hexane, ethanol and water. Where they differ is in their advantages and limitations.

Notwithstanding the simplicity of Method 1, the major advantage here is that it eliminates the need to individually divide the gradients of the probe liquid by that of the reference liquid. However, it must be stated that the major caveat of this method is that because only a single value of Q_{AB} is obtained, further statistical analysis, for instance, to determine whether the Q_{AB} value is significantly different to its corresponding F_l value, can be difficult—at best, the error associated with the average value can only be conservatively estimated through Propagation of Error Theory.

Alternatively, the gradients of the probe liquid can be individually divided by that of the reference liquid based on the procedures outlined in Method 2 or Method 3. In doing so, a distribution of values is obtained, which directly provides information about the precision of the experiment. However, the limitation of Method 2 is that the data is paired based on the sequence the data was conducted. Consequently, the appropriateness and the potential accuracy of the calculated Q_{AB} value or contact angles is arbitrarily set. Unlike Method 2, Method 3 aims to pair data rationally based on how similar the C_r value is to the C_p value, that is, the powder beds are matched by how likely their pore structures are similar to one another. Consequently, a higher precision is expected for Method 3, which was observed in both the calculated Q_{AB} and the contact angles.

However, it must be highlighted that as the Washburn equation is non-linear relative to the contact angle of a liquid, due to the presence of a $\cos(\theta)$ term, the effectiveness of these methods of analyses is dependent on the contact angle of the liquids used. However, in general, as the difference between the contact angles of the two liquids become larger or as the contact angles approach the upper end of the range, that is 90° , there is less difference in the effectiveness of the different methods of analyses. Consequently, the choice of which method to use to analyse liquid intrusion data is dependent on the system being studied. Additionally, the non-linear nature of the Washburn equation also has an effect on the amount of variability in the calculation of contact angles. If the contact angle of a liquid is towards the lower end of the range (that is, 0°), the variability in the average contact angle is likely to be larger, measured in whole degrees, while the converse is true for contact angles towards the upper range, where the variability is likely to be smaller, measured in fractions of a degree. This could explain the variability of the contact angle of water to the glass beads being less than 1° , especially with Method 1 and Method 3.

One possible criticism with the current experimental analysis is the use of glass beads as the spherical particles do not truly represent real powders within the pharmaceutical industry. However, the use of non-uniform or irregularly shaped powders is more likely to have a greater effect on the liquid intrusion profile, where, for instance, there may

be different “regions” within the profile such as step-wise changes in the squared mass gain versus time plots. This can make the identification of an LROI difficult. However, if a suitable LROI can be identified, the analysis of the data does not change regardless of which method was used as all the methods must assume that the packing of the powder bed is constant: ergo the term *material constant*.

3.3.5. Conclusions

This paper addressed three of the major limitations of the current established approach to the data analysis of liquid intrusion experiments for powders:

1. the selection of the reference liquid,
2. pore structure of different powder beds and
3. dealing with multiple sets of replicate experiments for probe and reference liquids.

It is proposed that the selection of the reference liquid should be based on experimental data where both the real world intrusion rate and the properties of the liquid are taken into account. In such an analysis, the liquid with the lower contact angle should be selected as the reference liquid.

In practice, the pore structure of different powder beds are not likely to be identical, that is $C_p \neq C_r$. This can lead to difficulties in data analysis where multiple replicate experiments are conducted for the probe and the reference liquid. Here, three methods of data analysis are proposed. The quickest and simplest method (Method 1) is to average the gradients of both the probe and reference liquid. The contact angle is then calculated based on the two averaged gradients. However, in doing this, a single contact angle is obtained. The variability associated with the average value, is estimated through the Propagation of Error Theory. The second method (Method 2) pairs the gradients based on the sequence the data was collected. The third method (Method 3) aims to rationally pair the data based on how similar the pore structure of the powder beds were based on the rank order of the respective material constants.

The selection of which method to use to pair data is dependent on the obtained data. The advantage of pairing data via Method 2 and Method 3 is that a distribution in the contact angle is obtained, which is not the case for Method 1. The advantage of Method 3 is that because the pairing of data is performed based on matching how similar the pore structure of the powder beds were (as measured by the material constants), the error associated in the calculation of the contact angle as a result of the non-identical nature of C_p and C_r is expected to be minimised.

3.3.6. Acknowledgements

The authors are grateful to Dr. A. Sudbury and Dr. D. Tokarev for the fruitful discussions. GT is thankful for the financial support of Graduate Research, Monash University, for providing a Monash Equity Scholarship.

3.3.7. References

- [1] Erbil HY, Surface chemistry of solid and liquid interfaces, Blackwell, Oxford, UK, 2006.
- [2] Davies P, Oral solid dosage forms, in: Gibson M (Ed.) Pharmaceutical preformulation and formulation: A practical guide from candidate drug selection to commercial dosage form, 2nd ed., Informa Healthcare, NY, USA, 2009, 367-430.
- [3] Parikh D, (Ed.) Handbook of pharmaceutical granulation technology. 3rd. ed., CRC Press, NY, USA, 2010.
- [4] Aulton ME, Banks M, Smith DK, The wettability of powders during fluidized bed granulation, J Pharm Pharmacol. 29(1977) 59P-P.
- [5] Schubert H, Food particle technology. Part I: Properties of particles and particulate food systems, J Food Eng. 6(1987) 1-32.
- [6] Rowley G, Pearson JT, Hussain MSH, Hartup E, Jones BE, A method for improving the wetting and dissolution properties of hydrophobic drugs of low aqueous solubility, J Pharm Pharmacol. 37(1985) 111P-P.
- [7] Kiesvaara J, Yliruusi J, Ahomäki E, Contact angles and surface free energies of theophylline and salicylic acid powders determined by the Washburn method, Int J Pharm. 97(1993) 101-9.
- [8] Neumann AW, Good RJ, Techniques of measuring contact angles, in: Good RJ, Stromberg RR (Eds.), Surface and Colloid Science, Plenum Press, NY, USA, 1979, 31-91.
- [9] Buckton G, Assessment of the wettability of pharmaceutical powders, J Adhes Sci Technol. 7(1993) 205-19.

- [10] Parsons GE, Buckton G, Chatham SM, The extent of the errors associated with contact angles obtained using liquid penetration experiments, *Int J Pharm.* 82(1992) 145-50.
- [11] Buckton G, Newton JM, Assessment of the wettability of powders by use of compressed powder discs, *Powder Technol.* 46(1986) 201-8.
- [12] Kiesvaara J, Yliruusi J, The effect of compression force and compression pressure on the surface free energy of tablets, *Acta Pharm Nord.* 3(1991) 171-7.
- [13] Young SA, Buckton G, Particle growth in aqueous suspensions: the influence of surface energy and polarity, *Int J Pharm.* 60(1990) 235-41.
- [14] Buckton G, Characterisation of small changes in the physical properties of powders of significance for dry powder inhaler formulations, *Advanced Drug Delivery Reviews.* 26(1997) 17-27.
- [15] Dove JW, Buckton G, Doherty C, A comparison of two contact angle measurement methods and inverse gas chromatography to assess the surface energies of theophylline and caffeine, *Int J Pharm.* 138(1996) 199-206.
- [16] Washburn EW, The dynamics of capillary flow, *Physical Review.* 17(1921) 273-83.
- [17] Grundke K, Boerner M, Jacobasch HJ, Characterization of fillers and fibres by wetting and electrokinetic measurements, *Colloids Surf.* 58(1991) 47-59.
- [18] Studebaker ML, Snow CW, The influence of ultimate composition upon the wettability of carbon blacks, *The Journal of Physical Chemistry.* 59(1955) 973-6.
- [19] Shi Q, Gardner DJ, Wang JZ, Surface properties of polymeric automobile fluff particles characterized by inverse gas chromatography and contact angle analysis. Fourth International Conference on Woodfiber-Plastic Composites; 1997; WI, USA: Forest Products Society; 1997. p. 245-56.
- [20] Teipel U, Mikonsaari I, Determining contact angles of powders by liquid penetration, *Part Part Syst Charact.* 21(2004) 255-60.
- [21] Galet L, Patry S, Dodds J, Determination of the wettability of powders by the Washburn capillary rise method with bed preparation by a centrifugal packing technique, *J Colloid Interface Sci.* 346(2010) 470-5.
- [22] Chen M, Wu S, Tang W, Gong J, Caking and adhesion free energy of maltitol: Studying of mechanism in adhesion process, *Powder Technol.* 272(2015) 235-40.
- [23] Hammes MV, Englert AH, Noreña CPZ, Cardozo NSM, Effect of water activity and gaseous phase relative humidity on microcrystalline cellulose water contact angle measured by the Washburn technique, *Colloids Surf, A.* 500(2016) 118-26.
- [24] Marmur A, Kinetics of penetration into uniform porous media: Testing the equivalent-capillary concept, *Langmuir.* 19(2003) 5956-9.
- [25] Jaine JE, Mucalo MR, Measurements of the wettability of catalyst support materials using the Washburn capillary rise technique, *Powder Technol.* 276(2015) 123-8.
- [26] Chibowski E, Perea-Carpio R, Problems of contact angle and solid surface free energy determination, *Adv Colloid Interface Sci.* 98(2002) 245-64.
- [27] Prestidge CA, Ralston J, Contact angle studies of particulate sulphide minerals, *Minerals Engineering.* 9(1996) 85-102.
- [28] Harkins WD, Feldman A, Films. The spreading of liquids and the spreading coefficient, *J Am Chem Soc.* 44(1922) 2665-85.
- [29] Buckton G, Newton JM, Assessment of the wettability and surface energy of a pharmaceutical powder by liquid penetration, *J Pharm Pharmacol.* 37(1985) 605-9.

[30] Haynes WM, Bruno TJ, Lide DR, (Eds.), Handbook of chemistry and physics. 95th ed., CRC Press, FL, USA, 2015.

Chapter 4:
**Evaluating the Flow of Surface
Modified Fine Powders with Varying
Amounts of Magnesium Stearate
Through Different Flowability Tests**

Geoffrey Tan

Bachelor of Pharmaceutical Sciences (Honours)

Drug Delivery, Disposition and Dynamics, Monash Institute of Pharmaceutical
Sciences. 381 Royal Parade, Parkville, VIC, 3052, Australia

Chapter 4: Evaluating the Flow of Surface Modified Fine Powders with Varying Amounts of Magnesium Stearate Through Different Flowability Tests

4.1. Commentary

In this chapter, Objective 2 “To measure the flowability of the fine powder as well as the surface modified powder” is addressed. The effect on the flowability of a fine powder (micron-sized glass beads) when dry coated with varying amounts of a pharmaceutical lubricant (magnesium stearate) was investigated. The flow behaviours of both uncoated and magnesium stearate coated micron-sized glass beads were evaluated and the results are discussed. Additionally, a comparison of the different techniques to assess the flow of the powders was made.

4.2. Abstract

Dry coating cohesive fine powders with a pharmaceutical lubricant can be an effective approach to improve the flow of poor flowing fine powders. In this study, micron-sized glass beads (MGB) were dry coated with varying amounts of magnesium stearate (MgSt). The flowability of the resultant powders was evaluated with different techniques: density measurements (expressed as the Carr index), compressibility, basic flowability energy, measurements of flow rate via the FlowPro and shear cell testing (cohesion, flow function and angle of internal friction).

The flow of the powders was dependent on both the amount of MgSt used as well as the method used. The minimum amount of MgSt required to improve flow was 0.1% w/w. Optimal flow was observed for powders with 0.1-0.25% w/w MgSt. With 0.05% w/w MgSt, the flow of the powder was observed to be complex. These powders were only able to flow better than MGB when undergoing unconfined flow or mechanically induced flow. Large amounts of MgSt increased the cohesiveness of the powder which resulted in suboptimal flowing powders.

4.3. Introduction

Fine powders are commonly used in the pharmaceutical industry largely due to their inherent advantages such as enhanced dissolution rates. However, their use can often present significant challenges, many of which can be attributed to their cohesive properties. For instance, the continuous, efficient and optimal manufacturing of quality pharmaceutical dosages such as tablets and capsules may not always be possible as many fine powders are inherently poor flowing. Consequently, production can come to a halt as pipes and hoppers can clog until manual intervention occurs to restore flow [1, 2]. Unsurprisingly, the poor flow of fine powders can ultimately lead to economic losses [2-5].

Furthermore, with the introduction of the Pharmaceutical Quality for the 21st Century initiative by the US Food and Drug Administration (FDA), which encompasses a Quality by Design (QbD) framework, along with guidelines from other regulatory bodies such as the International Conference on Harmonization on Technical Requirements (ICH) [6, 7], there is a greater emphasis on pharmaceutical manufacturers to better understand their manufacturing processes. Consequently, manufacturers need to determine which factors are important in determining the Critical Quality Attributes (CQA) of their final products and then monitor and control these factors to ensure the production of quality products. Among the important factors that impact the CQA of tablets and capsules is powder flow. Therefore, a practical method to improve and evaluate the flow behaviours of fine powders is of substantial importance.

Powder flow occurs as a result of an imbalance of two opposing forces: the flow promoting force and the cohesive force [2, 4, 8-11]. The flow promoting force, as its name suggests, is a force that acts to promote the flow of powders, for instance gravity [1]. Conversely, the cohesive force is an attractive force that results from the existence of inter-particle interactions such as van der Waals interactions and capillary forces between contacting surfaces. These inter-particle interactions limit the movement of particles and thus flow [1, 8, 12, 13]. In order for powders to flow, the flow promoting

force must be greater than the cohesive force to break the cohesive contacts, thereby allowing particle movement. However, for fine powders, as they are relatively light (due to their small size), the inter-particle interactions within the cohesive contacts can often overwhelm the flow promoting force, thus reducing powder flow [1, 14].

Powder flow is also influenced by a multitude of external factors, some of which include the hardness of the particles and the state of consolidation (or aeration) of the powder [11]. For instance, when powders consolidate and the particles compress against one another, the particles can deform and flatten around the regions where they contact [15]. As a result of this deformation, the contact area between adjacent particles increases. With more surface in contact, more inter-particle interactions can occur, which effectively increases the cohesiveness of the powder and thus results in poorer flowability [15]. Consequently, as softer particles are able to deform more easily than harder particles, particles that are relatively soft are more likely to flow more poorly than harder particles. The state of consolidation (or aeration) of powders can also have a pronounced effect on the flow behaviour of powders [4, 16]. For instance, a powder may show good flow while in a non-consolidated (or low consolidated) state but show poor flow under higher consolidation such as when flowing out of a hopper [16, 17]. With a very few exceptions, as powders consolidate their flow typically becomes poorer [18]. This decreased flowability occurs because of an increase in the average number of contacts between adjacent particles [3, 19]. Consequently there are more inter-particle interactions, thus increasing the overall cohesive force [3, 19]. Furthermore, not only can powders behave as solids when consolidated, they can also behave as liquids when aerated or even as gases when suspended in a gas [20].

To improve the flow of fine powders, particle engineering methods, such as the mechanofusion system (Hosokawa Micron Powder Systems, Japan), where the surfaces of fine powders are modified can be used. By subjecting the fine powder (host) and a coating powder (guest) to high stresses in a mechanofusion system, a thin coating of the guest particles can form on the surfaces of the host particles thereby effectively masking the surfaces of the host particles [21-24]. With a layer of guest particles, inter-particle interactions between contacting coated particles are likely to be

different to the original host particles. This would, in theory, also alter how the coated powder flows. For example, when fine powders were dry coated with magnesium stearate via mechanofusion, the fine powders flowed more easily [21, 25-30].

A practical ability to assess the flow behaviours of powders is also important. However, this can be challenging as there are numerous processes within pharmaceutical manufacturing where powders are required to flow under different conditions. For instance, powder flow occurs during blending and transporting; powders flow out of hoppers, silos and bins; and powder flow also occurs when filling tablet dies, capsule shells and sachets [5, 8, 31, 32]. Thus, powders may potentially exhibit different flow behaviours during the manufacturing process [4, 5, 8, 31, 32]. Consequently, there is no single method that is able to assess the various flow behaviours powders can potentially exhibit [32, 33]. Thus, to gain a more complete assessment of the flow behaviours powders can exhibit, it is often necessary to evaluate powders with a range of methods [32, 33]. Although there is no definitive list of what methods are recommended, the general guideline is to select a range of methods that closely resembles the different flow regimes the powder encounters during the manufacturing process [32, 33]. For instance, Carr index may be a useful method to predict potential problems with capsule filling in dosator capsuling operations [34]. Alternatively, to ensure optimal flow of powders out of hoppers, silos, bins or intermediate bulk containers (IBCs), shear cell testing may be performed to determine the optimal dimensions of manufacturing, transporting and storage equipment [16, 18]. Operations where powders undergo dynamic flow, for instance during blending, may correlate well with methods that assess dynamic flow behaviours, such as measuring basic flowability energy or powder avalanching [35]. Alternatively, dynamic flow measurements such as basic flowability energy may be a useful and practical method to aid in the determination of wet granulation end-point [36-39].

Despite the many different types of powder flow, the flow of powders can be very broadly categorised as confined, unconfined or consolidated flow. Confined flow occurs when powders start from an unconsolidated (or low consolidated) state and the flow of the powders results in significant increases in powder consolidation, while

unconfined flow occurs when the flow of powders does not result in significant increases in powder consolidation. In contrast to confined flow, when powders are already in a consolidated state, due to the presence of a consolidating pressure, and flow occurs while the powders are still under consolidation, then consolidated flow is said to have occurred.

Although there are a large number of available techniques to assess powder flow, only the most commonly used techniques to assess powder flow are used in this study and are briefly discussed below (for a more comprehensive discussion refer to Chapter 1: Section 1.8 Measuring the Flow of Powders and [2, 8, 33, 40]).

When poor flowing powders are freshly poured into containers, the powders naturally form powder beds with large voids and thus small *bulk densities*. The large voids result from relatively strong cohesive forces that prevent the particles from flowing past one another to fill the voids below [40-42]. Upon disturbances, for instance, from tapping, the supplied energy from each tap may be sufficient to break the relatively strong cohesive forces and allow the particles to flow past one another under the influence of gravity [8]. Consequently, the particles rearrange themselves to fill the voids below, thus consolidating the powder bed and increasing the density of the powder bed. This consolidated density is termed the *tapped density*.

The bulk and tapped densities of powders can be used to calculate their compressibility as described by Equation (4.1), this is known as the Carr index (*CI*) [43]:

$$CI = \frac{\rho_t - \rho_b}{\rho_t} \quad (4.1)$$

where ρ_b and ρ_t are the bulk and tapped densities of powders, respectively.

Because the flow of powders during density measurements results in powders flowing downwards into a confined space (as there are no openings at the bottom of the container) with each tap, the flowing powder will inevitably consolidate and because

powder flow occurs due to gravitational forces, Carr indices can be considered indirect measurements of confined gravitational flow. The advantages of the Carr index are: it is a quick, simple and cost-effective method to assess the relative strength of inter-particle interactions of powders. Limitations of this method includes its inability to take into account the effect of powder consolidation on powder flow and it is not suitable to assess the flow of highly cohesive powders that are very poor flowing.

As a rule, poor-flowing powders typically possess large Carr indices due to large increases in density after tapping. The exception to this are powders that are so cohesive that tapping is not energetic enough to break the strong cohesive force [44]. The small Carr indices calculated for highly cohesive powders misleadingly suggest good powder flow. More forceful methods to compress the powder bed, such as a mechanically driven piston, may overcome the limitation from tapping [45]. Such methods are referred to as compressibility measurements. Compressibility measurements can be considered indirect measurements of confined mechanical flow as the powders are mechanically made to flow into a confined space. The advantages of the compressibility measurements are: they are relatively simple methods to assess flow and are likely a suitable method to assess the flow of highly cohesive powders that are very poor flowing. The limitation of this method is that the consolidation effect on powder flow is also not taken into account.

An increasingly common method to evaluate flow is through the use of a powder rheometer such as the FT4 Powder Rheometer (Freeman Technology Ltd., UK). In the case of the FT4 Powder Rheometer, a motorised twisted blade (see Figure 4-1) is rotated through the powder bed at a controlled and constant speed [46].



Figure 4-1: Image of the twisted blade used with the FT4 Powder Rheometer (Freeman Technology Ltd., UK).

Flow is measured as the energy required to maintain constant rotation of the blade as the blade continuously moves down through the powder. This energy is termed the basic flowability energy (BFE). More flowable powders are expected to present less resistance to the rotating blade, thus requiring less energy to maintain the constant rotation of the blade, thereby resulting in lower BFE [46]. As there is a “bulldozing” effect on the powder while the twisted blade moves down through the powder, BFE measurements can be considered dynamic measures of confined mechanical flow. The advantage of this method is that the flow is assessed in a dynamic manner. The limitation of the BFE measurement is that such measurements are limited only to other measurements based on the FT4 Powder Rheometer thus difficulties may arise when comparing data from other instruments.

Measurements of the flow rate of powders through an orifice of a container per unit time are also dynamic measurements of flow [47-49]. Not surprisingly, more flowable powders typically have faster flow rates. As powders are able to flow out of the container through the orifice, significant increases in powder consolidation does not occur; thus, flow rate measurements can be considered as direct measurements of unconfined flow. Traditionally, measuring the flow of powders through an orifice has been limited to powders that are relatively flowable [42]. However, to aid in measuring the flow of cohesive powders, Intelligent Pharmaceuticals Oy recently released the FlowPro (Intelligent Pharmaceuticals Oy, Finland) [50]. In brief, it operates by vertically tapping a sample cuvette to induce powder flow of cohesive fine powders which is then measured via an inbuilt balance. Early studies have shown good promise in measuring the flow of cohesive powders [49-52]. However, it must be noted that measurements of the flow of powders through an orifice is often dependent on the experimental setup and thus measurements with the FlowPro may not necessarily be comparable with other instruments.

As the effect of consolidation on powder flow is of significant relevance to the handling of bulk powders in the pharmaceutical industry, shear cell testing is an important method to evaluate the flowability of powders [16, 45]. For example, powders at the bottom of bulk storage containers (hoppers, bins and silos) can experience high consolidation pressures [16]. Consequently, if the flow of a powder is susceptible to the effect of consolidation, the powder may show unsatisfactory flow out of bulk storage containers or even cause a blockage [17]. Thus, shear cell testing provides invaluable information on how powders flow especially when designing equipment for bulk powder storage and handling [16].

By measuring the shear stress required to cause powder flow whilst the powder is under varying levels of consolidation, mechanical properties such as the cohesion coefficient (or simply cohesion), flow function coefficient (or simply flow function, ff_c) and the angle of internal friction (AIF) can be determined. Typically, larger ff_c values correspond to better flowing powders with the general guidelines: $ff_c < 1$ = non-flowing, $1 < ff_c < 2$ = very cohesive, $2 < ff_c < 4$ = cohesive, $4 < ff_c < 10$ = easy flowing,

and $ff_c > 10$ = free flowing [16, 29, 53, 54]. Large cohesion and AIF values corresponds to poorer flowing powders. As powders undergo a pre-shear phase prior to each shear measurement (for a more detailed discussion on the shear cell procedure, the reader is invited to read [16, 18]), flow measurements from shear cell testing assesses the flowability of powders whilst the powder is under consolidative pressures. The advantage of shear cell testing is that it is able to take into account the effects of powder consolidation on powder flow. The limitation of shear cell testing is that it is not a quick nor simple measurement.

4.4. Materials and Methods

4.4.1. Materials

Micron-sized glass beads (MGB) ($d_{50} = 10 \mu\text{m}$) (Cospheric LLC, USA). MGB dry coated with varying amounts of magnesium stearate NF (MgSt) (Mallinckrodt Baker Inc., USA) (0.05, 0.1, 0.175, 0.25, 0.5, 0.75, 1 and 2% w/w MgSt). For details on the dry coating process, refer to Chapter 2: Surface Modification and Physical Characterisation of a Model Pharmaceutical Powder Section 2.3.1 Particle Engineering via Dry Coating. The dry coated powders are labelled as M-MGB-X where X is the weight percentage of the MgSt.

4.4.2. Methods

4.4.2.1. Sample Pre-conditioning

Unless otherwise stated powders were freshly sieved through a 250 μm mesh prior to flow measurements to remove the effects of powder history.

4.4.2.2. Powder Densities and their Carr Indices

To determine the Carr index, the bulk density, ρ_b , was measured by slowly pouring approximately 7-8 ml of freshly sieved powder into a calibrated 10 ml measuring

cylinder through a funnel held at a fixed height above the measuring cylinder. The mass and volume of the powder within the measuring cylinder were then measured. The tapped density, ρ_t , of the powder was determined by measuring the new volume of the powder bed after 1250 taps with an automated tapping apparatus (AUTOTAP™, Quantachrome Instruments, USA). The tapper operated with a 3.18 mm vertical tap and a tapping rate of 260 taps/min. Replicates of four were conducted for all powders. The Carr index, CI , for all powders was calculated with Equation (4.1).

4.4.2.3. Compressibility Measurements

The compressibility of the powders was evaluated with the FT4 Powder Rheometer (Freeman Technology Ltd., UK) using a vented piston. Details of the method can be found elsewhere [33, 46]. Briefly, a 10 ml split vessel was filled approximately 2 mm above the split level with freshly sieved powders. The powder was subjected to an automated conditioning step performed by the FT4 before the vessel was split to produce a powder bed with a flat surface. Compression of the powder bed was achieved with a normal stress of 1, 2, 4, 6, 8, 10, 12, and 15 kPa. All tests were conducted in triplicate.

4.4.2.4. Basic Flowability Energy

The basic flowability energy (BFE) was measured with a FT4 Powder Rheometer (Freeman Technology Ltd., UK) using a 23.5 mm diameter twisted blade and a 25 ml split vessel. Details of this test have been described elsewhere [33, 46]. Briefly, the split vessel was filled approximately 2 mm above the split level with freshly sieved powders. The powder was subjected to an automated conditioning step and the vessel was then split to produce a powder bed with a flat surface. The test cycle involved passing the twisted blade through the powder bed in a controlled path with a rotational speed of 10-100 mm/s. Replicates of three were conducted for all powders.

4.4.2.5. Flow Rate

The flow rate of the powders out of an orifice was measured with a FlowPro (Intelligent Pharmaceuticals Oy, Finland). Details of the instrument can be found elsewhere [33]. Briefly, the instrument consists of a balance to measure mass gain with time. Directly above the balance is a stainless-steel cylindrical cuvette with an orifice diameter of 3.0 mm with a vertically tapping motor. Approximately 1.75 g of powder was slowly poured into the cylindrical cuvette through a funnel at a fixed height above the sample cuvette. To retain the powder within the sample cuvette until the start of the measurement, the base of the sample cuvette was stoppered with parafilm. Analysis of the data was achieved with FlowPro software v1.1.1713. Replicates of four were conducted for all powders.

4.4.2.6. Shear Cell Testing

Shear cell testing was performed with a FT4 system (Freeman Technology, UK) using the 1 ml shear cell module. A detailed description of shear cell testing can be found elsewhere [55]. Briefly, approximately 2.5 g of freshly sieved powder was first conditioned by the FT4 system. After the conditioning step, the powder was compressed to 9 kPa with a vented piston and then the module was split to produce a 1 ml powder bed with a flat surface. The shear stress was measured with respect to each normal stress of 7, 6, 5, 4, and 3 kPa with a pre-shear normal stress of 9 kPa. Replicates of five were conducted for each powder.

4.4.2.7. Statistical Analysis

Statistical analysis was achieved with a one-way analysis of variance (ANOVA) with a Tuckey's *post hoc* analysis where a significant difference was obtained if $p < 0.05$ (IBM SPSS Statistics v23, IBM Corp., USA).

4.5. Results

Carr indices for the powders are presented in Figure 4-2. The Carr index of MGB was approximately 0.42 ± 0.01 , indicating that MGB is a poor flowing powder which agrees with visual observations of the powder.

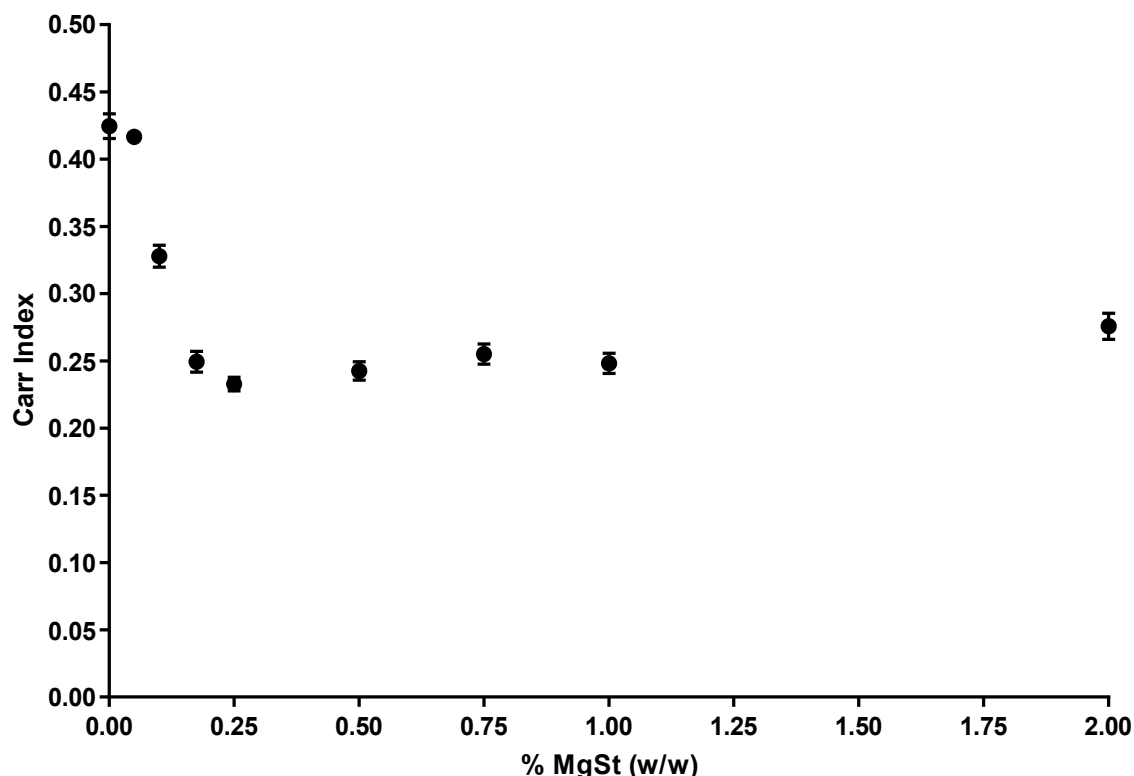


Figure 4-2: Carr index of MGB and MGB dry coated with varying amounts of MgSt. $n = 4$, error bars represent standard deviation. Note that some of the error bars are smaller than the symbols.

When MGB was dry coated with MgSt the Carr indices decreased indicating that the flow of the dry coated powders improved with a MgSt coating. Optimal flow was indicated for M-MGB-0.175 with a minimum Carr index of approximately 0.25 ± 0.01 . The Carr index of M-MGB-0.25 was not significantly different ($p > 0.05$) to the Carr index of M-MGB-0.175. Interestingly, the Carr index of M-MGB-0.05 was not significantly different ($p > 0.05$) to that of MGB, indicating that M-MGB-0.05 did not flow differently to uncoated MGB.

The Carr index of M-MGB-2 was significantly larger ($p < 0.05$) than the Carr indices of powders with 0.175-1% w/w MgSt. This indicates that M-MGB-2 flowed more poorly than the powders with 0.175-1% w/w MgSt. Similarly, previous studies also reported larger Carr indices when pharmaceutical powders were dry coated with large amounts of MgSt [27, 30]. For instance, dry coat lactose monohydrate ($d_{50} \approx 20 \mu\text{m}$) with 2% w/w MgSt showed a larger Carr index than that of lactose that had been dry coated with 1% w/w MgSt [27]. Alternatively, ibuprofen ($d_{50} \approx 44 \mu\text{m}$) that had been dry coated with 5% w/w MgSt had a larger Carr index than ibuprofen that had been dry coated with 1% w/w MgSt [30].

Figure 4-3 presents the compressibility of the powders. The compressibility of MGB was significantly lower after dry coating with MgSt. MGB was very compressible with a compressibility of approximately $30.1 \pm 0.5\%$, suggesting that the powder was poor flowing. The minimum compressibility occurred for M-MGB-0.175 with a compressibility of approximately $5.7 \pm 0.5\%$, thereby indicating that M-MGB-0.175 flowed best. This is in agreement with the Carr indices of the powders. M-MGB-0.05 was less compressible than uncoated MGB.

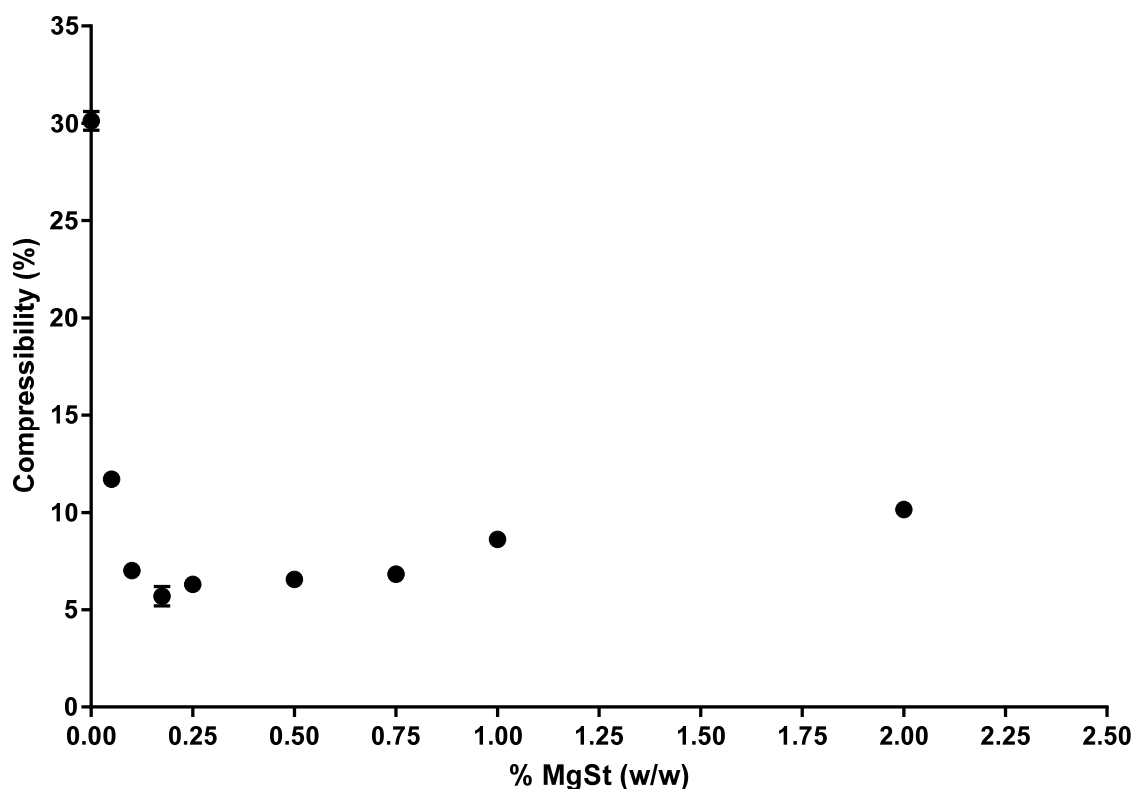


Figure 4-3: Compressibility of MGB and MGB dry coated with varying amounts of MgSt at a normal stress of 15 kPa. $n = 3$, error bars represent standard deviations. Note that some of the error bars are smaller than the symbols.

The compressibilities of the powders with 0.175% w/w MgSt or more remained the same until the amount of MgSt used reached at least 1% w/w. With 1% w/w MgSt or greater, the compressibilities of the powders were significantly larger ($p < 0.05$) than that of M-MGB-0.175. This suggests that the powders with 1% w/w MgSt or more flowed more poorly than powders with 0.175-0.75% w/w MgSt.

The basic flowability energies (BFE) of the powders are presented in Figure 4-4. The BFE of MGB was approximately 81.3 ± 6.6 mJ. Similar to the compressibility results, the BFE of M-MGB-0.05 was significantly lower ($p < 0.05$) than the BFE of MGB.

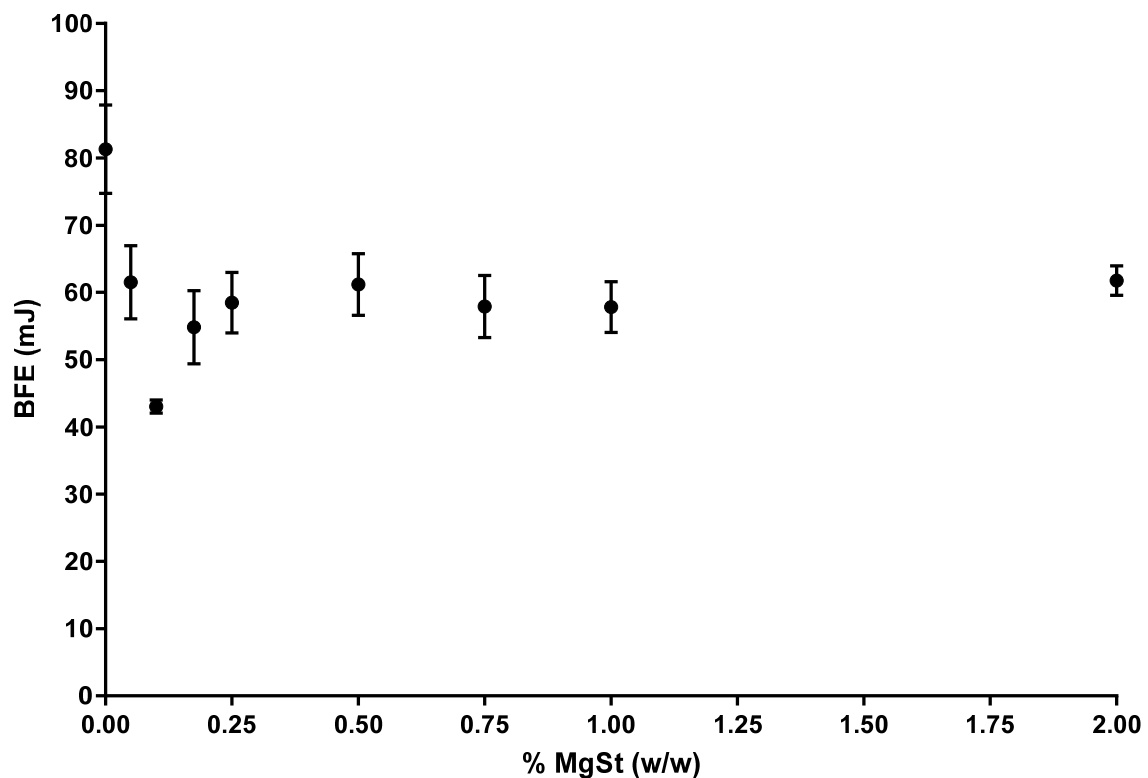


Figure 4-4: Basic flowability energy of MGB and MGB dry coated with varying amounts of MgSt. $n = 3$, error bars represent standard deviations.

The best powder flow was indicated for M-MGB-0.1 with a minimum BFE of approximately 43.0 ± 1.0 mJ. The BFE of the powders with 0.175% w/w MgSt or more were the same indicating that these powders flowed the same.

The flow rate of the powders was measured with a FlowPro. The results are presented in Figure 4-5. MGB was not very flowable with a flow rate of approximately 16.1 ± 1.2 mg/s. This agrees with the results from the other methods presented above. The low flow rate of MGB might also partially be the result of relatively large agglomerates (because of strong cohesive forces) that hindered flow through the orifice, especially as some of the agglomerates were too large to pass through the orifice.

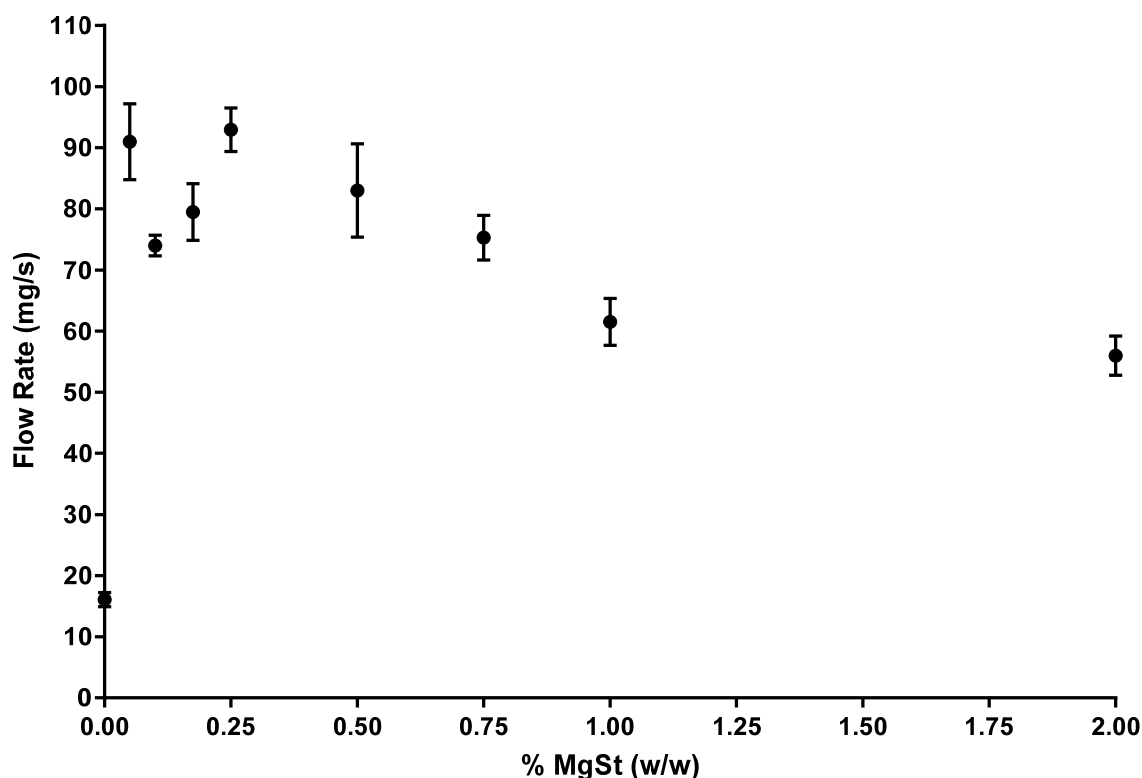


Figure 4-5: Flow rate of MGB and MGB dry coated with varying amounts of MgSt. $n = 4$, error bars represent standard deviation.

Interestingly, M-MGB-0.05 was significantly more flowable than MGB and M-MGB-0.1 and M-MGB-0.175. M-MGB-0.05, M-MGB-0.25 and M-MGB-0.5 had the same flow rate. Powders with 0.75% w/w or more MgSt were significantly less flowable ($p > 0.05$) than M-MGB-0.25.

The flowability of the powders under consolidation was evaluated through shear cell testing. Figure 4-6 presents the cohesion and flow function of the powders.

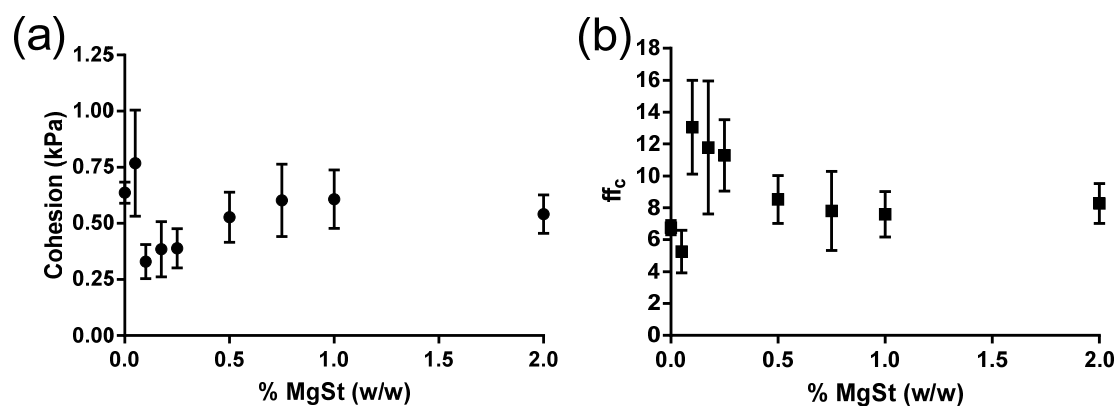


Figure 4-6: (a) Cohesion and (b) flow function of MGB and MGB dry coated with varying amounts of MgSt. $n = 5$, error bars represent standard deviation.

An interesting observation is the high variability in the cohesion and flow function of all powders with a MgSt coating. A similarly large variability in the cohesion and flow function was also reported for MgSt coated ibuprofen [56]. Consequently, these measurements were not very effective in discriminating between the flowabilities of the powders other than the largest differences in flow—that is, between the uncoated MGB and powders with 0.1-0.25% w/w MgSt. Nonetheless, these results conform with the general flow profile observed in the other methods to assess flow. That is, the flowability of MGB improved with the addition of small amounts of MgSt before decreasing with larger amounts of MgSt.

The angles of internal friction (AIF) of the powders are present in Figure 4-7. The AIF data was able to discriminate the flowability of powders with 0.1-0.175% w/w MgSt and powders with at least 0.5% w/w MgSt.

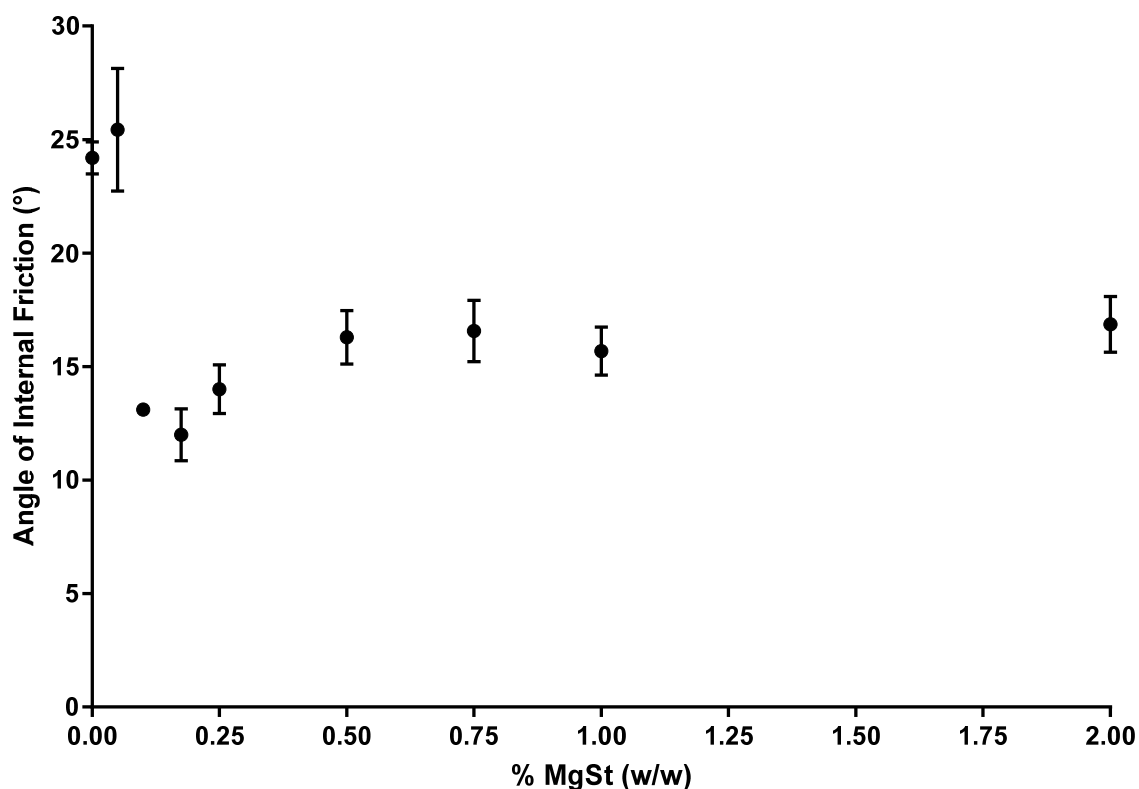


Figure 4-7: Angle of internal friction of MGB and MGB dry coated with varying amounts of MgSt. $n = 5$, error bars represent the standard deviation.

The AIF of MGB was approximately 24° . The AIF of M-MGB-0.05 was not significantly different to the AIF of MGB indicating that both MGB and M-MGB-0.05 flowed the same while undergoing consolidated flow. Interestingly, slip-stick behaviour (data not shown) was observed for M-MGB-0.05 during shear cell testing which occurs when the particles repeatedly transition between a lower cohesion state (slip phase) and a higher cohesion state (stick phase). This slip-stick behaviour may explain the relatively high variability of the AIF of M-MGB-0.05. Importantly, the slip-stick behaviour may indicate that MgSt may have only partially covered the surfaces of the MGB host particles—that is, the MgSt coating of M-MGB-0.05 was patchy or incomplete. An incomplete coating would lead to three different types of contacts: MgSt-MgSt, MgSt-glass and glass-glass. Transitions between these different contacts during particle movement may result in the slip-stick behaviour.

The AIF of powders with at least 0.1% w/w MgSt were smaller than the AIF of MGB. This suggests that these powders flowed better than MGB. However, powders with at least 0.5% w/w MgSt, were less flowable than the powders with 0.1-0.175% w/w MgSt.

4.6. Discussion

Dry coating MGB with a minimum of 0.1% w/w MgSt through mechanofusion was effective in improving the flow of MGB. The optimal amount of MgSt was approximately 0.1-0.25% w/w. However, it should be noted that the optimal amount of MgSt required is powder specific, specifically with respect to the specific surface area of the host powder [21, 27]. As particle size, size distribution and morphology of the powders remained unchanged after dry coating (Chapter 2: Surface Modification and Physical Characterisation of a Model Pharmaceutical Powder), the improved flow of the powders with 0.1% w/w MgSt was attributed to MgSt lowering the cohesive forces between the particles. With a smaller amount of MgSt than 0.1% w/w, MGB-0.05 did not flow better than MGB when flow was assessed through Carr index (see Figure 4-2) and AIF (see Figure 4-7). This was potentially due to M-MGB-0.05 only having a partial coating of MgSt that was unable to significantly diminish the strong cohesive forces between the particles. Similar observations from Zhou *et al.*, 2013 [21] were observed when studying salbutamol sulphate (SS, $d_{50} \approx 3.3 \mu\text{m}$) that had been dry coated with 0.5% w/w MgSt where it did not flow any better than uncoated SS.

However, flow rate measurements showed that M-MGB-0.05 flowed better than MGB, M-MGB-0.1 and M-MGB-0.175 (see Figure 4-5). The high flow rate of M-MGB-0.05 was attributed to M-MGB-0.05 forming small agglomerates (from visual inspection) that could flow through the orifice easily. These small agglomerates were responsible for the good flow of M-MGB-0.05.

When flow was assessed through Carr index and compressibility measurements, the flowability of M-MGB-2 was poorer than the flowability of powders with 0.175-1% w/w MgSt (see Figure 4-2 and Figure 4-3), despite M-MGB-2 having more MgSt. This coincides well with other reported studies where powders that had been dry coated

with excess amounts of MgSt showed poorer flow than powders with optimal amounts of MgSt [21, 27, 30, 57]. For instance, Zhou *et al.*, 2011 [27] studied the flow of lactose ($d_{50} \approx 20 \mu\text{m}$) that had been dry coated with varying amounts of MgSt. The authors of [27] reported that the flow of lactose that had been dry coated with 2% w/w MgSt was poorer than the flow of the optimal flowing powder (lactose dry coated with 1% w/w MgSt). Similarly, in a separate study, the authors of [21] reported that dry coating salbutamol sulphate (SS, $d_{50} \approx 3.3 \mu\text{m}$) with 10% w/w MgSt flowed significantly poorer to SS that had been dry coated with 5% w/w MgSt. The poorer flow observed for M-MGB-2 may be attributed to the thickness of the MgSt [21]. As MgSt is a relatively soft material, the thicker MgSt coating may be able to deform sufficiently, thereby increasing the contact area between adjacent particles [15]. Therefore, with more surface in contact, more inter-particle interactions can occur between the contacting surfaces, which manifests as increased cohesiveness [15].

The flowability of the powders was also influenced by the method used to assess flow. In contrast to the indicated poor flow of M-MGB-0.05 from its Carr index (see Figure 4-2), M-MGB-0.05 was more flowable than MGB when flow was assessed through compressibility (see Figure 4-3) and BFE (see Figure 4-4) measurements. This was likely attributed to the type of flow that occurred during these different flow assessments. As tapped density, compressibility and BFE measurements are all examples of confined flow, the flow of powders in these measurements resulted in increased powder consolidation as the powder continued to flow. Consequently, with more particles closer together, the average number of contact points between adjacent particles increased and thus resulted in greater net cohesive forces [3, 19]. Therefore, for tapped density measurements of M-MGB-0.05, as the powder consolidates with each tap, the increase in the cohesive force can increase to a point where the weight of the M-MGB-0.05 agglomerates was no longer sufficient to cause powder flow. However, in compressibility and BFE measurements of M-MGB-0.05 the flow of the powder was caused by a mechanical force exerted by a motor. As the motor was able to exert a mechanical force that was greater than the gravitational force, the flow promoting force was able to overcome the increasing cohesive force (due to powder consolidation), thereby resulting in greater powder flow.

Additionally, although the flow of powders in tapped density and flow rate measurements were the result of the gravitational force, M-MGB-0.05 showed different flowabilities in these two methods. M-MGB-0.05 exhibited significant improvements in flowability when assessed through flow rate measurements (see Figure 4-5), while M-MGB-0.05 flowed poorly when flow was assessed through Carr indices (see Figure 4-2). The improved flow of M-MGB-0.05 in flow rate measurements was attributed to the fact that flow rate measurements measure the unconfined flowabilities of powders. Consequently, during flow of the powder, consolidation of the powder does not occur (the powder can flow out of the orifice). Therefore, an increase in the cohesive force due to consolidation does not occur, thus allowing the weight of the M-MGB-0.05 agglomerates to maintain flow throughout the measurement. In contrast, the increasing cohesive force during tapped density measurements was able to increase to a point where it overwhelmed the weight of the M-MGB-0.05 agglomerates, thereby preventing further flow.

Moreover, optimal flow was observed for M-MGB-0.25 in flow rate measurements while M-MGB-0.175 showed optimal flow in Carr indices despite these two methods assess gravitational flow. This was attributed to flow rate measurements not experiencing increases in consolidation during powder flow. Consequently, M-MGB-0.25 was able to continue to flow throughout the measurement. This was not the case in tapped density measurements as significant powder consolidation can occur thereby increasing the cohesive force between adjacent particles to the point where it was able to overwhelm the weight of M-MGB-0.25 to limit further flow.

4.7. Conclusion

Dry coating MGB via mechanofusion with sufficient amounts of MgSt was able to improve the flow of MGB. The measured flow behaviour of the powders was dependent on both the amount of MgSt used and the method used to assess powder flow. The optimal amount of MgSt was in the range of 0.1-0.25% w/w as these powders showed significant flow improvements regardless of the method used to assess powder flow. With a sub-optimal amount of MgSt, improvements in the flow of M-MGB-

0.05 was more dependent on the method of flow assessment. M-MGB-0.05 was only able to flow more freely than MGB during unconfined flow (measured by flow rate) or confined mechanical flow (measured through compressibility or BFE measurements). In contrast, powders with large amounts of MgSt were unable to flow as freely as powders having 0.1-0.25% w/w MgSt. This was attributed to the MgSt coating being able to deform sufficiently which ultimately resulted in increased cohesion of the powder.

Both the Carr index and compressibility measurements were quick and simple methods to assess the confined flow of the powders and both showed similar results on the flowabilities of the powders. However, as the Carr index was the more cost-effective and simpler of the two methods, the Carr index is the recommended method to assess the confined flow of powders. For powders with a partial coating, such as M-MGB-0.05, compressibility measurements are recommended instead of the Carr index. BFE measurements were less effective at assessing the flow of the powders undergoing confined flow compared to both the Carr index and compressibility. The FlowPro was effective at measuring the flow of the powders. In contrast, shear cell testing was shown to be highly variable when assessing the flow of MgSt coated powders. Consequently, shear cell testing may not necessarily be a suitable method to assess the flow of MgSt coated powders.

4.8. Acknowledgements

GT is thankful for the financial support of Graduate Research, Monash University, for providing a Monash Equity Scholarship.

4.9. References

- [1] Pietsch WB, Adhesion and agglomeration of solids during storage, flow and handling - A survey, *J Eng Ind.* 91(1969) 435-49.
- [2] Juliano P, Barbosa-Canovas GV, Food powders flowability characterization: Theory, methods and applications, *Annu Rev Food Sci Technol*, Annual Reviews, CA, USA, 2010, 211-39.

- [3] Ganesan V, Rosentrater KA, Muthukumarappan K, Flowability and handling characteristics of bulk solids and powders – a review with implications for DDGS, *Biosystems Engineering*. 101(2008) 425-35.
- [4] Prescott JK, Barnum RA, On powder flowability, *Pharm Technol*. 24(2000) 60.
- [5] Baxter T, Barnum R, Prescott JK, Flow: General principles of bulk solids handling, in: Augsburger LL, Hoag SW (Eds.), *Pharmaceutical dosage forms - Tablets: Unit operations and mechanical properties*, 3rd ed., Informa Healthcare, NY, USA, 2008, 75-110.
- [6] FDA, Pharmaceutical quality for the 21st century – A risk-based approach progress report. [internet] 2010 2010-Nov-03 [cited 2015 Jun 28]; Available from: <http://www.fda.gov/aboutfda/centersoffices/officeofmedicalproductsandtobacco/cder/ucm128080.htm>
- [7] ICH, Quality guidelines. [internet] [cited 2015 Jun 28]; Available from: <http://www.ich.org/products/guidelines/quality/article/quality-guidelines.html>
- [8] Aulton ME, (Ed.) *Pharmaceutics: The science of dosage form design*. 2nd ed., Churchill Livingstone, Edinburgh, UK, 2002.
- [9] Orband JLR, Geldart D, Direct measurement of powder cohesion using a torsional device, *Powder Technol*. 92(1997) 25-33.
- [10] Sutton H, Flow properties of powders and the role of surface character, in: Parfitt G, Sing K (Eds.), *Characterization of powder surfaces*, Academic Press, NY, USA, 1976, 107-58.
- [11] Peleg M, Flowability of food powders and methods for its evaluation — A review, *J Food Process Eng*. 1(1977) 303-28.
- [12] Zimon AD, *Adhesion of dust and powder*, Plenum Press, New York, USA, 1969.
- [13] Zeng XM, Martin G, Marriott C, *Particulate interactions in dry powder formulations of inhalation*, Taylor & Francis, NY, USA, 2000.
- [14] Stewart PJ, Particle interaction in pharmaceutical systems, *Pharm Int*. 7(1986) 146-9.
- [15] Israelachvili JN, *Intermolecular and surface forces*, 3rd ed., Academic Press, MA, USA, 2011.
- [16] Jenike AW, *Storage and flow of solids*, University of Utah, Utah, USA, 1964.
- [17] Svarovsky L, *Powder testing guide: methods of measuring the physical properties of bulk powders*, Elsevier Applied Science, London, UK, 1987.
- [18] Schulze D, *Powders and bulk solids: Behavior, characterization, storage and flow*, Springer, Berlin, Germany, 2008.
- [19] Rietema K, *The dynamics of fine powders*, Elsevier Applied Science, London, UK, 1991.
- [20] Igwe GJI, *Powder technology and multiphase systems: Gas permeametry and surface area measurement*, Ellis Horwood, NY, USA, 1991.
- [21] Zhou QT, Qu L, Gengenbach T, Larson I, Stewart PJ, Morton DAV, Effect of surface coating with magnesium stearate via mechanical dry powder coating approach on the aerosol performance of micronized drug powders from dry powder inhalers, *AAPS PharmSciTech*. 14(2013) 38-44.
- [22] Zhou QT, Armstrong B, Larson I, Stewart PJ, Morton DAV, Understanding the influence of powder flowability, fluidization and de-agglomeration characteristics on the aerosolization of pharmaceutical model powders, *Eur J Pharm Sci*. 40(2010) 412-21.

- [23] Kunnath K, Huang Z, Chen L, Zheng K, Davé R, Improved properties of fine active pharmaceutical ingredient powder blends and tablets at high drug loading via dry particle coating, *Int J Pharm.* 543(2018) 288-99.
- [24] Jallo LJ, Ghoroi C, Gurumurthy L, Patel U, Davé RN, Improvement of flow and bulk density of pharmaceutical powders using surface modification, *Int J Pharm.* 423(2012) 213-25.
- [25] Zhou Q, Qu L, Larson I, Stewart PJ, Morton DAV, Effect of mechanical dry particle coating on the improvement of powder flowability for lactose monohydrate: A model cohesive pharmaceutical powder, *Powder Technol.* 207(2011) 414-21.
- [26] Zhou QT, Qu L, Larson I, Stewart PJ, Morton DAV, Improving aerosolization of drug powders by reducing powder intrinsic cohesion via a mechanical dry coating approach, *Int J Pharm.* 394(2010) 50-9.
- [27] Zhou Q, Qu L, Gengenbach T, Denman JA, Larson I, Stewart PJ, et al., Investigation of the extent of surface coating via mechanofusion with varying additive levels and the influences on bulk powder flow properties, *Int J Pharm.* 413(2011) 36-43.
- [28] Paw R, Goggin P, Bajwa G, Feasibility study to investigate the application of mechanofusion to improve flow properties of a cohesive API, *J Pharm Pharmacol.* 62(2010) 1435-6.
- [29] Zhou Q, Armstrong B, Larson I, Stewart PJ, Morton DAV, Improving powder flow properties of a cohesive lactose monohydrate powder by intensive mechanical dry coating, *J Pharm Sci.* 99(2010) 969-81.
- [30] Qu L, Zhou Q, Gengenbach T, Denman JA, Stewart PJ, Hapgood KP, et al., Investigation of the potential for direct compaction of a fine ibuprofen powder dry-coated with magnesium stearate, *Drug Dev Ind Pharm.* 41(2015) 825-37.
- [31] Masuda H, Higashitani K, Yoshida H, (Eds.), *Powder technology handbook*. 3rd ed., Taylor & Francis Group, FL, USA, 2006.
- [32] Copley M, A test of quality. *Manufacturing Chemist.* 2008:31-3.
- [33] Tan G, Morton DAV, Larson I, On the methods to measure powder flow, *Current Pharmaceutical Design.* 21(2015) 5751-65.
- [34] Osorio JG, Muzzio FJ, Effects of powder flow properties on capsule filling weight uniformity, *Drug Dev Ind Pharm.* 39(2013) 1464-75.
- [35] Boateng AA, Barr PV, Modelling of particle mixing and segregation in the transverse plane of a rotary kiln, *Chem Eng Sci.* 51(1996) 4167-81.
- [36] Cassidy O, Thomas W, Characterisation of wet masses using a powder rheometer, Poster session 1 — Pharmaceuticals, *J Pharm Pharmacol.* 54(2002) 25-46.
- [37] Rowe RC, Characterization of wet powder masses using a mixer torque rheometer. 4. Effect of blade orientation, *Int J Pharm.* 133(1996) 133-8.
- [38] Luukkonen P, Schæfer T, Podcizek F, Newton M, Hellén L, Yliruusi J, Characterization of microcrystalline cellulose and silicified microcrystalline cellulose wet masses using a powder rheometer, *Eur J Pharm Sci.* 13(2001) 143-9.
- [39] Dave RH, Wu SH, Contractor LD, To determine the end point of wet granulation by measuring powder energies and thermal properties, *Drug Dev Ind Pharm.* 38(2012) 439-46.
- [40] Staniforth JN, Powder flow, in: Aulton ME (Ed.) *Pharmaceutics: The science of dosage form design*, 2nd ed., Churchill Livingstone, Edinburgh, UK, 2002, 197-211.
- [41] Hausner H, Friction conditions in a mass of metal powder, *Int J Powder Metall.* 3(1967) 7-13.

- [42] Powder flow, United States Pharmacopeia, US Pharmacopial Convention, MA, USA, 2011, 723-6.
- [43] Carr RL, Evaluating flow properties of solids, Chem Eng. 72(1965) 163-8.
- [44] Kulkarni PA, Berry RJ, Bradley MSA, Review of the flowability measuring techniques for powder metallurgy industry, Proc Inst Mech Eng Part E-J Process Mech Eng. 224(2010) 159-68.
- [45] Thalberg K, Lindholm D, Axelsson A, Comparison of different flowability tests for powders for inhalation, Powder Technol. 146(2004) 206-13.
- [46] Freeman R, Measuring the flow properties of consolidated, conditioned and aerated powders — A comparative study using a powder rheometer and a rotational shear cell, Powder Technol. 174(2007) 25-33.
- [47] Hammerness FC, Thompson HO, A study of the effect of lubricant and fines on a tablet granulation, J Am Pharm Assoc. 47(1958) 58-61.
- [48] Chowhan ZT, Yang IC, Powder flow studies IV. Tensile strength and orifice flow rate relationships of binary mixtures, Int J Pharm. 14(1983) 231-42.
- [49] Seppälä K, Heinämäki J, Hatara J, Seppälä L, Yliruusi J, Development of a new method to get a reliable powder flow characteristics using only 1 to 2 g of powder, AAPS PharmSciTech. 11(2010) 402-8.
- [50] Genina N, Räikkönen H, Ehlers H, Heinämäki J, Veski P, Yliruusi J, Thin-coating as an alternative approach to improve flow properties of ibuprofen powder, Int J Pharm. 387(2010) 65-70.
- [51] Soppela I, Airaksinen S, Murtomaa M, Tenho M, Hatara J, Räikkönen H, et al., Investigation of the powder flow behaviour of binary mixtures of microcrystalline celluloses and paracetamol, Journal of Excipients and Food Chemicals. 1(2010) 55-67.
- [52] Sandler N, Reiche K, Heinämäki J, Yliruusi J, Effect of moisture on powder flow properties of theophylline, Pharmaceutics. 2(2010) 275-90.
- [53] Ghoroi C, Gurusurthy L, McDaniel DJ, Jallo LJ, Davé RN, Multi-faceted characterization of pharmaceutical powders to discern the influence of surface modification, Powder Technol. 236(2013) 63-74.
- [54] Yu WL, Muteki K, Zhang L, Kim G, Prediction of bulk powder flow performance using comprehensive particle size and particle shape distributions, J Pharm Sci. 100(2011) 284-93.
- [55] Schwedes J, Review on testers for measuring flow properties of bulk solids (based on an IFPRI-Report 1999), Granular matter. 5(2003) 1-43.
- [56] Qu L, Zhou Q, Denman JA, Stewart PJ, Hapgood KP, Morton DAV, Influence of coating material on the flowability and dissolution of dry-coated fine ibuprofen powders, Eur J Pharm Sci. 78(2015) 264-72.
- [57] Wei G, Mangal S, Denman J, Gengenbach T, Lee Bonar K, Khan RI, et al., Effects of coating materials and processing conditions on flow enhancement of cohesive acetaminophen powders by high-shear processing with pharmaceutical lubricants, J Pharm Sci. 106(2017) 3022-32.

Chapter 5:

Characterising the Surface Properties of Surface Modified Fine Powders

Geoffrey Tan

Bachelor of Pharmaceutical Sciences (Honours)

Drug Delivery, Disposition and Dynamics, Monash Institute of Pharmaceutical
Sciences. 381 Royal Parade, Parkville, VIC, 3052, Australia

Chapter 5: Characterising the Surface Properties of Surface Modified Fine Powders

5.1. Commentary

To better understand how MgSt altered the flowability of the powders, this chapter aims to address Thesis Objective 4 “*to measure the surface energy of the fine powder as well as the surface modified powder*” and Thesis Objective 5 “*to measure the surface hydrophobicity of the fine powder as well as the surface modified powder*”.

The surface energy of MGB and MGB dry coated with 0.05% to 0.75% w/w MgSt was measured via IGC at infinite dilution. The hydrophobicity of the powders was determined by measuring the contact angle of water to the powders via the liquid intrusion method. Also included in this chapter is the characterisation of the surface composition of the powders to provide further insights into results reported in Chapter 4. ToF-SIMS experiments were conducted by Dr. John Denman and XPS experiments were conducted by Dr. Thomas Gengenbach.

5.2. Abstract

In this study the surfaces of surface modified powders were characterised to better understand how the modified surface alters the surface properties of the powders. Time-of-flight secondary ion mass spectrometry (ToF-SIMS) analysis showed that the extent and thickness of the MgSt coating can vary from a thin partial coating to a thin near-complete coating to a thicker near-complete coating of MgSt. Additionally, results from x-ray photoelectron spectroscopy (XPS) suggested that the hydrocarbon tail of MgSt was facing outwards. Inverse gas chromatography (IGC) was used to characterise the surface energy of the powders, while the contact angle of water to the powders was measured via the liquid intrusion method. The change in the surface energy of the powders coincided well with the extent of the MgSt coating. With a coating of MgSt, the surface energy of the powders was significantly lower than that of uncoated MGB. The contact angle of water to MGB was relatively high with a value

of approximately 80° . Thus, the capillary force for MGB was likely to be relatively weak. Liquid intrusion did not occur for powders with a MgSt coating, which indicated that the contact angle of water to MgSt coated powders was $\geq 90^\circ$. Consequently, a coating of MgSt was able to eliminate the presence of capillary forces between powders.

5.3. Introduction

Pharmaceutical manufacturing can often be challenging when using fine powders as they are inherently cohesive [1-6]. Thus, fine powders often lack the necessary flowability to enable optimal and efficient manufacturing of pharmaceutical dosages [2]. The cohesive property of these powders is the result of relatively strong cohesive forces between adjacent particles [1-6]. These cohesive forces are a collection of attractive inter-particle interactions, such as van der Waals interactions and capillary forces, that exist between the contacting surfaces of adjacent particles. Such attractive contacts are termed *cohesive contacts* that act to keep particles in contact with one another [1]. Consequently, cohesive forces limit the movement of particles and thus reduce powder flow [1, 7-9].

Contact mechanics describes the pull-off force to be proportional to the surface energy of the powder. For the case of two identical spherical particles and without external loading (that is, the particles are not pushed together), the pull-off force, F_{po} , in the absence of other forces is given by Equation (5.1):

$$F_{po} = -\frac{3}{2}\pi w_c r \quad (5.1)$$

where r is the radii of the particles and $w_c = 2\gamma_s$ and is termed the *work of cohesion*. γ_s is the surface energy of the particles.

The surface energy, γ_s , (sometimes specified as *total surface energy*, γ_s^T , see below) of solids is an intrinsic property of solids as it stems from the net inward intermolecular forces exerted by the molecules at the surface and is analogous to the surface tension of liquids. Surface energy is defined as the energy required to create a unit area of

new surface [1, 10]. The surface energy is comprised of two major interactions [11]. The first is the innate dispersive (London) interaction which is present between all molecules. The second is the polar interaction (sometimes referred to as the acid-base interaction as it is only evident when an acidic moiety interacts with a basic moiety and vice versa) [11, 12]. Therefore, the surface energy of any solid material can be split into their major components—a dispersive component, γ_S^D , which is always present and a polar component, γ_S^P , which only arises when acid-base interactions are evident and the sum of these components gives the total surface energy (or simply surface energy) [13].

Thus, the work of cohesion, w_C , can be written in its surface energy component form [14-16]:

$$w_C = 2(\gamma_S^D + \gamma_S^P) \quad (5.2)$$

For powders with a large surface energy, the pull-off force is large; thus, the powders are expected to flow poorly.

The surface energy of powders is commonly characterised via inverse gas chromatography (IGC) [17-22]. In this technique, the sample of interest forms the stationary phase of the IGC, while the mobile phase carries a series of standard vapour probes to characterise the dispersive and polar components of the surface energy of the sample [23, 24]. IGC measurements can be performed under two different conditions: infinite dilution or finite concentration [23, 25]. In infinite dilution, very small amounts of the vapour probes are carried through the stationary phase [23, 25]. Under infinite dilution, only the highest surface energy sites are probed; thus, measurements of IGC at infinite dilution only provide information on these high energy sites [26-28]. To probe a wider range of the surface energy distribution, IGC at finite concentration can be used where larger amounts of the probe vapours are carried through the stationary phase, thereby probing a wider area of the powder surface [23, 28].

In contrast to van der Waals interactions, capillary forces only exist when there is a liquid bridge between adjacent particles. The capillary force is a strong force that can potentially dominate the van der Waals interactions [29]. The strength of the capillary force is proportional to the cosine of the angle water makes to the particles [29-31]. For two identical smooth spherical particles, the capillary force, F_c , is given by Equation (5.3) [30]:

$$F_c = -2\pi\gamma_l r \cos \theta \quad (5.3)$$

where γ_l is the surface tension of the liquid and θ is the angle the liquid makes to the particles.

As the strength of the capillary force is dependent on the hydrophilicity/hydrophobicity (in the context of water) of powders, the maximum capillary force occurs when water perfectly wets the powder, that is, when $\theta = 0^\circ$. For powders where water makes larger contact angles (that is, more hydrophobic powders), the capillary force is weaker thus the powders are expected to flow more freely.

For the case of powders, the contact angle of liquids is traditionally measured through methods where powders are adhered to scaffolds to act as Wilhelmy plates or the powder is compacted to form dense bodies on which sessile drops can form [32-38]. Clearly, neither of these methods are ideal as the powder is no longer in its natural form. Alternatively, the liquid intrusion method proposed by Washburn, 1921 [39], relates the contact angle of liquids to powders as a function of the rate at which liquids intrude into powder beds. For a more detailed discussion on the liquid intrusion method as well as some methods to accommodate some of the limitations of the liquid intrusion method, refer to Chapter 3: Development of New Experimental Methods – Part II: Strategies to Analyse Data Obtained from Liquid Intrusion Experiments of Loose Porous Materials. In brief, Washburn showed that the relationship between the intrusion rate of liquids and their contact angles to powders is given by Equation (5.4) [39, 40]:

$$\frac{m^2}{t} = \frac{C\rho^2\gamma_L \cos \theta}{\eta} \quad (5.4)$$

where, m is the mass of the intruded liquid at time, t . C is the *material constant* and is a measure of the pore structure of the powder bed, ρ is the density of the liquid, γ_L is the surface tension of the liquid, θ is the contact angle of the liquid, and η is the viscosity of the liquid.

The use of a perfectly wetting ($\theta = 0^\circ$) reference liquid allows the determination of the material constant. Assuming that powder beds are composed of the same powder material and are prepared by a standardised packing procedure, it is assumed that the material constant is just that, constant [41-46]. Consequently, Equation (5.4) can be modified to give Equation (5.5):

$$\cos \theta_p = \frac{\rho_r^2 \gamma_{Lr} \eta_p}{\rho_p^2 \gamma_{Lp} \eta_r} \cdot \frac{m_p^2 t_r}{m_r^2 t_p} \quad (5.5)$$

where subscripts p and r refer to probe and reference liquids, respectively.

With the impact of the surfaces of fine powders on their inter-particle interactions, particle engineering through surface modification appears to be a logical approach to improve the flow of fine powders [3, 9]. Dry coating methods such as the mechanofusion system (Hosokawa Micron Powder Systems, Japan) achieves surface modification by subjecting the powder of interest (host powder) and a coating material (guest powder) to high shear stresses [47, 48]. As the guest powders are typically smaller and/or softer than the host powder, the high stresses exerted by the dry coating process can delaminate, smear and/or spread the guest powder over the surfaces of the host particles [48-51]. In doing so, a thin coating of the guest particles is formed on the host particles thereby effectively masking the surfaces of the host particles [49, 52-54]. Consequently, dry coating methods can alter the inter-particle interactions and therefore the flowability of fine powders. Thus, the selection of the coating material may be strategically selected to optimise the flowability of fine powders.

In the design of pharmaceutical formulations, pharmaceutical lubricants such as magnesium stearate (MgSt) are used to improve the manufacturability of pharmaceutical dosages such as tablets [55]. The functionality of MgSt is attributed to its ability to not only reduce friction but also the cohesive inter-particle forces [55]. For this reason, MgSt has been explored as a coating material to improve the flowability of fine powders [52, 56-58]. For instance, the flow of cohesive fine powders has been shown to improve significantly after dry coating through mechanofusion with the pharmaceutical lubricant magnesium stearate [48, 49, 56, 59-62]. Similarly, measurements detailed in the previous chapter (Chapter 4: Evaluating the Flow of Surface Modified Fine Powders with Varying Amounts of Magnesium Stearate Through Different Flowability Tests) found that dry coating micron-sized glass beads (MGB, d_{50} approximately 10 μm) with varying amounts of MgSt (0.05% to 2% w/w) via mechanofusion improved the flowability of MGB.

The mechanisms by which surface coatings such as MgSt alter the flow of fine powders remain relatively poorly understood. Changes in the flow of fine powders with a MgSt coating have largely been attributed to the MgSt lowering the surface energy of the fine powder [18, 51, 63-65]. However, other mechanisms may also contribute to the improved flow of MgSt coated powders. For example, as the powders are now coated with a hydrophobic material (due to the aliphatic hydrocarbon tail of MgSt), the contact angle of water to the MgSt coated powder may also have increased. With an increased contact angle, the magnitude of the capillary force is decreased and this may contribute to the improvement in the flow of the surface modified fine powder.

This study aims to better understand how altering the surface composition of a fine powder alters the surface properties of the powder. To this end, a fine powder was dry coated with varying amounts of MgSt to form surface modified powders with varying amounts of MgSt and their surface compositions, surface energies and hydrophobicities were characterised.

5.4. Materials and Methods

5.4.1. Materials

Micron-sized glass beads (MGB, $d_{50} = 10 \mu\text{m}$ with a span of 1.1 ± 0.04) were obtained from Cospheric LLC (CA, USA) which served as a model pharmaceutical powder. Magnesium stearate NF (MgSt) was obtained from Mallinckrodt Baker Inc. (NJ, USA). Commercially available $250 \mu\text{m}$ pre-silanized glass beads were used as carrier particles (CGB), which was procured from Sigma-Aldrich Co. LLC. (MO, USA). GC grade decane, nonane, octane, heptane, hexane, dichloromethane, and toluene were procured from Sigma-Aldrich Co. LLC. (MO, USA). Silanized glass wool and pre-silanized glass columns were purchased from Surface Measurement Systems Ltd. (London, UK). Absolute ethanol and acetone were purchased from Merck KGaA (Hesse, Germany). All materials were used as received. Milli-Q water was produced from a Direct-Q[®] 3 UV Water Purification System (Merck KGaA, Hesse, Germany).

5.4.2. Methods

5.4.2.1. Time-of-Flight Secondary Ion Mass Spectrometry

Time-of-Flight Secondary Ion Mass Spectrometry (ToF-SIMS) experiments were performed using a Physical Electronics Inc. PHI TRIFT V nanoTOF instrument equipped with a pulsed liquid metal ^{79}Au primary ion gun (LMIG), operating at 30 keV energy. Experiments were performed under a vacuum of 5×10^{-6} Pa or better. “Unbunched” Au₁ instrumental settings were used to optimise spatial resolution for the collection of +SIMS images. Surface analyses were performed at four locations per sample using a $50 \times 50 \mu\text{m}$ raster area.

Region-of-interest spectra were extracted from the collected raw data using WincadenceN software (Physical Electronics Inc., MN, USA). This resulted in spectra collected from the surface of 20 particles per sample.

Spectra were calibrated and integrated peak values of selected ions were normalised to the total selected secondary ion intensities to correct for differences in total ion yield between analyses and samples. The resulting data were then compared qualitatively by preparing plots of average normalised counts (with 95% confidence intervals) for each species of interest. Chemical maps were also prepared from the raw data to show the spatial distribution of species of interest.

5.4.2.2. X-ray Photoelectron Spectroscopy

X-ray photoelectron spectroscopy (XPS) analysis was performed using an AXIS Ultra DLD spectrometer (Kratos Analytical Inc., Manchester, UK) with a monochromated Al K_{α} source at a power of 144 W (12 kV \times 12 mA), a hemispherical analyser operating in the fixed analyser transmission mode and the standard aperture (analysis area was approximately 0.3 x 0.7 mm). The total pressure in the main vacuum chamber during analysis was typically between 10^{-9} to 10^{-8} mbar. Survey spectra were acquired at a pass energy of 160 eV. To obtain more detailed information about chemical structure, oxidation states etc., high resolution spectra were recorded from individual peaks at 40 eV pass energy (yielding a typical peak width for polymers of <1.0 eV).

Each specimen was analysed at an emission angle of 0° as measured from the surface normal. Since the actual emission angle is ill-defined in the case of particles (ranging from 0° to 90°) the sampling depth ranges from 0 nm to approximately 10 nm.

Data processing was performed using CasaXPS processing software v2.3.15 (Casa Software Ltd., Teignmouth, UK). All elements present were identified from survey spectra. The atomic concentrations of the detected elements were calculated using integral peak intensities and the sensitivity factors supplied by the manufacturer. Binding energies were referenced to the aliphatic hydrocarbon C 1s peak at 285.0 eV (Appendix: Figure A.1) in order to correct for the shift in peak positions that occurs because of sample charging during analysis [66]. Sample charging was compensated for using a low-kinetic energy electron flood gun in combination with a magnetic immersion lens. The latter directs the electrons from the flood gun towards the sample

and generates a uniform and stable electron potential across the sample surface. The accuracy associated with quantitative XPS is approximately 10-15%. Precision (that is, reproducibility) depends on the signal/noise ratio but is usually much better than 5%. The latter is relevant when comparing similar samples.

5.4.2.3. Surface Energy Measurements

The surface energy of the powders was determined via inverse gas chromatography (iGC 2000, Surface Measurement Systems Ltd., London, UK) at infinite dilution. Approximately 1.2 g of MGB were packed into pre-silanized glass columns (300 x 4 mm ID). As MgSt coated MGB naturally forms high packing efficiency powder beds which results in over-pressuring the IGC, it was necessary to blend the MgSt coated MGB with 70% w/w MgSt (refer to Chapter 3: Section 3.2 Part I: A Strategy to Evaluate the Surface Energy of High Packing Efficiency Fine Powders via Inverse Gas Chromatography). Given the volume constraints of the IGC columns, blends of approximately 0.7 g of surface MgSt coated MGB with 70% w/w CGB (refer to [67] for details on the blending method) were packed into pre-silanized glass columns (300 x 4 mm ID). It was previously shown that the reduced mass of 0.7 g of MgSt coated MGB does not affect the surface energy measurement [67]. Both ends of the columns were loosely stoppered with silanized glass wool to prevent powder movement. Packed columns were then gently tapped until no visible signs of voids, channels or cracks within the powder.

Prior to surface energy measurements, the powders were pre-conditioned with a stream of helium at a flow rate of 10 sccm (standard cubic centimetre per minute) for a period of 120 mins at 303.15 K and 0% RH (relative humidity). To measure surface energy, helium at 10 sccm was used to carry a series of *n*-alkanes probes (decane, nonane, octane, heptane, and hexane) and specific probes (dichloromethane and toluene) through the stationary phase to determine the dispersive surface energy, γ_S^D , and the specific free energy, ΔG^{SP} , respectively. The concentration used for all probes was at 0.03 p/p_0 (where p is the partial pressure and p_0 is the saturation vapour pressure) and the system was kept at 303.15 K and 0% RH. Dead volumes were

based on the elution time of methane gas at 0.03 p/p_0 . The detection of the probes was achieved through a flame ionization detector (FID). Results were analysed with SMS-iGC analysis software v1.3 (Surface Measurement Systems Ltd., London, UK). Replicates of three were conducted for all powders.

γ_S^D of the powder and ΔG^{SP} of both dichloromethane and toluene was calculated with the Schultz method [25]. However, through this method, ΔG^{SP} is obtained in units of energy per mole (kJ/mol), while γ_S^D is in units of energy per area (mJ/m²). The harmonization of these units was achieved through the use of Avogadro's number and the cross-sectional area of the vapour probe (refer to Table 5-1) [68-71]. ΔG^{SP} is related to the polar surface energy, γ_S^P , through the concept presented by Good-van Oss [13, 72], Equation (5.6) and Equation (5.7):

$$\Delta G^{SP} = 2aN_A(\sqrt{\gamma_L^+\gamma_S^-} + \sqrt{\gamma_L^-\gamma_S^+}) \quad (5.6)$$

$$\gamma_S^P = 2\sqrt{\gamma_S^+\gamma_S^-} \quad (5.7)$$

where a is the cross-sectional area of the probe, N_A is Avogadro's number, γ_L^+ is the electron-acceptor parameter of the acidic probe, γ_S^- is the electron-donor parameter of the powder surface (basic site), γ_L^- is the electron-donor parameter of the basic probe, and γ_S^+ is the electron-acceptor parameter of the powder surface (acidic site).

Table 5-1: The electron-acceptor parameter, γ_L^+ , electron-donor parameter, γ_L^- , and cross-sectional area, a , of dichloromethane and toluene (Surface Measurement Systems Ltd., London, UK).

Probe	γ_L^+ (mJ/m ²)	γ_L^- (mJ/m ²)	a (x10 ⁻¹⁹ m ²)
Dichloromethane	5.20	0	2.45
Toluene	0	2.30	4.60

The total surface energy, γ_S^T , is given by Equation (5.8) [13]:

$$\gamma_S^T = \gamma_S^D + \gamma_S^P \quad (5.8)$$

5.4.2.4. Surface Hydrophobicity Measurements

Liquid intrusion experiments were performed with an automated tensiometer (Attension Sigma 700, Biolin Scientific, Stockholm, Sweden).

Powder beds of the powders were prepared by pouring approximately 1.24 g of MGB or 0.7 g of surface modified powder through a funnel at a fixed height above a custom-made borosilicate glass column (50 x 10 mm ID) (Platinum Laboratory Services, Melbourne, Australia). The column contained a POR 2 borosilicate sintered glass frit (pore size of 40-100 μm) to retain the powder. In order to ensure the integrity of the glass frit, 1 layer of filter paper (pre-cut 10 mm diameter Whatman Grade 1 filter paper, Whatman PLC., Kent, UK) was placed in the column prior to loading the powder. The column was cleaned prior to each experiment by washing and rinsing with Milli-Q water, ethanol, and acetone before drying with a stream of dry compressed air.

Powder beds of MGB were prepared by tapping the columns 200 times with an automated tapping instrument (AUTOTAP™, Quantachrome Instruments, FL, USA). To prevent powder beds of surface modified powders from lifting during the liquid intrusion experiments, powder beds were prepared by tapping the columns 1250 times with an automated tapping instrument before the powder beds were compressed with a compressive stress of approximately 152 kPa. The tapper operated with a 3.18 mm vertical tap at a tapping rate of 260 taps/min.

All liquid intrusion studies were performed at $25 \pm 2^\circ \text{C}$ with freshly prepared powder beds. Water was used as the probe liquid, while ethanol was used as the reference liquid [73]. Replicates of five were completed for all powders with all liquids, unless otherwise specified. Table 5-2 presents the liquid properties (density, viscosity, and surface tension) of all liquids used at 25°C .

Table 5-2: Liquid properties of water and ethanol at 25° C [30].

Liquid	Density (kg/m ³)	Viscosity (Pa·s)	Surface tension (N/m)
Water	997.047	0.000890	0.07199
Ethanol	784.855	0.001074	0.02197

The contact angle of the probe liquid to the powders was calculated based on the rank order of the material constants (method presented in [73]).

5.4.2.5. Statistical Analysis

Statistical analysis was achieved with a one-way analysis of variance (ANOVA) with a Tuckey's *post hoc* analysis where a significant difference was obtained if $p < 0.05$ (IBM SPSS Statistics v23, IBM Corp., NY, USA).

5.5. Results and Discussion

5.5.1. Surface Composition of MGB After Dry Coating with Varying Amounts of MgSt

Both ToF-SIMS and XPS are highly surface specific techniques that provide chemical information about the upper-most portion of the surfaces of solids [74-76]. The depth resolution for ToF-SIMS is approximately 1-2 nm while the depth resolution of XPS is approximately 5-10 nm for flat surfaces [77]. However, due to the spherical morphology of MGB, it is very difficult to give an exact depth resolution of both ToF-SIMS and XPS. Consequently, data from ToF-SIMS and XPS analysis can only be used as a qualitative indicator of the relative thickness of the MgSt coatings.

Figure 5-1 presents the normalised counts of Si and Mg signals. The coverage of the MgSt coating was qualitatively assessed by spatial distribution maps of Si and Mg as a function of the weight percentage of MgSt used, which are presented in Figure 5-2. The presence of a Mg signal in the uncoated MGB, see Figure 5-1a, indicates there

were sources of magnesium in the glass. Consequently, Mg signals from powders dry coated with MgSt may originate from the glass and/or the MgSt. However, the Si signal, Figure 5-1b, only originates from glass.

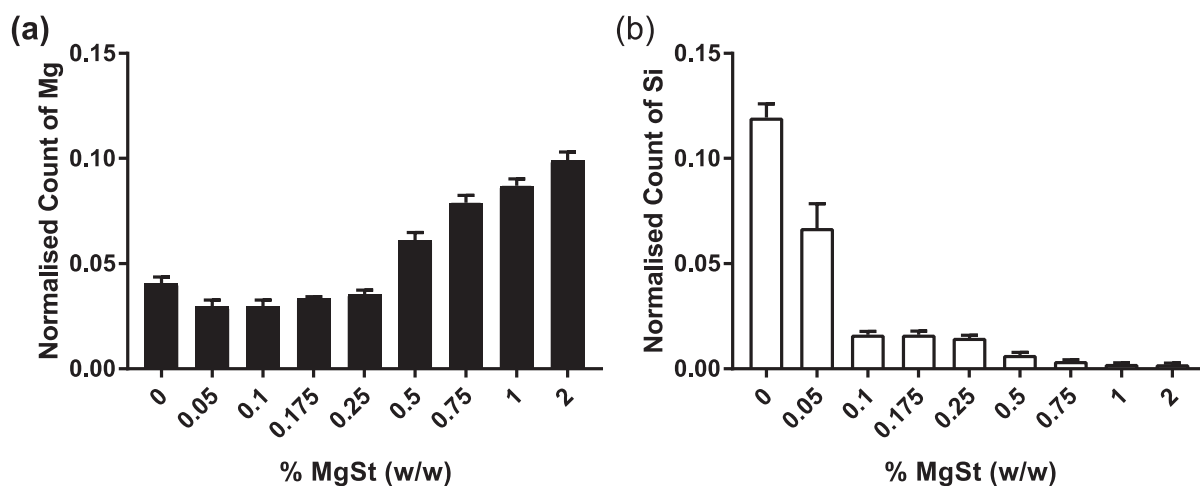


Figure 5-1: Normalised counts of (a) Mg and (b) Si signals over the total spectral peak of MGB and MGB dry coated with varying amounts of MgSt measured using ToF-SIMS at a scan area of 50 x 50 μm . $n = 20$ for each powder, error bars represent 95% confidence intervals.

Despite the addition of additional sources of magnesium in the form of MgSt, the normalised count of Mg in M-MGB-0.05 decreased compared to uncoated MGB. However, this small decrease was likely the result of a “matrix effect” as ToF-SIMS is highly sensitive to the chemical state of the target surface [74]. The matrix of MGB is the uncoated glass particle while for M-MGB-0.05 the matrix is the glass particle plus MgSt.

The normalised count of Si decreased significantly ($p < 0.05$) with only 0.05% w/w MgSt, suggesting there was sufficient amounts of MgSt on the glass particles to cover some of the Si. However, there was insufficient amounts of MgSt to “hide” all the Si as the normalised count of Si for M-MGB-0.05 remained relatively high. Therefore, the MgSt coating of M-MGB-0.05 was likely to be a thin partial coating.

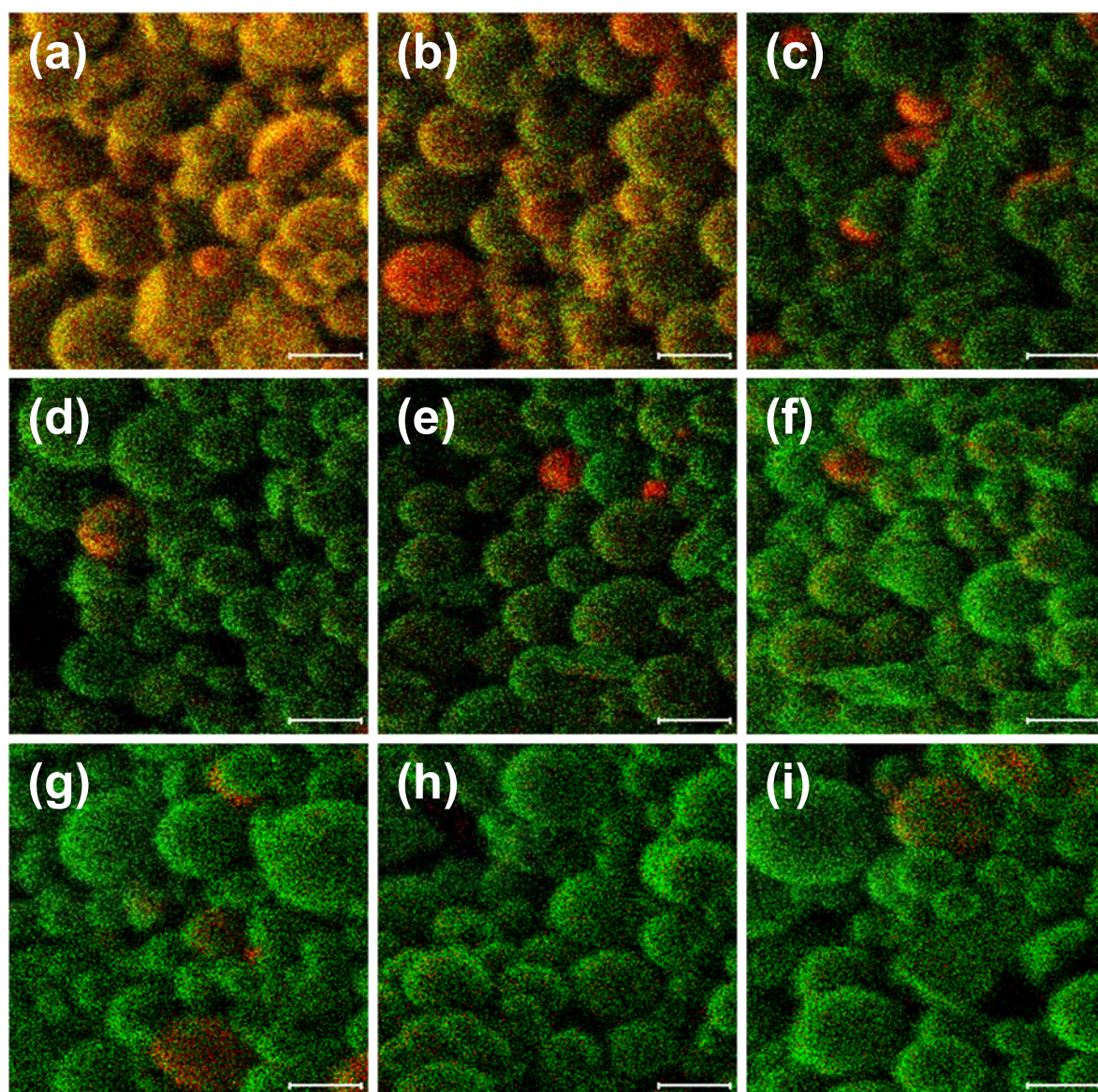


Figure 5-2: Representative spatial distribution of Si and Mg of: (a) MGB, (b) M-MGB-0.05, (c) M-MGB-0.1, (d) M-MGB-0.175, (e) M-MGB-0.25, (f) M-MGB-0.5, (g) M-MGB-0.75, (h) M-MGB-1, and (i) M-MGB-2. Scale bar equates to 10 μm . Red represents a Si signal and green represents a Mg signal. Note: the brightness of the images was increased to improve the visibility of the spatial distribution of Si and Mg.

With greater amounts of MgSt (0.1-0.25% w/w), the normalised count of Si was significantly lower ($p < 0.05$) than M-MGB-0.05 (see Figure 5-1b). However, despite this decrease in the normalised count of Si, the normalised count of Mg was not significantly different ($p > 0.05$) to M-MGB-0.05 (see Figure 5-1a). Furthermore, from Figure 5-2c to Figure 5-2e, it was observed that there was an overall increase in the

distribution of Mg over the surface of the particles while the overall distribution of Si over the surface of the particles decreased. Consequently, the MgSt coating on the powders with 0.1-0.25% w/w MgSt was likely to be a thin near-complete coating of MgSt. The normalised count of Mg significantly ($p < 0.05$) increased with increasing amounts of MgSt above 0.25% w/w MgSt (see Figure 5-1a) while the normalised count of Si decreased (see Figure 5-1b). Consequently, the MgSt coating with a minimum of 0.5% w/w MgSt was likely a thicker near-complete coating that was able to effectively “hide” more of the Si from being detected (see Figure 5-2f to Figure 5-2i). These observations indicate that the MgSt coating builds up and becomes thicker as the amount of MgSt used during dry coating increases. That is, with increasing amounts of MgSt, a new layer of MgSt is added to the previous layer of MgSt. This coincides well with the observations from Zhou *et al.*, 2011 [60], where the authors suggested that the coating of MgSt on lactose monohydrate (d_{50} approximately 20 μm) was thicker when the amount of MgSt used increased from 1% w/w to 5% w/w MgSt.

From the spatial distribution maps of Si and Mg of the powders (see Figure 5-2), it appears that MgSt might not have necessarily completely coated the entire surface of all the particles as a small number of patches where Si was still largely detected, even with a MgSt amount as high as 2% w/w, see Figure 5-2i.

XPS was used to determine the Mg and Si composition of the surfaces of the powders. The surface compositions of the powders are reported as atomic ratios relative to carbon and are presented in Figure 5-3.

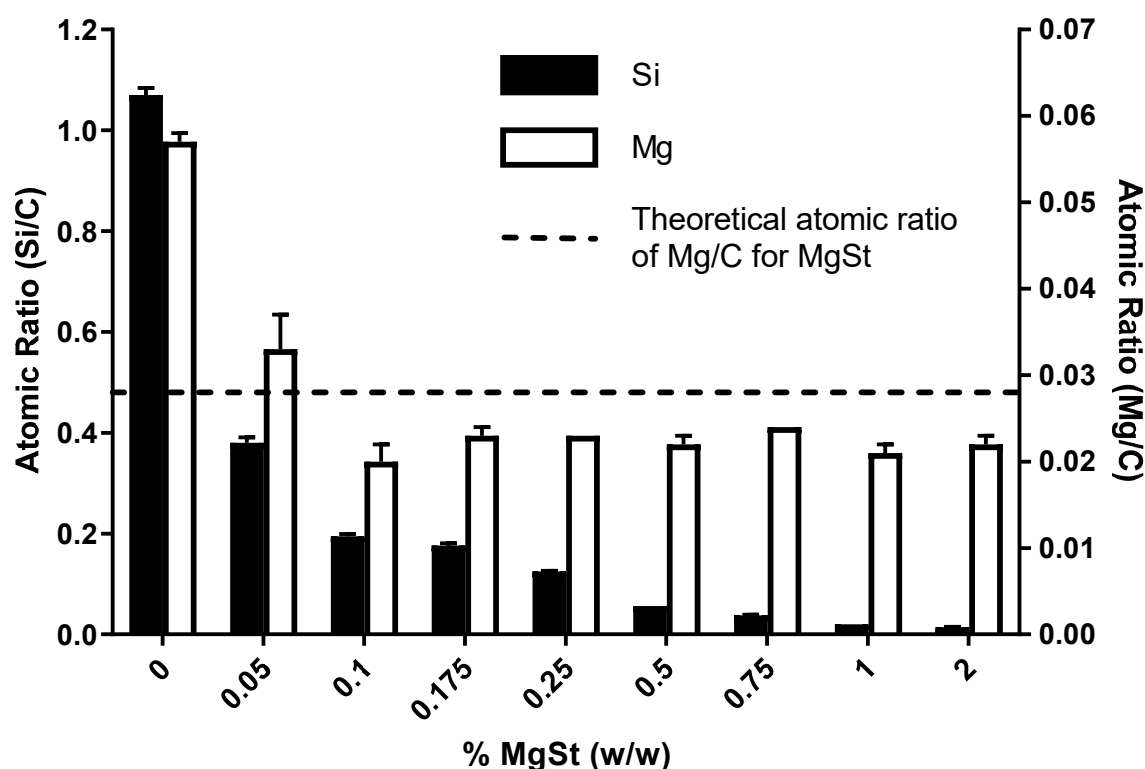


Figure 5-3: Atomic ratio of Si and Mg relative to carbon for MGB and MGB dry coated with varying amounts of MgSt. $n = 2$, error bars represent the deviation from the mean.

The atomic ratio of Si/C was observed to decrease with increasing weight percentage of MgSt used. This suggests the MgSt coating increased in thickness with increasing amounts of MgSt used, which is in good agreement with the ToF-SIMS analysis. Of interest was the atomic ratio of Mg/C for M-MGB-0.05 which was above the theoretical atomic ratio of Mg/C for MgSt, which is 0.028. This indicates that additional sources of Mg were detected, likely from the MGB host particles, which coincides well with the ToF-SIMS data in suggesting that the MgSt coating for M-MGB-0.05 was likely a thin partial coating.

Although it was not possible to provide a definitive description of the structure of the MgSt coating, XPS analysis does, however, suggest that the MgSt was likely orientated so that the Mg/carboxylic acid portion of MgSt was “buried” beneath the hydrocarbon tail of MgSt. That is, the hydrocarbon tail of MgSt was likely presented at the surface of the MgSt coated powders. This is because the atomic ratios of Mg/C for

the powders with 0.1% w/w MgSt or greater were all below the theoretical atomic ratio of Mg/C for MgSt, which is 0.028 (see Figure 5-3). Moreover, as ToF-SIMS and XPS only probes the upper-most portion of the surface of solids and Si from the MGB host particles was still detectable (see Figure 5-1 and Figure 5-3), the coating of MgSt must not have been thicker than the depth resolution of both ToF-SIMS and XPS, which was estimated to be approximately 10 nm. Consequently, despite the increasing thickness of the MgSt coating, the overall thickness of the coating itself was likely to be very thin (no more than approximately 10 nm). From previous studies of x-ray powder diffraction of MgSt powder the computed d -spacing for the long crystal spacing was reported to be approximately 4.8 nm [78]. This may suggest the MgSt coating of surface modified powders were likely a multi-laminar structure. Furthermore, as the atomic ratios of Mg/C for powders with 0.1-2% w/w MgSt were similar to one another, the MgSt was likely orientated in a similar way with increasing amounts of MgSt used. One possible structure of the MgSt coating is depicted in Figure 5-4.

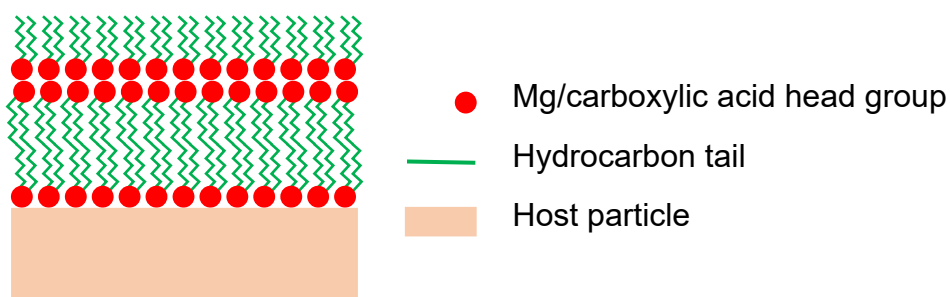


Figure 5-4: One possible structure of MgSt on the surface of the host particle after dry coating where the hydrocarbon tail of MgSt covers the Mg/carboxylic acid portion of MgSt. The number of layers of MgSt may vary depending on the amount of MgSt used relative to the total surface area of the host powder. Image not to scale.

5.5.2. The Effect of a MgSt Coating on the Surface Energy of MGB

The surface energy of the powders was evaluated via inverse gas chromatography at infinite dilution and the results are presented in Figure 5-5. The total surface energy, γ_S^T , of MGB was approximately 250 ± 9 mJ/m².

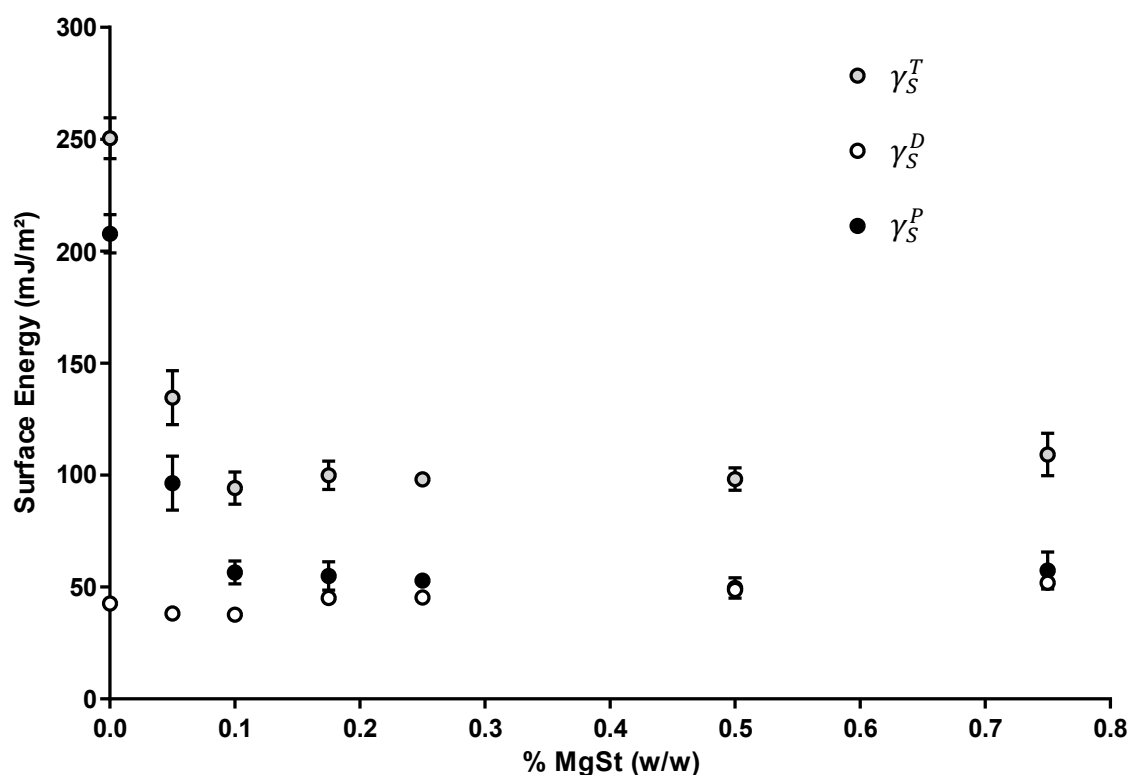


Figure 5-5: Surface energy of MGB and MGB dry coated with varying levels of MgSt. $n = 3$, error bars represent standard deviations.

When dry coated with 0.1% w/w MgSt, the γ_S^T of M-MGB-0.1 was lowered to approximately 94 ± 7 mJ/m². The surface energy of the powders with a minimum of 0.1% w/w MgSt remained unchanged despite having greater amounts of MgSt than 0.1% w/w. This indicates that the MgSt coatings for these powders were near-complete and showed similar chemistry. This is in good agreement with the ToF-SIMS and XPS results, which suggested that the hydrocarbon tail was presented at the surface of the MGB host particles. As the surfaces of the powders with 0.1% w/w or more MgSt were largely covered by MgSt (see Figure 5-2c to Figure 5-2i) and the hydrocarbon tail of MgSt was facing outwards (see Figure 5-3), the surface energies of M-MGB-1 and M-MGB-2 were therefore likely to be similar to the surface energy of the 0.1% w/w MgSt powder.

Not surprisingly, the γ_S^T of M-MGB-0.05 was lower than that of MGB but higher than the γ_S^T of the powders with a minimum of 0.1% w/w MgSt. This was attributed to the

MgSt coating covering the highest energy sites of the MGB host particles thus effectively masking these high energy sites during surface energy measurements via IGC at infinite dilution. Consequently, the measured γ_S^T of M-MGB-0.05 was between the surface energy MGB and 0.1% w/w MgSt coated MGB.

To better understand the change in the total surface energy of the powders, γ_S^T was split into its components: the dispersive surface energy, γ_S^D , and the polar surface energy, γ_S^P , also presented in Figure 5-5. The decrease seen in γ_S^T was primarily caused by a decrease in γ_S^P . Dry coating MGB with 0.175% w/w MgSt or more significantly increased ($p < 0.05$) γ_S^D by a small amount (see Figure 5-5). This was likely attributed to the increase in the dispersive nature of the powders with increasing amounts of MgSt, thereby also increasing the affinity of the dispersive probes to the stationary phase. This is in good agreement with the XPS analysis which suggested that MgSt was orientated with the hydrocarbon tail presenting outwards.

5.5.3. Hydrophobicity of MgSt Coated MGB

The hydrophobicity of the powders was measured via the liquid intrusion method with water as the probe liquid and ethanol as the reference liquid. The contact angle of water to the powders are presented in Table 5-3. Water did not intrude into powder beds of powders with 0.1% w/w MgSt or more.

Table 5-3: Contact angle of water to powders at 25° C. Ethanol was used as the reference liquid. Parentheses indicate standard deviation.

Powder	θ (°)	<i>n</i>
MGB	80 (0.3)	5
M-MGB-0.05	89 (0.2)	4
M-MGB-0.1+	>90	

The contact angle of water to MGB was $80 \pm 0.3^\circ$. With such a high contact angle, the strength of the capillary forces in MGB was likely relatively weak. Not surprisingly, water made a higher contact angle to M-MGB-0.05 where it was approximately

$89\pm 0.2^\circ$. Thus, with a coating of MgSt, the hydrophobicity of the powder increased. However, the intrusion rate of water into powder beds of M-MGB-0.05 was very slow and highly variable (as indicated by a large percentage of coefficient of variance, approximately 19% compared to approximately 6% for the intrusion rate of water into powder beds of MGB), refer to Figure 5-6.

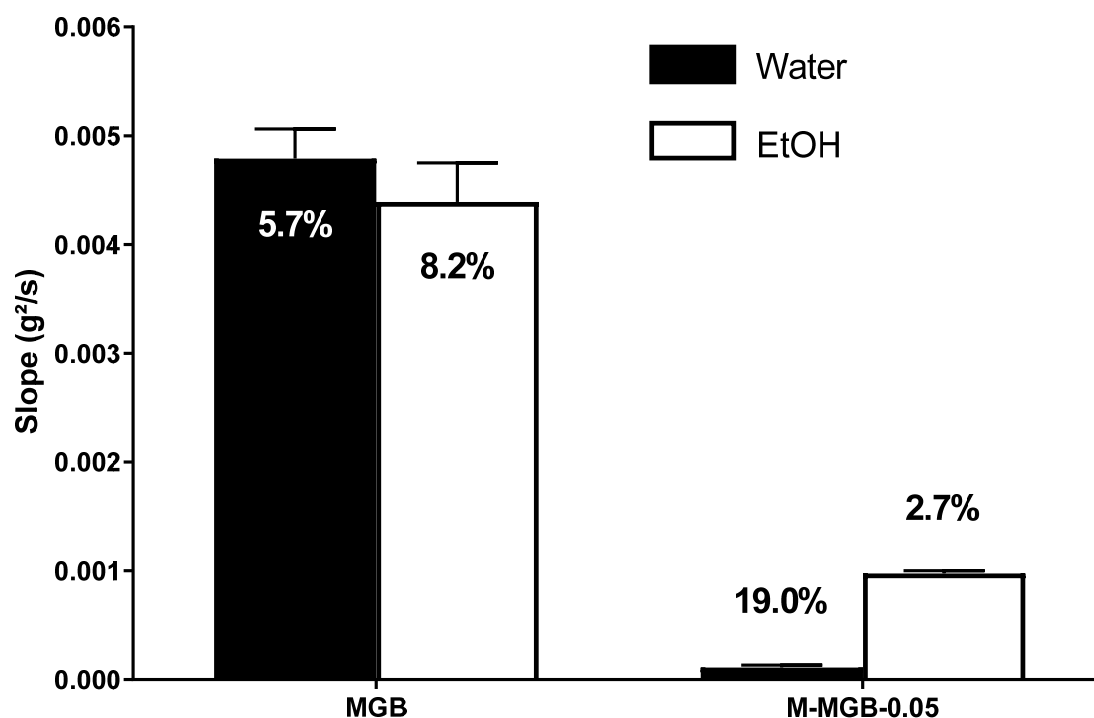


Figure 5-6: Rate of intrusion of water and ethanol into powder beds of MGB ($n = 5$) and M-MGB-0.05 ($n = 4$). Error bars represent standard deviation. The percentage coefficient of variation is presented numerically for each liquid and powder.

The poor and variable intrusion rate of water into powder beds of M-MGB-0.05 was likely attributed to the MgSt having a water contact angle of approximately 118° , which is large enough to prevent water intrusion from occurring [79]. However, as M-MGB-0.05 was only partially coated with MgSt, portions of the surface of the powder were glass (from the MGB host particle). Consequently, the intrusion of water into powder beds of M-MGB-0.05 was likely the result of preferential wetting of the uncoated portions of the particles. These powder beds also appeared partially dry after liquid intrusion experiments (data not shown). Water did not intrude into powders with a near-

complete MgSt coating (0.1% w/w MgSt or more). Consequently, dry coating MGB with MgSt was able to eliminate the effect of capillary forces on the flowability of powders with a MgSt coating, see Equation (5.3).

5.6. Conclusion

Dry coating MGB with MgSt was an effective approach to modify the surface composition of MGB by forming a coating of MgSt on the surfaces of the MGB host particles. The thickness and extent of the MgSt coating was dependent on the amount of MgSt used. The coating varied from being a thin partial coating (0.05% w/w MgSt) to a thin near-complete coating (0.1-0.25% w/w MgSt) to a thicker near-complete coating (0.5% w/w MgSt or more). Furthermore, XPS analysis suggested that MgSt was orientated so that the hydrocarbon tail was likely presented at the surface of the MgSt coated powders.

The surface energy of MGB was lowered with increasing amounts of MgSt. The decrease in the surface energy of the MgSt coated powders was primarily the result of MgSt lowering the polar surface energy. In contrast, the dispersive surface energy increased by a small amount after dry coating MGB with MgSt, which agrees with the XPS analysis suggesting that the hydrocarbon tail of MgSt oriented outwards. Furthermore, the surface energy of the powders remained unchanged once a near-complete MgSt coating was present on the MGB host particles. This was attributed to the MgSt coated powders all showing a similar surface: the hydrocarbon tail of MgSt.

The contact angle of water to uncoated MGB was approximately 80° , indicating that MGB was hydrophilic. However, with such a relatively high water contact angle, the strength of the capillary force within MGB was likely to be relatively weak. The hydrophobicity of MGB was increased after dry coating with MgSt. Liquid intrusion of water into beds of powders coated with more than 0.05% w/w MgSt did not occur. Consequently, a coating of MgSt was able to eliminate the presence of capillary forces within the MgSt coated powders.

5.7. Acknowledgements

The authors acknowledge the facilities, and scientific and technical assistance of the Australian Microscopy & Microanalysis Research Facility at the South Australian Regional Facility (SARF), University of South Australia, a facility that is funded by the University, and State and Federal Governments.

5.8. References

- [1] Aulton ME, (Ed.) *Pharmaceutics: The science of dosage form design*. 2nd ed., Churchill Livingstone, Edinburgh, UK, 2002.
- [2] Juliano P, Barbosa-Canovas GV, *Food powders flowability characterization: Theory, methods and applications*, Annu Rev Food Sci Technol, Annual Reviews, CA, USA, 2010, 211-39.
- [3] Orband JLR, Geldart D, Direct measurement of powder cohesion using a torsional device, *Powder Technol.* 92(1997) 25-33.
- [4] Sutton H, Flow properties of powders and the role of surface character, in: Parfitt G, Sing K (Eds.), *Characterization of powder surfaces*, Academic Press, NY, USA, 1976, 107-58.
- [5] Prescott JK, Barnum RA, On powder flowability, *Pharm Technol.* 24(2000) 60.
- [6] Peleg M, Flowability of food powders and methods for its evaluation — A review, *J Food Process Eng.* 1(1977) 303-28.
- [7] Zimon AD, *Adhesion of dust and powder*, Plenum Press, New York, USA, 1969.
- [8] Zeng XM, Martin G, Marriott C, *Particulate interactions in dry powder formulations of inhalation*, Taylor & Francis, NY, USA, 2000.
- [9] Pietsch WB, Adhesion and agglomeration of solids during storage, flow and handling - A survey, *J Eng Ind.* 91(1969) 435-49.
- [10] Johnson KL, Kendall K, Roberts AD, Surface energy and the contact of elastic solids, *Proc R Soc Lond A.* 324(1971) 301-13.
- [11] Fowkes FM, Determination of interfacial tensions, contact angles, and dispersion forces in surfaces by assuming additivity of intermolecular interactions in surfaces, *The Journal of Physical Chemistry.* 66(1962) 382-.
- [12] van Oss CJ, Acid—base interfacial interactions in aqueous media, *Colloids Surf, A.* 78(1993) 1-49.
- [13] van Oss CJ, Good RJ, Chaudhury MK, Additive and nonadditive surface tension components and the interpretation of contact angles, *Langmuir.* 4(1988) 884-91.
- [14] Girifalco LA, Good RJ, A theory for the estimation of surface and interfacial energies: 1. Derivation and application to interfacial tension, *J Phys Chem.* 61(1957) 904-9.
- [15] Fowkes FM, Attractive forces at interfaces, *Ind Eng Chem.* 56(1964) 40-52.
- [16] Owens DK, Wendt RC, Estimation of the surface free energy of polymers, *J Appl Polym Sci.* 13(1969) 1741-7.

- [17] Hadjittofis E, Zhang GGZ, Heng JYY, Influence of sample preparation on IGC measurements: the cases of silanised glass wool and packing structure, *RSC Advances*. 7(2017) 12194-200.
- [18] Jong T, Li J, Morton DAV, Zhou Q, Larson I, Investigation of the changes in aerosolization behavior between the jet-milled and spray-dried colistin powders through surface energy characterization, *J Pharm Sci*. 105(2016) 1156-63.
- [19] Steele DF, Moreton RC, Staniforth J, Young P, Tobyn M, Surface energy of microcrystalline cellulose determined by capillary intrusion and inverse gas chromatography, *The AAPS journal*. 10(2008) 494-503.
- [20] Smith RR, Shah UV, Parambil JV, Burnett DJ, Thielmann F, Heng JYY, The effect of polymorphism on surface energetics of D-mannitol polymorphs, *The AAPS Journal*. (2016) 1-7.
- [21] Lapčík L, Otyepka M, Otyepková E, Lapčíková B, Gabriel R, Gavenda A, et al., Surface heterogeneity: Information from inverse gas chromatography and application to model pharmaceutical substances, *Current Opinion in Colloid & Interface Science*. 24(2016) 64-71.
- [22] Rückriem M, Enke D, Hahn T, Inverse gas chromatography (IGC) as a tool for an energetic characterisation of porous materials, *Micropor Mesopor Mat*. 209(2015) 99-104.
- [23] Braun J-M, Guillet J, Study of polymers by inverse gas chromatography, *Mechanisms of Polyreactions-Polymer Characterization*, Springer, Berlin, Germany, 1976, 107-45.
- [24] Belgacem MN, Gandini A, Inverse gas chromatography as a tool to characterize dispersive and acid-base properties of the surface of fibers and powders, in: Pefferkorn E (Ed.) *Interfacial Phenomena In Chromatography*, Marcel Dekker Inc., NY, USA, 1999, 41-124.
- [25] Schultz J, Lavielle L, Martin C, The role of the interface in carbon fibre-epoxy composites, *J Adhesion*. 23(1987) 45-60.
- [26] Sircar S, Role of adsorbent heterogeneity on mixed gas adsorption, *Ind Eng Chem Res*. 30(1991) 1032-9.
- [27] Do DD, Dynamics of adsorption in heterogeneous solids, in: Rudziński W, Steele WA, Zgrablich G (Eds.), *Equilibria and dynamics of gas adsorption on heterogeneous solid surfaces*, Elsevier, Amsterdam, The Netherlands, 1997, 777-835.
- [28] Yla-Maihaniemi P, Heng J, Thielmann F, Williams D, Inverse gas chromatographic method for measuring the dispersive surface energy distribution for particulates, *Langmuir*. 24(2008) 9551-7.
- [29] Zimon AD, *Adhesion of dust and powder*, 2nd ed., Consultants Bureau, NY, USA, 1982.
- [30] Cross NL, Picknett RG, Particle adhesion in the presence of a liquid film. in: Johnson HR, Littler DJ, (Eds.), *The mechanism of corrosion by fuel impurities*; 1963; Marchwood, UK: Butterworths; 1963. p. 383-90.
- [31] Thomson W, On the equilibrium of vapour at a curved surface of liquid. *Proc R Soc Edinb*; 1870; Edinburgh, UK; 1870. p. 63-8.
- [32] Kiesvaara J, Yliruusi J, The effect of compression force and compression pressure on the surface free energy of tablets, *Acta Pharm Nord*. 3(1991) 171-7.
- [33] Buckton G, Characterisation of small changes in the physical properties of powders of significance for dry powder inhaler formulations, *Advanced Drug Delivery Reviews*. 26(1997) 17-27.

- [34] Buckton G, Assessment of the wettability of pharmaceutical powders, *J Adhes Sci Technol.* 7(1993) 205-19.
- [35] Shanker RM, Baltusis PJ, Hruska RM, Development of a new technique for the assessment of wettability of powders, *Pharm Res.* 10(1995) S-243.
- [36] Dove JW, Buckton G, Doherty C, A comparison of two contact angle measurement methods and inverse gas chromatography to assess the surface energies of theophylline and caffeine, *Int J Pharm.* 138(1996) 199-206.
- [37] Pepin, Blanchon S, Couarraze G, A new approach for determination of powder wettability, *Int J Pharm.* 152(1997) 1-5.
- [38] Ahfat NM, Buckton G, Burrows R, Ticehurst MD, An exploration of inter-relationships between contact angle, inverse phase gas chromatography and triboelectric charging data, *Eur J Pharm Sci.* 9(2000) 271-6.
- [39] Washburn EW, The dynamics of capillary flow, *Physical Review.* 17(1921) 273-83.
- [40] Grundke K, Boerner M, Jacobasch HJ, Characterization of fillers and fibres by wetting and electrokinetic measurements, *Colloids Surf.* 58(1991) 47-59.
- [41] Studebaker ML, Snow CW, The influence of ultimate composition upon the wettability of carbon blacks, *The Journal of Physical Chemistry.* 59(1955) 973-6.
- [42] Shi Q, Gardner DJ, Wang JZ, Surface properties of polymeric automobile fluff particles characterized by inverse gas chromatography and contact angle analysis. Fourth International Conference on Woodfiber-Plastic Composites; 1997; WI, USA: Forest Products Society; 1997. p. 245-56.
- [43] Teipel U, Mikonsaari I, Determining contact angles of powders by liquid penetration, *Part Part Syst Charact.* 21(2004) 255-60.
- [44] Galet L, Patry S, Dodds J, Determination of the wettability of powders by the Washburn capillary rise method with bed preparation by a centrifugal packing technique, *J Colloid Interface Sci.* 346(2010) 470-5.
- [45] Chen M, Wu S, Tang W, Gong J, Caking and adhesion free energy of maltitol: Studying of mechanism in adhesion process, *Powder Technol.* 272(2015) 235-40.
- [46] Hammes MV, Englert AH, Noreña CPZ, Cardozo NSM, Effect of water activity and gaseous phase relative humidity on microcrystalline cellulose water contact angle measured by the Washburn technique, *Colloids Surf, A.* 500(2016) 118-26.
- [47] Alonso M, Satoh M, Miyanami K, Mechanism of the combined coating-mechanofusion processing of powders, *Powder Technol.* 59(1989) 45-52.
- [48] Zhou Q, Armstrong B, Larson I, Stewart PJ, Morton DAV, Improving powder flow properties of a cohesive lactose monohydrate powder by intensive mechanical dry coating, *J Pharm Sci.* 99(2010) 969-81.
- [49] Zhou QT, Qu L, Gengenbach T, Larson I, Stewart PJ, Morton DAV, Effect of surface coating with magnesium stearate via mechanical dry powder coating approach on the aerosol performance of micronized drug powders from dry powder inhalers, *AAPS PharmSciTech.* 14(2013) 38-44.
- [50] Stank K, Steckel H, Physico-chemical characterisation of surface modified particles for inhalation, *Int J Pharm.* 448(2013) 9-18.
- [51] Zhou Q, Denman JA, Gengenbach T, Das S, Qu L, Zhang HL, et al., Characterization of the surface properties of a model pharmaceutical fine powder modified with a pharmaceutical lubricant to improve flow via a mechanical dry coating approach, *J Pharm Sci.* 100(2011) 3421-30.

- [52] Zhou QT, Armstrong B, Larson I, Stewart PJ, Morton DAV, Understanding the influence of powder flowability, fluidization and de-agglomeration characteristics on the aerosolization of pharmaceutical model powders, *Eur J Pharm Sci.* 40(2010) 412-21.
- [53] Kunnath K, Huang Z, Chen L, Zheng K, Davé R, Improved properties of fine active pharmaceutical ingredient powder blends and tablets at high drug loading via dry particle coating, *Int J Pharm.* 543(2018) 288-99.
- [54] Jallo LJ, Ghoroi C, Gurumurthy L, Patel U, Davé RN, Improvement of flow and bulk density of pharmaceutical powders using surface modification, *Int J Pharm.* 423(2012) 213-25.
- [55] Morin G, Briens L, The effect of lubricants on powder flowability for pharmaceutical application, *AAPS PharmSciTech.* 14(2013) 1158-68.
- [56] Zhou QT, Qu L, Larson I, Stewart PJ, Morton DAV, Improving aerosolization of drug powders by reducing powder intrinsic cohesion via a mechanical dry coating approach, *Int J Pharm.* 394(2010) 50-9.
- [57] Koskela J, Morton DAV, Stewart PJ, Juppo AM, Lakio S, The effect of mechanical dry coating with magnesium stearate on flowability and compactibility of plastically deforming microcrystalline cellulose powders, *Int J Pharm.* 537(2018) 64-72.
- [58] Lau M, Young PM, Traini D, Investigation into the manufacture and properties of inhalable high-dose dry powders produced by comilling API and lactose with magnesium stearate, *AAPS PharmSciTech.* 18(2017) 2248-59.
- [59] Zhou Q, Qu L, Larson I, Stewart PJ, Morton DAV, Effect of mechanical dry particle coating on the improvement of powder flowability for lactose monohydrate: A model cohesive pharmaceutical powder, *Powder Technol.* 207(2011) 414-21.
- [60] Zhou Q, Qu L, Gengenbach T, Denman JA, Larson I, Stewart PJ, et al., Investigation of the extent of surface coating via mechanofusion with varying additive levels and the influences on bulk powder flow properties, *Int J Pharm.* 413(2011) 36-43.
- [61] Paw R, Goggin P, Bajwa G, Feasibility study to investigate the application of mechanofusion to improve flow properties of a cohesive API, *J Pharm Pharmacol.* 62(2010) 1435-6.
- [62] Qu L, Zhou Q, Gengenbach T, Denman JA, Stewart PJ, Hapgood KP, et al., Investigation of the potential for direct compaction of a fine ibuprofen powder dry-coated with magnesium stearate, *Drug Dev Ind Pharm.* 41(2015) 825-37.
- [63] Han X, Jallo L, To D, Ghoroi C, Davé R, Passivation of high-surface-energy sites of milled ibuprofen crystals via dry coating for reduced cohesion and improved flowability, *J Pharm Sci.* 102(2013) 2282-96.
- [64] Jallo LJ, Schoenitz M, Dreizin EL, Dave RN, Johnson CE, The effect of surface modification of aluminum powder on its flowability, combustion and reactivity, *Powder Technol.* 204(2010) 63-70.
- [65] Chen L, Ding X, He Z, Fan S, Kunnath KT, Zheng K, et al., Surface engineered excipients: II. Simultaneous milling and dry coating for preparation of fine-grade microcrystalline cellulose with enhanced properties, *Int J Pharm.* 546(2018) 125-36.
- [66] Baer DR, Artyushkova K, Cohen H, Easton CD, Engelhard M, Gengenbach TR, et al., XPS guide: Charge neutralization and binding energy referencing for insulating samples, *Journal of Vacuum Science & Technology A.* 38(2020) 031204.

- [67] Tan G, Qu L, Morton DAV, Larson I, A strategy to evaluate the surface energy of high packing efficiency fine powders via inverse gas chromatography, *Powder Technol.* 320(2017) 470-3.
- [68] Cline D, Dalby R, Predicting the quality of powders for inhalation from surface energy and area, *Pharm Res.* 19(2002) 1274-7.
- [69] Traini D, Young PM, Thielmann F, Acharya M, The influence of lactose pseudopolymorphic form on salbutamol sulfate–lactose interactions in DPI formulations, *Drug Dev Ind Pharm.* 34(2008) 992-1001.
- [70] Thielmann F, Naderi M, Burnett D, Jervis H, Investigation of the acid-base properties of an MCM-supported ruthenium oxide catalyst by inverse gas chromatography and dynamic gravimetric vapour sorption, in: Jackson SD, Hargreaves JSJ, Lennon D (Eds.), *Catalysis in Application*, The Royal Society of Chemistry, Cambridge, UK, 2003, 233-9.
- [71] Das SC, Behara SRB, Bulitta JB, Morton DAV, Larson I, Stewart PJ, Powder strength distributions for understanding de-agglomeration of lactose powders, *Pharm Res.* 29(2012) 2926-35.
- [72] van Oss CJ, Chaudhury MK, Good RJ, Monopolar surfaces, *Adv Colloid Interface Sci.* 28(1987) 35-64.
- [73] Tan G, Morton DAV, Larson I, Strategies to analyse data obtained from liquid intrusion experiments of loose porous materials, *J Pharm Biomed Anal.* 145(2017) 711-7.
- [74] Fearn S, *An introduction to Time-of-Flight Secondary Ion Mass Spectrometry (ToF-SIMS) and its application to materials science.* Morgan & Claypool Publishers, CA, USA, 2015.
- [75] Grams J, *New trends and potentialities of ToF-SIMS in surface studies,* Nova Science Publishers, NY, USA, 2007.
- [76] *Surface science techniques,* Springer, Berlin, Germany, 2013.
- [77] Mangal S, Meiser F, Tan G, Gengenbach T, Denman J, Rowles MR, et al., Relationship between surface concentration of l-leucine and bulk powder properties in spray dried formulations, *Eur J Pharm Biopharm.* 94(2015) 160-9.
- [78] Sharpe SA, Celik M, Newman AW, Brittain HG, Physical characterization of the polymorphic variations of magnesium stearate and magnesium palmitate hydrate species, *Structural Chemistry.* 8(1997) 73-84.
- [79] Zografi G, Tam SS, Wettability of pharmaceutical solids: Estimates of solid surface polarity, *J Pharm Sci.* 65(1976) 1145-9.

Chapter 6:

Conclusions and Future Work

Geoffrey Tan

Bachelor of Pharmaceutical Sciences (Honours)

Drug Delivery, Disposition and Dynamics, Monash Institute of Pharmaceutical
Sciences. 381 Royal Parade, Parkville, VIC, 3052, Australia

Chapter 6: Conclusions and Future Work

6.1. Conclusions

This thesis investigates the mechanisms of how modifying the surface of a model cohesive fine powder with the pharmaceutical lubricant MgSt alters the flowability of the powder. To this end, micron-sized glass beads (MGB, $d_{50} \approx 10 \mu\text{m}$) were dry coated via mechanofusion with 0.05-2% w/w MgSt and the flow of the powders assessed with a number of methods. To understand the mechanisms of the changes in powder flow, the surface properties and surface coatings of the powders were measured.

Morphological studies and particle sizing showed that dry coating MGB with MgSt did not alter the morphology (Chapter 2: Figure 2-2) nor particle size or size distribution of the powders (Chapter 2: Figure 2-1 and Chapter 2: Table 2-1).

Dry coating MGB with MgSt was effective in increasing the flowability of MGB (Chapter 4: Evaluating the Flow of Surface Modified Fine Powders with Varying Amounts of Magnesium Stearate Through Different Flowability Tests). As the particle size and morphology of the powders were unaffected by the dry coating process, the improved flow of MgSt coated powders was attributed to the surface coating of MgSt. The improved flow was dependent on the amount of MgSt used as well as the method used to assess flow. The minimum amount of MgSt required to improve flow was 0.1% w/w regardless of the method used to assess flow. The amount of MgSt to induce best flow was within the range of 0.1-0.25% w/w MgSt. With a suboptimal amount of MgSt, M-MGB-0.05 was only able to flow more freely when it was undergoing unconfined flow (measured through flow rate) or confined mechanical flow (assessed through compressibility and BFE measurements). Powders with excess MgSt did not flow as easily as powders with optimal amounts of MgSt.

ToF-SIMS and XPS analysis of the powders showed that a coating of MgSt was formed on the MGB host particles after dry coating (Chapter 5: Characterising the

Surface Properties of Surface Modified Fine Powders). ToF-SIMS analysis showed that the thickness and extent of the MgSt coating was dependent on the amount of MgSt used and varied from being a thin partial coating (0.05% w/w MgSt) to a thin near-complete coating (0.1-0.25% w/w MgSt) to a thicker near-complete MgSt coating (0.5% w/w MgSt or more). XPS analysis showed that the coating of MgSt was orientated such that the hydrocarbon tail was facing outwards thus forming the surface of the powder (Chapter 5: Figure 5-4).

Inverse gas chromatography showed that the surface energy of MGB was significantly lower after dry coating with MgSt (Chapter 5: Figure 5-5). The decrease in the surface energy was primarily facilitated by a significant decrease in the polar surface energy. This can be understood through the XPS data suggesting that the hydrocarbon tail was presented at the surface of powders. Powders with 0.1% w/w MgSt or more had the same surface energies. This unchanged surface energy can be explained by the ToF-SIMS results showing a near-complete coating at these amounts of MgSt (Chapter 5: Figure 5-2).

The hydrophobicity of MGB, measured by the liquid intrusion method, increased after dry coating with MgSt. This increase in hydrophobicity was able to eliminate the presence of capillary forces for powders with a MgSt coating. However, as the contact angle of water to MGB was approximately 80° and the strength of the capillary force is proportional to the cosine of the contact angle ($F_c \propto \cos \theta$, see Equation (5.3)), the capillary force in MGB was likely to be relatively weak (Chapter 5: Table 5-3). Therefore, the elimination of the capillary force for MgSt coated powders was not likely to have had a large contribution to the increased flow of the MgSt coated powders.

Consequently, the principal mechanism by which the MgSt improved the flow of MgSt coated powders was due to the MgSt significantly lowering the surface energy of the constituent particles while the elimination of capillary forces only had a minor impact on the improvement in flow of MgSt coated powders.

Figure 6-1 presents the relationship between the surface energies of the powders and the flow of the powders as they undergo confined gravitational flow.

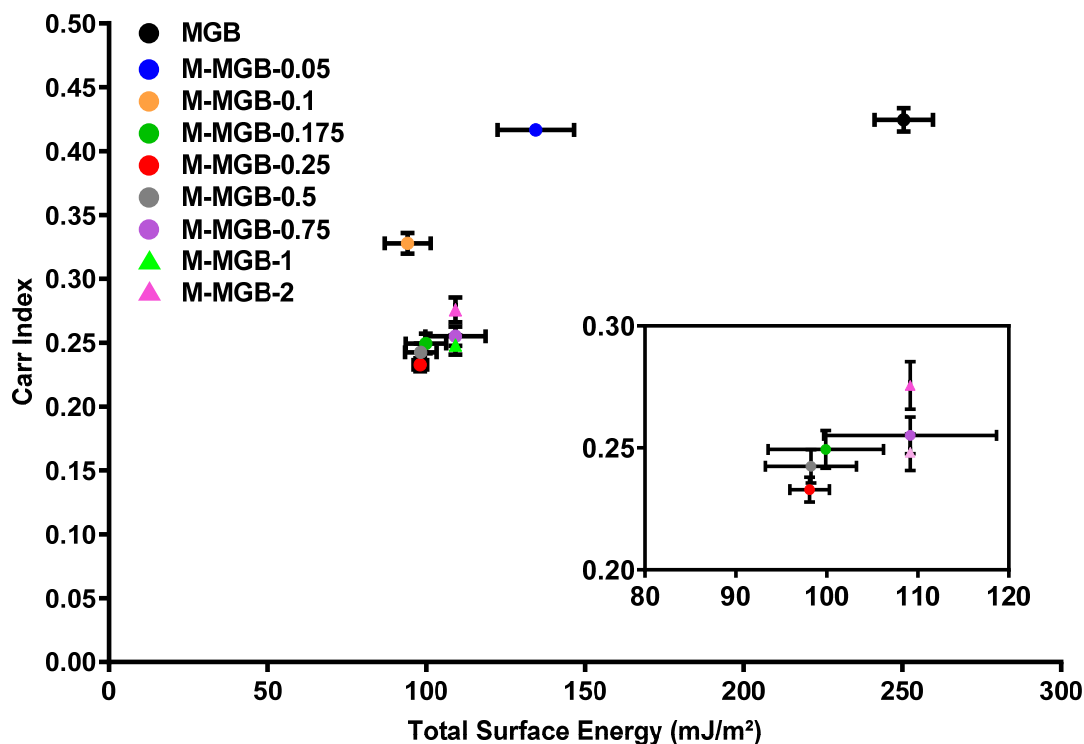


Figure 6-1: Relationship between the total surface energies of the powders and confined gravitational flow as assessed via Carr indices. Inset provides a zoomed in view of the clustered data.

From the data presented in Figure 6-1, powders with lower surface energies exhibited better flow. M-MGB-0.05 was the exception where M-MGB-0.05 and MGB exhibited the same flow despite M-MGB-0.05 had a significantly lower surface energy than MGB. This indicates that factors other than the surface energy were influencing the flow of M-MGB-0.05. Because M-MGB-0.05 was only partially coated by MgSt, both glass (from the MGB host particles) and MgSt were present on the surfaces of the M-MGB-0.05 particles. Consequently, three types of contacts were possible between particles of M-MGB-0.05: glass-glass, MgSt-glass and MgSt-MgSt. As the glass-glass contacts were the strongest of the three possible contacts (as glass had a significantly higher surface energy and a smaller water contact angle than MgSt), the glass-glass

contacts would therefore have occurred more often than any of the other possible contacts as M-MGB-0.05 flowed. Furthermore, as the flow of powders in tapped density measurements causes increased powder consolidation, the cohesive force between agglomerates of M-MGB-0.05 can increase to a point where the strength of the gravitational force is insufficient to break the strong contacts between the constituent particles.

Although the surface energies of M-MGB-0.1 and M-MGB-0.175 were the same, M-MGB-0.175 exhibited better flow than M-MGB-0.1. This may be attributed to M-MGB-0.175 having more MgSt thus was able form a MgSt coating that covered a greater portion of the MGB host particle compared to M-MGB-0.1. With this greater coverage of MgSt, less glass-glass contacts can form and thus result in greater flow. Expectedly, powders with similar surface energies (0.175 - 1% w/w MgSt) had similar flows, see inset in Figure 6-1. As the surface energies were similar, the cohesive forces between the constituent particles were also similar.

M-MGB-2 exhibited poorer flow than powders with 0.175 - 1% w/w MgSt (Chapter 5: Characterising the Surface Properties of Surface Modified Fine Powders). This poorer flow was likely attributed to the thickness of the MgSt coating. As MgSt is a relatively soft material, it can potentially deform. Therefore, with a sufficiently thick MgSt coating, the coating can deform when significant powder consolidation occurs, such as during tapped density measurements. This deformation results in greater contact areas between adjacent particles, see Figure 6-2 [1].

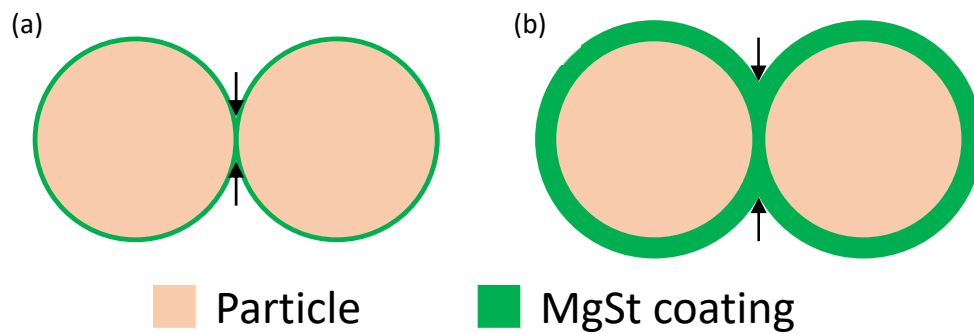


Figure 6-2: Two spherical particles with a MgSt coating in contact showing: (a) deformation of a thin coating of MgSt and (b) deformation of a thick coating of MgSt. The region in contact is indicated by arrows.

With more of the surface in contact, more inter-particle interactions can occur between adjacent particles [1]. The net result of having more inter-particle interactions is an increase in the cohesiveness of the powder and thus poorer flow.

Figure 6-3 presents the relationship between the surface energies of the powders and the flow of the powders as they undergo confined mechanical flow.

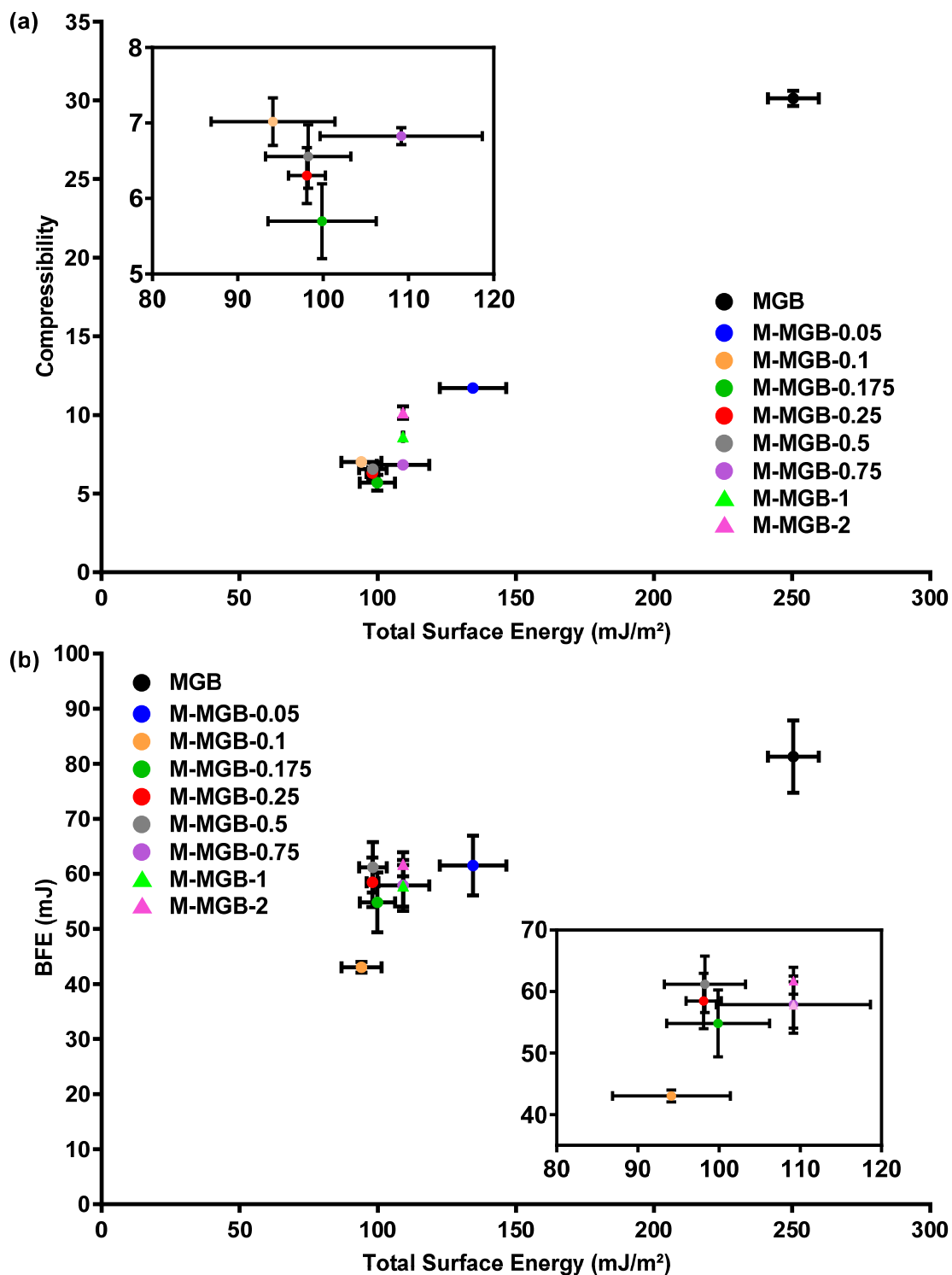


Figure 6-3: Relationship between the total surface energies of the powders and confined mechanical flow as assessed via (a) compressibility and (b) BFE measurements. Inset provides a zoomed in view of the clustered data.

As can be seen in Figure 6-3, powders with a lower surface energy undergoing confined mechanical flow were able to flow more freely. As per confined gravitational flow, powders with unchanged surface energies also exhibited unchanged confined mechanical flow, see inset figures in Figure 6-3. Powders with large amounts of MgSt also showed poorer confined mechanical flow than powders with less MgSt. The difference in confined mechanical flow compared to confined gravitational flow was that the poorer flow was exhibited with a smaller amount of MgSt. For instance, in compressibility measurements, M-MGB-1 exhibited poorer flow than powders with 0.1-0.75% w/w MgSt (see Figure 6-3a). The poorer flow of M-MGB-1 was likely the result of the stronger flow promoting force (mechanical force) exerted by the instrument. Therefore, the strong mechanical force was able to deform the MgSt coating sufficiently which increases the contact area between adjacent particles [1]. This therefore enables more inter-particle interactions to occur between adjacent particles which ultimately manifest as increased cohesiveness, thus poorer flow.

Figure 6-4 presents the relationship between the surface energies of the powders and the flow of the powders as they undergo unconfined flow.

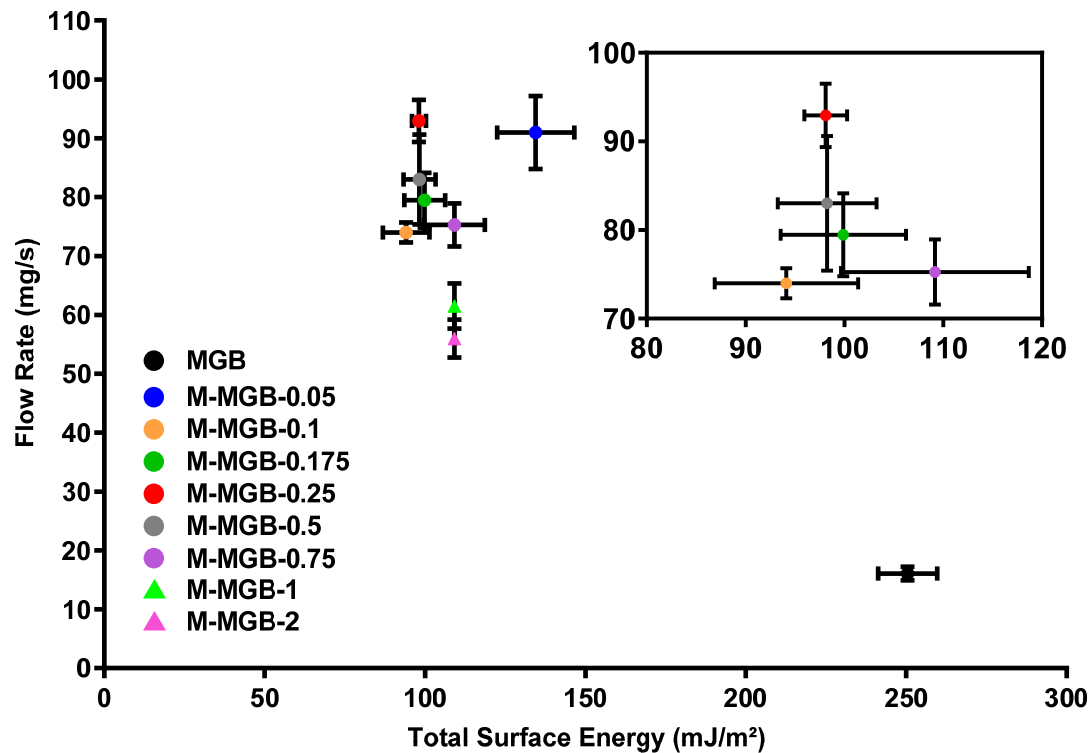


Figure 6-4: Relationship between the total surface energies of the powders and unconfined flow as measured through the flow rate of the powders. Inset provides a zoomed in view of the clustered data.

The data in Figure 6-4 shows that powders with a lower surface energy exhibited better unconfined flow. Powders with 0.75% w/w MgSt or more exhibited poorer flow than M-MGB-0.25, despite the powders all having the same surface energies. This is likely attributed to the relatively thick MgSt coating deforming sufficiently to increase the contact area between adjacent particles, which ultimately results in increased cohesiveness and thus poorer flowing powders [1].

Figure 6-5 presents the relationship between the surface energies of the powders and the flow of the powders as they undergo consolidated flow.

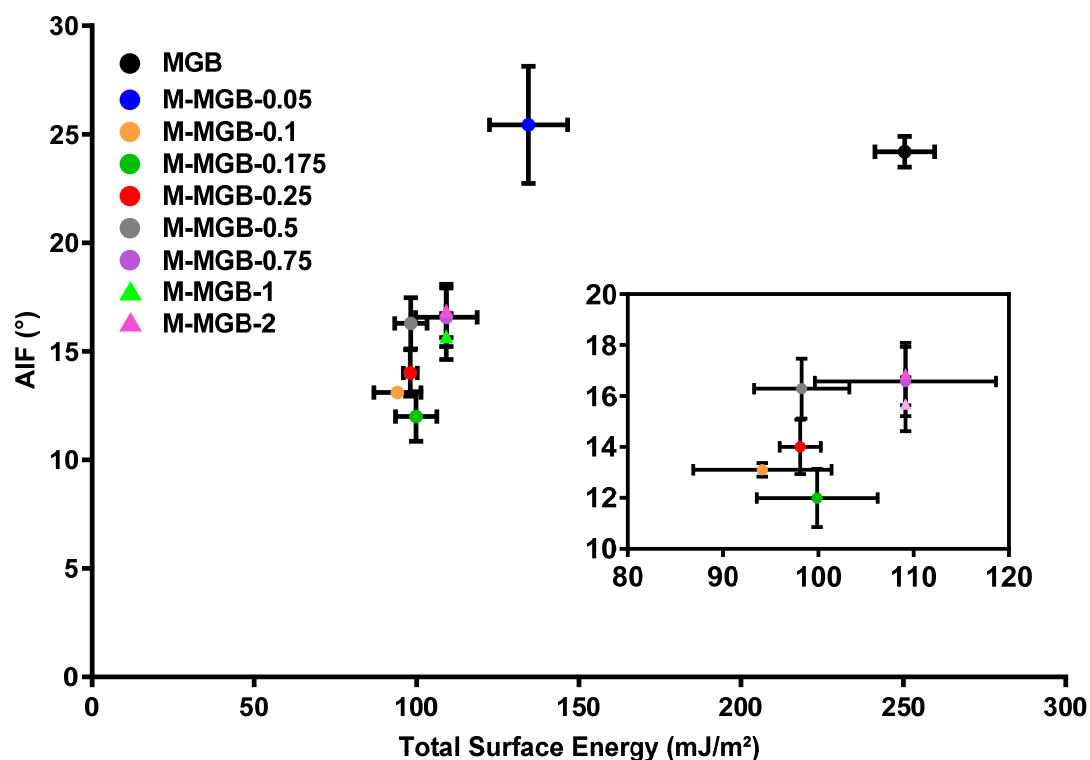


Figure 6-5: Relationship between the total surface energies of the powders and consolidated flow as assessed via AIF. Inset provides a zoomed in view of the clustered data.

In agreement with the other kinds of flow, decreasing the surface energy of the powders resulted in improved consolidated flow. M-MGB-0.05 showed slip-stick behaviour that affected its flow (Chapter 4: Evaluating the Flow of Surface Modified Fine Powders with Varying Amounts of Magnesium Stearate Through Different Flowability Tests). Powders with a minimum of 0.5% w/w MgSt flowed more poorly than powders with less MgSt (0.1-0.175% w/w), despite the powders all having the same surface energies. This is due to the high consolidative pressures exerted on the powders during shear cell testing. Consequently, the relatively thick MgSt coating was able to deform sufficiently which resulted in increased cohesiveness, hence poorer flow [1].

6.1.1. Thesis Summary

The work presented in this thesis demonstrates that modifying the surfaces of cohesive fine powders with a lubricant such as MgSt can have a complex effect on the flow of surface modified fine powders. The improved flow of the coated powders was the result of reduced cohesive forces between the constituent particles. This reduction was primarily facilitated by the coating significantly lowering the surface energy of the powder and, to a lesser extent, the elimination of capillary forces. Furthermore, the flow of surface modified powders was also influenced by the extent and thickness of the MgSt coating. Partial coatings of MgSt affect the type of contacts that are possible during powder flow. Thicker coatings of MgSt may result in small increases in cohesivity as deformation of the coating may occur (Chapter 6). This is especially true when powders undergo flow processes where consolidation either results from the flow (for example as shown in compressibility measurements) or was pre-consolidated (for example as shown in shear cell testing).

Consequently, this thesis provided valuable insights into the mechanisms of how the commonly used surface coating MgSt alters the flow of a model cohesive fine powder, thereby addressing the Thesis Statement of this thesis.

Thesis Objective 1: *“to modify the surfaces of a fine powder with magnesium stearate through mechanofusion”* was addressed in Chapter 2: Surface Modification and Physical Characterisation of a Model Pharmaceutical Powder.

Thesis Objective 2: *“to measure the flowability of the fine powder as well as the surface modified powder”* was addressed in Chapter 4: Evaluating the Flow of Surface Modified Fine Powders with Varying Amounts of Magnesium Stearate Through Different Flowability Tests

Thesis Objective 3: *“to measure the surface energy of the fine powder as well as the surface modified powder”* was addressed in Chapter 5: Characterising the Surface Properties of Surface Modified Fine Powders

Thesis Objective 4: *“to measure the surface hydrophobicity of the fine powder as well as the surface modified powder”* was addressed in Chapter 5: Characterising the Surface Properties of Surface Modified Fine Powders

Thesis Objective 5: *“to evaluate the relationship of the surface energy and hydrophobicity of the powders to the flowability of the powders”* was addressed in Chapter 6: Conclusions and Future Work

6.2. Future Work

In this study, the surface energies of the powders were measured via IGC at infinite dilution. As IGC at infinite dilution uses small concentrations of vapour probes, only the highest surface energy sites are probed. However, the surface energy of powders does not exist as a single value. Instead, surface energy exists as a distribution of surface energies. In order to investigate the role of surface energy distribution on the flow of fine powders with and without coatings, future studies could include IGC at finite concentration measurements, where greater amounts of vapour probes are used to probe for a wider portion of the surface energy distribution.

The coating material used in this thesis was a hydrophobic material (MgSt) while the host powder was hydrophilic (glass). Future studies could investigate the effect of coating materials with varying properties (such as hydrophobicities/hydrophilicities, hydrates, polymorphic forms etc.) on the flow of fine powders with varying characteristics (such as hydrophobicities/hydrophilicities, surface roughness, morphologies etc.). Such studies may lead to a broader understanding of how surface coatings generally influence the flow of fine powders.

As MGB was spherical, accurate measurements of the percentage surface coverage of the MgSt coating was not possible. Consequently, future studies where powders with relatively flat sides may allow for measurements of the extent of surface coverage of coatings such as MgSt. Alternatively, different coating methods may be explored such as the layer-by-layer approach where designed polymers with defined

proportions of functional groups may be used as coating materials. Such investigations may have industrial relevance as this may allow for more efficient use of materials and resources in the manufacturing of pharmaceutical dosages thus potentially lowering their cost of production.

6.3. References

[1] Israelachvili JN, Intermolecular and surface forces, 3rd ed., Academic Press, MA, USA, 2011.

Appendix

Table A.1: Q_{AB} values of *n*-hexane (Liquid A) to ethanol (Liquid B) when Method 1 and Method 2 were used. $F_l = 2.028$ (*n*-hexane to ethanol at 25° C). Note: SD for Method 1 was estimated through Propagation of Error Theory.

<i>n</i>	Q_{AB}	
	Method 1	Method 2
1	-	1.343
2	-	1.610
3	-	2.462
4	-	1.309
5	-	1.606
Average	1.648	1.666
SD	0.394	0.467
RSD	23.9	28.0

Appendix

Table A.2: Q_{AB} values of *n*-hexane (Liquid A) to ethanol (Liquid B) when Method 3 was used. $F_l = 2.028$ (*n*-hexane to ethanol at 25° C).

Collection Sequence						Ranked (Smallest to Largest)				
n_A	Hexane (g ² /s)	C_A ($\times 10^{-16}$ m ⁵)	n_B	Ethanol (g ² /s)	C_B ($\times 10^{-16}$ m ⁵)	C_A ($\times 10^{-16}$ m ⁵)	Hexane (g ² /s)	C_B ($\times 10^{-16}$ m ⁵)	Ethanol (g ² /s)	Q_{AB}
1	0.00557	2.181	1	0.00415	3.291	2.181	0.00557	3.139	0.00396	1.408
2	0.00699	2.737	2	0.00434	3.447	2.400	0.00613	3.291	0.00415	1.479
3	0.00974	3.812	3	0.00396	3.139	2.737	0.00699	3.447	0.00434	1.610
4	0.00613	2.400	4	0.00468	3.716	3.032	0.00774	3.716	0.00468	1.654
5	0.00774	3.032	5	0.00482	3.828	3.812	0.00974	3.828	0.00482	2.019
Average	0.00724	2.833		0.00439	3.484					1.634
SD	0.00163	0.636		0.000362	0.287					0.237
RSD	22.5	22.5		8.2	8.2					14.5

Appendix

Table A.3: Contact angle of water to glass beads when Method 1 and Method 2 were used. Ethanol was used as the reference liquid. Note: SD for Method 1 was estimated through Propagation of Error Theory.

<i>n</i>	θ (°)	
	Method 1	Method 2
1	-	79.7
2	-	80.9
3	-	78.7
4	-	80.1
5	-	81.1
Average	80.2	80.1
SD	0.02	1.0
RSD	0.022	1.2

Appendix

Table A.4: Contact angle of water to glass beads when Method 3 was used. Ethanol was used as the reference liquid.

Collection Sequence						Ranked (Smallest to Largest)				
n_r	Ethanol (g ² /s)	C_r (×10 ⁻¹⁶ m ⁵)	n_p	Water (g ² /s)	C_p (×10 ⁻¹⁶ m ⁵)	C_r (×10 ⁻¹⁶ m ⁵)	Ethanol (g ² /s)	C_p (×10 ⁻¹⁶ m ⁵)	Water (g ² /s)	θ (°)
1	0.00415	3.291	1	0.00473	3.443	3.139	0.00396	3.206	0.00441	79.9
2	0.00434	3.447	2	0.00441	3.206	3.291	0.00415	3.443	0.00473	79.7
3	0.00396	3.139	3	0.00493	3.588	3.447	0.00434	3.445	0.00474	80.2
4	0.00468	3.716	4	0.00514	3.739	3.716	0.00468	3.588	0.00493	80.5
5	0.00482	3.828	5	0.00474	3.445	3.828	0.00482	3.739	0.00514	80.4
Average	0.00439	3.484		0.00479	3.484					80.1
SD	0.000362	0.287		0.000272	0.198					0.3
RSD	8.2	8.2		5.7	5.7					0.4

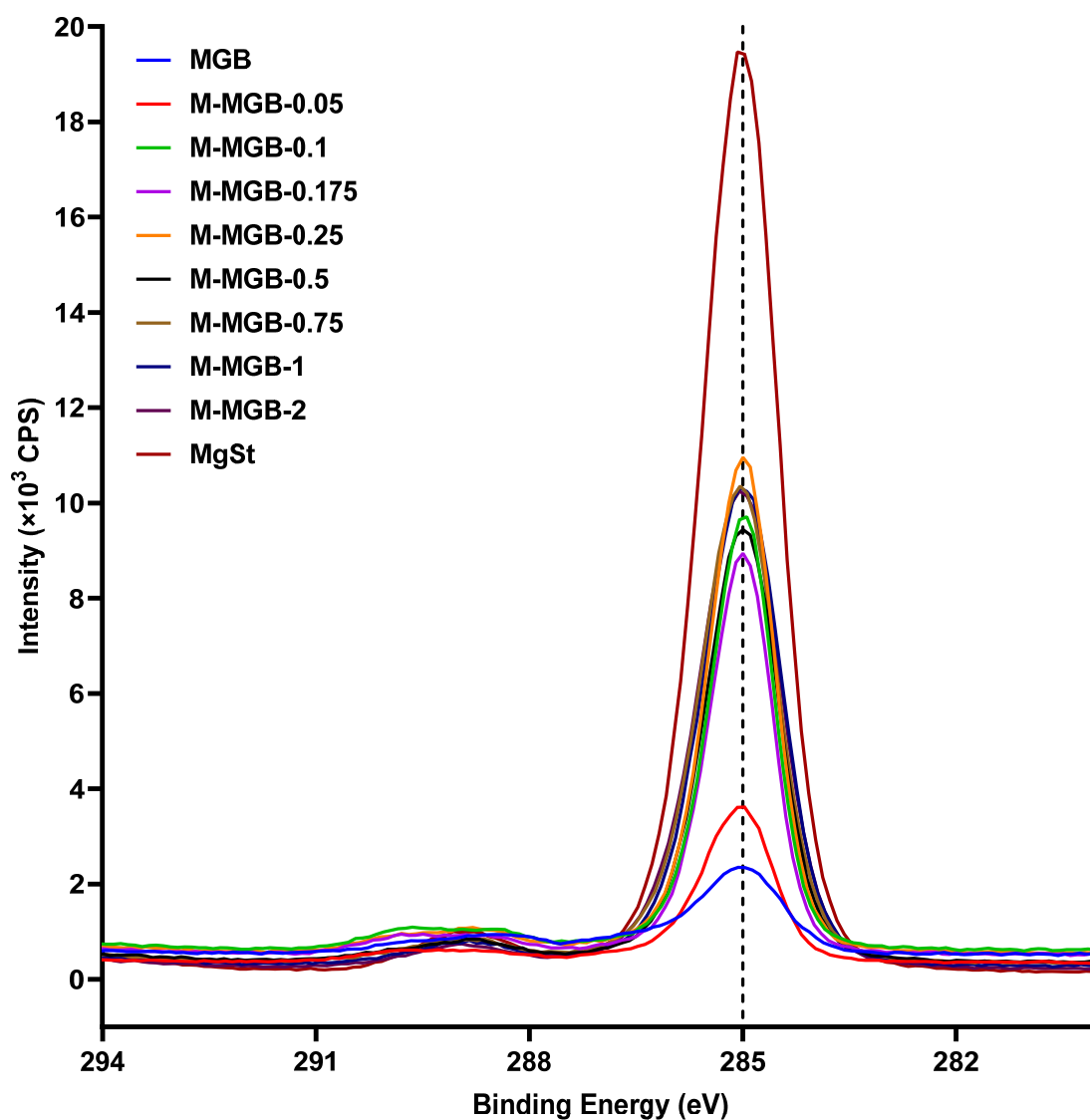


Figure A.1: C 1s high resolution spectra of MgSt, MGB and MGB dry coated with varying levels of MgSt.